Università degli Studi di Napoli "Federico II"

Facoltà di Scienze MM.FF.NN.

Dottorato in Fisica Fondamentale ed Applicata
XXIV ciclo

Davide Bianco

A thesis submitted for the degree of Philosophiae Doctor

Microscopic approaches to complex excitations in nuclei

Advisor:
Prof. N. Lo Iudice

Referees:
Prof. A. Brondi
Dr. L. Coraggio

Coordinator:
Prof. R. Velotta

Contents

Chapter 1

Introduction

The study of the spectroscopic properties of nuclei in terms of their nucleonic degrees of freedom is one of the most challenging task in nuclear structure. In order to accomplish it, one needs first a reliable nucleon-nucleon interaction, and then a many-body theory which allows to solve the nuclear eigenvalue problem.

Several nucleon-nucleon potentials have been developed, exploiting results from phase-shift analysis and mesonic theories. A large part of this potentials present a strong repulsive core. More recently, effective field theories rooted into quantum chromodynamics, have derived the so-called chiral potential, which reproduces the scattering data and the properties of deuteron and other light nuclei, and has the virtue of being smooth even at short internucleonic distances.

In principle the Shell Model (SM) allows to solve exactly the nuclear eigenvalue problem starting from the bare nucleon-nucleon potential. It provides, in fact, a precise recipe for deriving an effective Hamiltonian within a restricted model space and, then, for solving the eigenvalue equations in such a space.

In practice, the derivation of the effective Hamiltonian has to rely on several approximations, even if the accuracy of the methods for generating such a Hamiltonian have increased considerably in recent years.

Also using a restricted model space, the solution of the eigenvalue problem requires the diagonalization of the effective Hamiltonian in configuration space whose dimensions grow very rapidly with the number of active nucleons.

Hence, the necessity of efficient diagonalization algorithms which allow to face larger and larger spaces. Very successful and sophisticated diagonalization codes exist now, based on the Lanczos (Arnoldi) algorithm, which allows to find extremal eigenvalues and eigenvectors of a symmetric (Hermitean) matrix. In addition, stochastic and non-stochastic methods for sampling the shell model basis states have been developed.

Here we present the implementation within the spin-uncoupled scheme of an iterative algorithm formulated few years ago, together with its endowed sampling procedure for achieving an effective cut of the space dimensions. We will study the performance of the method by investigating the convergence of the iterative process, stating its limit of applicability. The algorithm, dubbed APL, is then used to perform a comprehensive study of the low-energy spectroscopy in medium-heavy nuclei. The method is then used to provide a comprehensive description of the low-energy spectroscopy in heavy Xenon isotopes.

Due to the limitations in space dimensions, shell model calculations for medium-heavy nuclei are not able to provide a complete picture of the low energy collective modes and high energy resonances.

The microscopic description of this nuclear states has been attempted within the Tamm-Dancoff Approximation (TDA), which describes the excitations in terms of 1-particle 1-hole, or even 2-quasiparticle, configurations, and the Random Phase Approximation (RPA), which includes higher order correlation. Due to their microscopic nature, these approaches account for some fragmentation of the modes and resonances. This fragmentation, however, is not sufficient to reproduce experimental data. A more complete description has to include more complex configuration.

Here we reformulate an equation of motion method for generating iteratively a basis of multiphonon states, built out of TDA phonons. This basis is then used for solving the eigenvalue problem without approximations.

We will describe this method in its spin-uncoupled and spin-coupled form as well as in its particle-hole and quasiparticle formulations. The first (ph) is suited to closed shell nuclei, the second to open-shell nuclear systems.

We will show how the method can be implemented and applied to the closed shell ^{16}O and to neutron rich oxygen isotopes. We will use realistic effective Hamiltonians in a space which includes up to $n = 3$-phonon states. We will study the effect of these complex states mainly on the giant dipole resonance (GDR) and on the so-called pygmy resonance in neutron rich isotopes.

1.1 Organization of the material

This thesis is divided into two parts. The first part is composed of chapters 2 to 6 and deals with the Nuclear Shell Model.

In chapter 2 we outline briefly the SM and its theoretical foundations. In particular, we describe how the nuclear eigenvalue problem for A nucleons interacting trough the bare nucleon-nucleon interaction can be turned into an equivalent eigenvalue problem, formulated in a restricted space, for a number of valence nucleons interacting trough an effective interaction.

The chapter 3 reviews different currently adopted methods for diagonalizing the SM Hamiltonian matrix. We discuss first the Lanczos algorithm, which is the most widely adopted method for Large Scale Shell Model calculations. We then present the stochastic Shell Model Monte Carlo, which is well suited to study the property of the ground state and to compute the strength functions. The chapter continues with an illustration of the Quantum Monte Carlo Diagonalization (QMCD) method. The QMCD achieves a truncation of the SM space by sampling the basis states, relevant to the Hamiltonian matrix diagonalization. Another method, known as Density Matrix Renormalization Group, borrowed from Solid State Physics, is finally outlined.

In chapter 4 the APL algorithm is presented. It is in particular shown that the algorithm is naturally endowed with a sampling procedure which allows to truncate the space.

In chapter 5, we illustrate how the algorithm can be implemented in the uncoupled M-scheme, and point out the simplifications which come out from using such a basis.

The first part ends with chapter 6, where some numerical applications to medium-heavy nuclei are presented. The results of the calculations are discussed. Special attention is paid to the low energy spectroscopic properties of heavy Xe isotopes.

The second part is composed of chapters 7 to 9 and deals with nuclear collective excitations.

In chapter 7, after a brief semiclassical description, we discuss Tamm-Dancoff (TDA) and Random-Phase (RPA) approximations, which are the most traditional and simple microscopic approaches to collective modes. These methods have basically an harmonic character. In order to account for anharmonic effects, one has to go beyond the harmonic approximation. Among the several extensions, we discuss the quasiparticle-phonon model (QPM).

Most of these extensions are still based on the so called quasi-boson approximation (QBA), underlying the RPA. This was the motivation for the formulation of the present method, known as Equations of Motion Phonon Method (EMPM). This approach is described in chapter 8.

We present a particle-hole (ph) and a quasiparticle formulation of the method. The first one is suited to closed shell nuclei. The second allows to study open-shell nuclei.

In chapter 9 we present the application of the method to oxygen isotopes, and study in particular the nuclear response to electromagnetic probes.

Some final remarks, together with some appendices, conclude the thesis.

PART ONE

The Nuclear Shell Model

Chapter 2

The Shell Model

2.1 The nuclear eigenvalue problem

The nuclear shell model originates from the independent particle model introduced by Mayer (1) and Jensen (2). The assumption of this model is to absorb the effects of the nucleon-nucleon interaction into an average potential. Under this assumption the nuclear Hamiltonian is just

$$H_0 = \sum_i h_i \ , \tag{2.1}$$

whit

$$h = t + U \ , \tag{2.2}$$

where t is the kinetic energy and U the mean-field potential.

The average potentials can be determined empirically or by performing an Hartree-Fock calculation B. The most widely adopted empirical potentials are the Woods-Saxon (WS) (3) and the Nilsson (4; 5) potentials. The first is composed of a radial and a spin-orbit part

$$U_{WS} = U(r) + \frac{\partial U(r)}{\partial r} l \cdot s \ , \tag{2.3}$$

where

$$U(r) = -\frac{U_0}{1 + exp[(r-R)/a]} \ . \tag{2.4}$$

The parameters U_0, a and R are fixed by a best fit of the experimental data (6).

The eigenvalue equation with a WS Hamiltonian has to be solved numerically. A simpler alternative, which allows an analytical solution, is represented by the Nilsson Modified Harmonic Oscillator potential

$$U_{HO} = \frac{1}{2}\hbar\omega_0\rho^2 - \kappa\hbar\omega_0\Big[2l \cdot s + \mu(l^2 - \langle l^2 \rangle)\Big] \ ; \qquad \rho = \left(\frac{M\omega_0}{\hbar}\right)^{1/2} r \ , \tag{2.5}$$

where the parameters ω_0, κ and μ are fitted to the data.

The nuclear eigenstates are given by the Slater determinants

$$\Phi_i = \frac{1}{(A!)^{1/2}} \mathcal{A} \left(\varphi_{\nu_1}(1)\varphi_{\nu_2}(2) \cdots \varphi_{\nu_A}(A)\right)_i , \tag{2.6}$$

where

$$h_i \varphi_\nu(i) = (t + U)\, \varphi_\nu(i) = \epsilon_\nu \varphi_\nu(i) \ , \tag{2.7}$$

are the eigensolution of the one body Hamiltonian, h, and $i \equiv \{\nu_1 \cdots \nu_i \cdots \nu_A\}$ labels the quantum numbers of each Slater determinant.

The independent particle model explains such nuclear properties as ground state spins and parities and the existence of "magic number".

For a realistic description of nuclear structure one has to take into account the residual interaction which is not absorbed by the mean field potential. In principle one has to solve the eigenvalue problem

$$H\Psi_\alpha(1,2,\dots,A) = E_\alpha\Psi_\alpha(1,2,\dots,A) \ , \tag{2.8}$$

in a infinite dimensional space spanned by the Slater determinants. This is clearly impossible. On the other hand, one is interested in few eigenvalues and eigenstates. The modern Shell Model provides the recipes for turning the eigenvalue problem in an infinite dimensional space into an equivalent one formulated in a restricted model space.

2.2 Model space and effective operators

We start with decomposing the nuclear Hamiltonian as

$$H = H_0 + V, \tag{2.9}$$

where H_0 is the unperturbed one-body Hamiltonian, given by Eq. 2.1, and V is the residual two-body potential. In the basis of the eigenstates of H_0, one obtains for the full Hamiltonian the eigenvalue equations

$$\sum_l \left[\epsilon_i\delta_{li} + (\Phi_i\, ,\, V\Phi_l)\right] c^l_\alpha = E_\alpha c^i_\alpha. \tag{2.10}$$

The solution of the above equations yields the eigenstates of H

$$\Psi_\alpha = \sum_i c^i_\alpha \Phi_i \ . \tag{2.11}$$

The eigenvalue problem defined by the equation above is formulated in a SM space of infinite dimensions, and requires the solution of a system of infinite equations, namely the diagonalization of an infinite dimension Hamiltonian matrix. On the other hand, according to the Shell Model theory, we can formulate an equivalent eigenvalue problem in a drastically truncated space. The truncation criterion is dictated by the fact that in general, in nuclear spectroscopy, one is interested in low energy excitations, which are mostly promoted by the valence nucleons.

In SM, one decomposes the full space into a d-dimensional model D plus an excluded Q space

$$I = P + Q \ , \tag{2.12}$$

$$P = \sum_{i=1,d} |i\rangle\langle i|, \qquad Q = I - P \ , \tag{2.13}$$

where

$$|i\rangle = |\nu_1, \cdots \nu_i, \cdots \nu_v\langle \ . \tag{2.14}$$

Thus, the model space is confined to the subspace of the v valence nucleons only.

Let us consider the eigenvalue equation in the full space

$$H\Psi^\alpha = E_\alpha\Psi^\alpha. \tag{2.15}$$

The goal is to transform the above eigenvalue equation into one formulated in the model space

$$H_{eff}\Psi^\alpha_0 = E^\alpha\Psi^\alpha_0, \tag{2.16}$$

under the request that the d eigenvalues of the model effective Hamiltonian H_{eff} coincide with the exact ones of H in the full space.

In order to derive H_{eff}, one makes the further request that the model eigenfunctions are obtained from the corresponding eigenstates of H in the full space by projection

$$\Psi_0^\alpha = P\Psi^\alpha \ . \tag{2.17}$$

The further step is to define the wave operator Ω

$$\Psi^\alpha = \Omega\Psi_0^\alpha \ , \tag{2.18}$$

so as establish a a complete link between model and full space.

In virtue of the above definition, the eigenvalue equation (2.15) becomes

$$H\Omega\Psi_0^\alpha = E^\alpha\Omega\Psi_0^\alpha \ . \tag{2.19}$$

Following now the procedure developed by Lee and Suzuki (8) and generalized by Andreozzi (9), one may left multiply by the inverse of Ω obtaining

$$\mathcal{H}\Psi_0^\alpha = E^\alpha\Psi_0^\alpha \ , \tag{2.20}$$

where $\mathcal{H}$ is related to the full Hamiltonian H by the similarity transformation

$$\mathcal{H} = \Omega^{-1}H\Omega \ . \tag{2.21}$$

The transformed Hamiltonian shares d eigenvalues with H, but still couples the model space and its complement.

On the other hand, Eq. (2.18) does not completely define Ω. Thus, without loss of generality, one can write the similarity transformation in the form

$$\left(\begin{array}{cc} P\Omega P & P\Omega Q \\ Q\Omega P & Q\Omega Q \end{array} \right) = \left(\begin{array}{cc} I_P & 0 \\ \omega & I_Q \end{array} \right) \ . \tag{2.22}$$

The eigenvalue equation in the complete space for the transformed Hamiltonian then reads

$$\left(\begin{array}{cc} P\mathcal{H}P & P\mathcal{H}Q \\ Q\mathcal{H}P & Q\mathcal{H}Q \end{array} \right) \left(\begin{array}{c} \Psi_0^\alpha \\ Q\Psi^\alpha - \omega\Psi_0^\alpha \end{array} \right) = E^\alpha \left(\begin{array}{c} \Psi_0^\alpha \\ Q\Psi^\alpha - \omega\Psi_0^\alpha \end{array} \right) \ . \tag{2.23}$$

The exact separation for the Hamiltonian of the model space from its orthogonal complement is achieved by imposing the condition

$$Q\mathcal{H}P = QHP + QHQ\omega - \omega PHP - \omega PHQ\omega = 0 \ . \tag{2.24}$$

Since $H = H_0 + V$, this relation can be written as

$$QVP + QH_0Q\omega + QVQ\omega - \omega PH_0P - \omega PVP - \omega PVQ\omega = 0 \ , \tag{2.25}$$

where use has been made of the fact that QH_0P and PH_0Q are identically zero, and that $\omega P = Q\omega = \omega$.

If the condition (2.24) is fulfilled, one can define the effective Hamiltonian as the transformed Hamiltonian operating within the model space

$$H_{eff} = P\mathcal{H}P = PHP + PVQ\omega \ . \tag{2.26}$$

The task is then to solve the decoupling equation in order to derive an explicit expression of the effective Hamiltonian. Assuming degeneracy in the P-space, one can use the following simplifying relation

$$PH_0P = \epsilon_0 P \,, \tag{2.27}$$

where ϵ_0 is the degenerate space energy. The Eq. (2.25) then reads

$$(\epsilon_0 - QHQ)\,\omega = QVP - \omega V_{eff} \,, \tag{2.28}$$

where the effective interaction is defined as

$$V_{eff} = P\mathcal{H}P - PH_0P = PVP + PVQ\omega \,. \tag{2.29}$$

Eq. (2.28) can be solved iteratively. One obtains

$$\omega = \sum_{k=0}^{\infty}(-1)^k \frac{1}{(\epsilon_0 - QHQ)^{k+1}} QVP(V_{eff})^k \,. \tag{2.30}$$

Upon insertion into Eq. (2.29), one obtains for the model effective potential the recursive formula

$$V_{eff} = \hat{Q}(\epsilon_0) + \sum_{k=1}^{\infty} \hat{Q}_k(\epsilon_0)(V_{eff})^k \,, \tag{2.31}$$

where

$$\hat{Q}(\epsilon_0) = PVP + PVQ\frac{1}{(\epsilon_0 - QHQ)}QVP \,, \tag{2.32}$$

is a Q-box and Q_k its k-derivative given by

$$\hat{Q}_k(\epsilon_0) = \frac{1}{k!}\frac{d^k}{d\epsilon^k}\hat{Q}(\epsilon)\bigg|_{\epsilon=\epsilon_0} = (-1)^k PVQ\frac{1}{(\epsilon_0 - QHQ)^{k+1}}QVP \,, \tag{2.33}$$

It can be shown (10) that the terms contributing to the Q-box diagrammatic expansion are only irreducible valence-linked diagrams, which can be divided into a one-body set, the so called S-box, and two-body contributions.

As clearly shown by the above defining equations, the model effective potential is given by an infinite series in the free nucleon-nucleon (NN) potential.In general, it is difficult to treat this series perturbatively, mainly because of the strong repulsive character of the NN potential at short distance. Thus, in order to evaluated V_{eff}, one has to try to obtain an effective convergence by summing subsets of an infinite number of properly selected terms of the series. A notable and widely adopted summation consists in summing the so called ladder diagrams

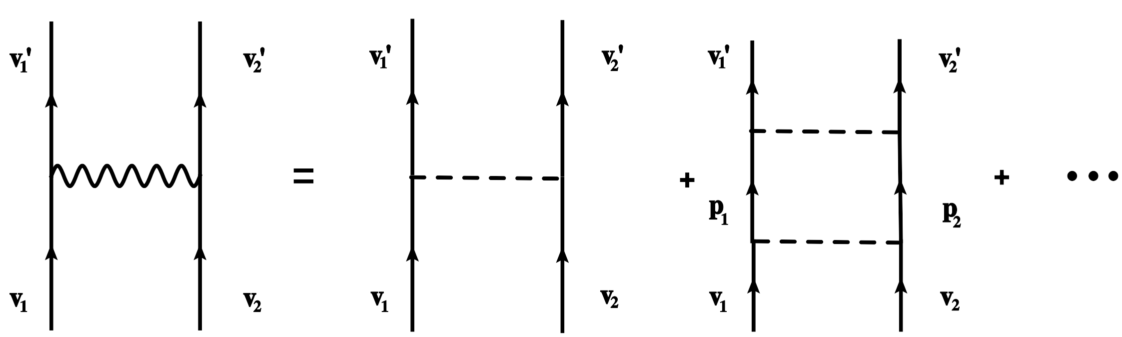

Figure 2.1: Diagrammatic representation of the G matrix.

(Fig. 2.1). This sum defines the well known Brueckner G matrix (11)

$$G(\omega) = V + V\frac{Q_{2p}}{\omega - H_0}G(\omega)\ , \tag{2.34}$$

where $Q_{2p} = \sum_{p_1p_2} |p_1p_2 >< p_1p_2|$ projects into the the space of the two-particle states excluded from the model space. The starting energy ω includes not only the excitation energy of the two-particle state $|p_1p_2>$ but also the energy of other excited nucleons in the many-body intermediate state. In practice, ω is a parameter.

The above defining equation can be written as

$$G(W) = \frac{V}{1 - V\frac{Q}{W-H_0}} = \frac{1}{\frac{1}{V} - \frac{Q}{W-H_0}}\ , \tag{2.35}$$

which shows clearly that the G-matrix has a smooth behavior even if V becomes infinite.

Once rearranged and expressed in term of the G matrix, the series does not converge. It still contains infinite terms describing the coupling of the valence particles with the excitations of the core. The lowest order term of this kind is the bubble diagram introduced in the pioneering work of Kuo and Brown (12) (Fig. 2.2) . Also the other higher order terms are important and make the redefined series non convergent. In order to account for these terms,

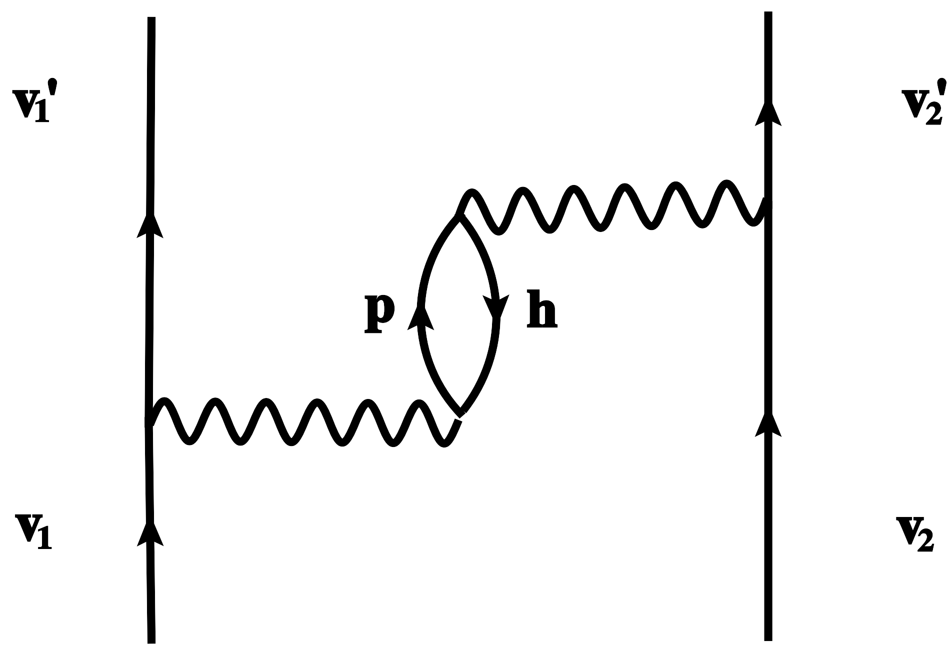

Figure 2.2: The lowest order core polarization diagram.

other summation techniques have been developed. One is due to Krenciglowa and Kuo (13) and consists in computing the most relevant perturbative terms of the Q-Box and then sum these Q-Boxes to all orders. Another method is non perturbative and relies on the similarity transformation of Andreozzi-Lee-Suzuki.

The calculation of the G matrix is cumbersome and based on approximations (the starting energy, for instance) which are not under full control. Thus alternative methods have been attempted.

A successful one is the so-called V_{low-k} method (14; 15). This applies the theory of effective interaction outlined above to the system of two nucleons in the vacuum. More specifically, it defines a "model" space spanned by NN states of low relative momenta and a Q-space covered by high-momentum states. The effective interaction theory is adopted to define an effective potential, dubbed V_{low-k}, which accounts for the coupling with the excluded high-momentum states. The V_{low-k} depends on the cutoff in the momentum space which separates the model from the Q space. Such a cutoff is basically a parameter. It has been shown in Ref. (15) that a cutoff $\sim 2.1\ fm^{-1}$ is a reasonable choice.

The V_{low-k} represents a useful alternative to the G matrix. It is, in fact, free of singularity and can be directly used as a potential in SM calculations after core polarization terms have been included by one of the mentioned summation techniques, like for instance the Q-Box method. In this form, it has been used with success for low-energy spectroscopic studies (16).

A crucial ingredient of the effective interaction is the NN potential. This is determined either empirically from the NN scattering data or from mesonic theories or from combining both procedures. We mention the Nijmegen I and II potentials (17), the AV18 (18) and the charge-dependent CD-Bonn potentials (19). Recently, important advances have been made with the derivation of NN potentials within effective field theories. The chiral Idaho-A and B (20; 21) are notable examples. A version of the chiral potential, dubbed N3LOW, is smooth even at short range and, therefore, has been used directly in SM calculations (22).

Chapter 3

Hamiltonian diagonalization methods

Standard diagonalization methods cannot be adopted for large scale shell model calculations, since they require $O(N^3)$ operations, N being the dimension of the matrix (23). The dimensions of the shell model Hamiltonian matrix increase very rapidly with the number of valence nucleons and shells. They become prohibitively large in medium nuclei with few valence neutrons and protons, even if they are confined within a major shell.

On the other hand, one is often interested only in few low-lying nuclear states. Thus, in the past decades, an intensive research activity was devoted to the search of methods and corresponding implementation codes for determining few low-lying eigenvalues and eigenfunctions of the nuclear Hamiltonian in large shell model spaces. These activities were strongly stimulated by the increasing power of computer facilities.

Lanczos algorithm (23; 24; 25) is certainly the most important and most exploited method. Indeed, it has been adopted with success in many branches of physics and in other disciplines, and the most powerful nuclear shell model codes are based on the Lanczos algorithm (26).

Even these highly sophisticated codes are not able to face most of the medium-heavy nuclei where the Hamiltonian matrices reach soon dimensions $N \gg 10^9$. This limitation has stimulated the search for alternative methods which circumvent the direct diagonalization of the Hamiltonian matrix. A notable one is the Shell Model Monte Carlo (SMMC) (32; 33). This stochastic method can handle spaces with larger dimensions. On the other hand, it can compute only ground state quantities and strength functions. It is, therefore, unable to provide detailed information on levels and transitions.

In this respect, a better use of the stochastic approach was made in the so called Quantum Monte Carlo Diagonalization (QMCD) (35). This methods adopts the stochastic Monte Carlo procedure to sample the nuclear basis states. In this reduced base the nuclear Hamiltonian is then diagonalized. The QMCD has the virtue of providing a criterion for truncating the shell model space and, therefore, opens the possibility of facing very large configuration spaces.

Another truncation method, based on the Density Matrix Renormalization Group (DMRG), the use of which was first proposed in condensed matter physics, (37; 36), has been successfully used in nuclear structure physics (38).

In this chapter, the different approaches mentioned above are briefly reviewed. Their presentation follows the order adopted in this introductory part.

3.1 Lanczos algorithm

The goal of Lanczos algorithm (24) is to construct a basis which brings the Hamiltonian matrix H to tridiagonal form T. This is achieved through the similarity transformation

$$T = Q^T H Q \quad \longrightarrow \quad HQ = QT \ , \tag{3.1}$$

where Q is the orthogonal matrix representing the overlap between the old and the new basis vectors.

This transformation is equivalent to the request that the new basis vectors, $|i\rangle$, fulfill the condition

$$H|i\rangle = \beta_{i-1}|i-1\rangle + \alpha_i|i\rangle + \beta_i|i+1\rangle \ , \tag{3.2}$$

where

$$\beta_i = \langle i+1|H|i\rangle \ , \quad \alpha_i = \langle i|H|i\rangle \ , \tag{3.3}$$

and

$$\beta_0 = \beta_n = 0 \ . \tag{3.4}$$

The action of H on a starting (pivot) vector, $|0\rangle$, decomposes the space into two orthogonal pieces,

$$H|0\rangle = \alpha_0|0\rangle + |w_1\rangle \ , \tag{3.5}$$

where

$$\alpha_0 = \langle 0|H|0\rangle \ , \tag{3.6}$$

and the vector $|w_1\rangle$, orthogonal to $|0\rangle$, is unnormalized. We can then define the normalized vector

$$|1\rangle = \frac{|w_1\rangle}{\langle w_1|w_1\rangle^{1/2}} \ , \tag{3.7}$$

and obtain

$$\beta_1 = \langle 1|H|0\rangle = \langle w_1|w_1\rangle^{1/2} \ . \tag{3.8}$$

The second state, $|1\rangle$, of the new basis, is thereby determined. The remaining $N-2$ basis vectors are found by iterating the procedure. One operates on the generic state, $|k\rangle$, obtaining the orthogonal decomposition (3.2). The tridiagonal matrix so obtained is to be diagonalized at each iterative step k until convergence to a selected sets of eigenvalues is reached.

The Lanczos procedure is a fast and efficient tool for determining the Hamiltonian eigenstates in nuclear shell model calculations. Its numerical implementation, however, deserves special care. The vectors $|k\rangle$ of the basis which yield a tridiagonal matrix are mathematically, but not numerically, orthogonal, because of the limited precision of digital computers. Though initially small, the errors so induced propagates rapidly with the number of iterations and may yield spurious solutions.

Several codes which employ the Lanczos algorithm for diagonalizing the nuclear Shell Model Hamiltonian are now available. They can be divide into two groups, depending on the calculation scheme used. One group is composed of the codes which use a $j-j$ coupled basis, the second of the codes which are based on the uncoupled m-scheme.

The $j-j$ scheme is adopted by the codes Nathan (26; 27; 28) and Nushell (29). It has the advantage of yielding SM Hamiltonian matrices of relatively small dimensions. On the other hand, these matrices are very dense and, since of the complex algebraic structure, the evaluation of their matrix elements is lengthy and cumbersome.

The m-scheme was first adopted in the pioneering Glasgow code (30), and fully exploited by the Antoine code (26; 31). The uncoupled basis yield a SM Hamiltonian matrix of much larger dimensions. However, it is sparse, and its matrix elements are much easier to be evaluated, due to the simple structure of the scheme.

3.2 Shell Model Monte Carlo

The Shell Model Monte Carlo (SMMC) method (32; 33) is an alternative approach to the solution of the Hamiltonian matrix eigenvalue problem. It is based on the imaginary-time evolution operator

$$U = e^{-\beta H} \ , \tag{3.9}$$

where β is a real number, for instance the inverse of the temperature $\beta = 1/T$. The action of the imaginary time evolution operator (3.9) on a generic state many-body state $|\Phi\rangle$ yields

$$e^{-\beta H}|\Phi\rangle = \sum_{\sigma} c_i^{(0)} e^{-\beta E_i}|\Phi_i\rangle \ , \tag{3.10}$$

where E_i and $|\Phi_i\rangle$ are the eigenvalues and eigenstates of the Hamiltonian H and $c_i^{(0)}$ are the expansion coefficients of $|\Phi\rangle$ in terms of the eigenstates $|\Phi_i\rangle$. We then have

$$lim_{\beta\rightarrow\infty} e^{-\beta H}|\Phi\rangle = c_0^{(0)}|\Psi\rangle \ , \tag{3.11}$$

where $|\Psi\rangle$ is the ground state wave function. Thus, for large β, the evolution operator $e^{-\beta H}$ acts as a ground state projection operator. The expectation value of an operator Ω on a the generic state $|\Phi\rangle$ is

$$\langle\Omega\rangle = \frac{\langle\Phi|e^{-\frac{\beta}{2}H}\Omega e^{-\frac{\beta}{2}H}|\Phi\rangle}{\langle\Phi|e^{-\beta H}|\Phi\rangle} = \frac{Tre^{-\beta H}\Omega}{Tre^{-\beta H}} \ . \tag{3.12}$$

In the limit of large β, one gets the ground state expectation value

$$\lim_{\beta\rightarrow+\infty}\langle\Omega\rangle = \frac{\langle\Psi|\Omega|\Psi\rangle}{\langle\Psi|\Psi\rangle} \ . \tag{3.13}$$

Difficulties in calculating explicitly the expectation value of the above relation arise from the two body part of the Hamiltonian. As a matter of fact, let us consider the following schematic expression for H

$$H = \epsilon O + \frac{1}{2}VOO \ , \tag{3.14}$$

where O is a one-body operator, V the two-body potential and ϵ the single-particle energy. If there were only one operator O, the two-body part of the Hamiltonian would be quadratic, and the time evolution would be simply linearized by mean of the Hubbard-Stratonovich transformation

$$e^{-\beta H} = e^{-\beta(\epsilon O + \frac{1}{2}VO^2)} = \sqrt{\frac{\beta|V|}{2\pi}}\int_{-\infty}^{\infty} d\sigma e^{-\frac{1}{2}\beta|V|\sigma^2} e^{-\beta h} \ , \tag{3.15}$$

where σ is a c-number and h has the form

$$h = \epsilon O + sV\sigma O \ , \tag{3.16}$$

with $s = 1$ if $V < 0$, and $s = i$ if $V > 0$.

Using this transformation, and defining $U_\sigma \equiv e^{-\beta h}$, the expectation value of an operator takes the form

$$\langle\Omega\rangle = \frac{\int d\sigma e^{-\frac{\beta}{2}|V|\sigma^2} TrU_\sigma\Omega}{\int d\sigma e^{-\frac{\beta}{2}|V|\sigma^2} TrU_\sigma} \ , \tag{3.17}$$

which is equivalent to

$$\langle\Omega\rangle = \frac{\int d\sigma W_\sigma \Omega_\sigma}{\int d\sigma W_\sigma} \ , \tag{3.18}$$

where

$$W_\sigma = G_\sigma TrU_\sigma \ ; \quad G_\sigma = e^{-\frac{\beta}{2}|V|\sigma^2} \ ; \quad \Omega_\sigma = \frac{TrU_\sigma\Omega}{TrU_\sigma} \ . \tag{3.19}$$

The problem has been then reduced to calculating two integrals, which can be evaluated with the Monte Carlo procedure.

Unfortunately, a realistic nuclear Hamiltonian of the form (3.14) includes the sum over several one-body operators,

$$H = \sum_{\alpha} \left(\epsilon^*_\alpha \bar{O}_\alpha + \epsilon_\alpha O_\alpha\right) + \frac{1}{2}\sum_{\alpha} V_\alpha \{O_\alpha \, , \, \bar{O}_\alpha\} \, , \tag{3.20}$$

which in general do not commute. In this equation, $\bar{O}_\alpha$ is the time-reverse of O_α. In this way the Hamiltonian is written in a time-reversal invariant form.

In order to linearize the time evolution, one have to split the interval β into N_t time slices of length $\Delta_\beta = \beta/N_t$, so that the evolution operator can be written as

$$e^{-\beta H} = \left[e^{-\Delta\beta H}\right]^{N_t} \, . \tag{3.21}$$

In each of these slices one can perform the transformation (3.15), obtaining

$$e^{-\Delta\beta H} \approx \int \prod_n \left(\frac{d\sigma_{\alpha n} d\sigma^*_{\alpha n} \Delta\beta |V_\alpha|}{2\pi}\right) e^{-\Delta\beta \sum_\alpha |V_\alpha||\sigma_{\alpha n}|^2} e^{-\Delta\beta h_n} \, , \tag{3.22}$$

where

$$h_n = \sum_\alpha (\epsilon^*_\alpha + s_\alpha V_\alpha \sigma_{\alpha n})\bar{O}_\alpha + (\epsilon_\alpha + s_\alpha V_\alpha \sigma^*_{\alpha n}) O_\alpha \, . \tag{3.23}$$

The expectation value can then be written again as the ratio

$$\langle \Omega \rangle = \frac{\int D\sigma W_\sigma \Omega_\sigma}{\int D\sigma W_\sigma} \, , \tag{3.24}$$

where

$$\begin{gathered} W_\sigma = G_\sigma Tr U \, , \quad G_\sigma = e^{-\Delta\beta \sum_{\alpha n} |V_\alpha||\sigma_{\alpha n}|^2} \, , \quad \Omega_\sigma = \tfrac{Tr U \Omega}{Tr U} \, , \\ D\sigma \equiv \prod_n \prod_\alpha d\sigma_{\alpha n} \left(\tfrac{\Delta\beta |V_\alpha|}{2\pi}\right) \, , \end{gathered} \quad . \tag{3.25}$$

Here U is given by

$$U = U_{N_t} \cdots U_2 U_1 \, . \tag{3.26}$$

For a high accuracy, the number of time slices N_t must be very large. Since there is a variable for each operator at each time slice, the dimension D of these integrals is very large and might exceed 10^5. With this method, one is also able to estimate the momenta of an operator in the ground state.

The mean value (3.24) has the structure

$$< \Omega >= \int D_\sigma P_\sigma \Omega_\sigma, \tag{3.27}$$

where

$$P_\sigma = \frac{W_\sigma}{\int D\sigma W_\sigma} \tag{3.28}$$

can be considered a probability density, since $P_\sigma \geq 0$ and $\int D\sigma P_\sigma = 1$. Thus, $< \Omega >$ comes out to be the average of Ω_σ weighted by P_σ. One may choose randomly a set S of configuration σ_s with probability P_σ and approximate $< \Omega >$ with

$$< \Omega >= \int D_\sigma P_\sigma \Omega_\sigma \approx \frac{1}{S} \sum_{s=1,S} O_s, \tag{3.29}$$

where Ω_s is the value of Ω_σ at the field configuration σ_s. The same $<\Omega>$, depending on the random choice of the field configurations, is a random variable. In virtue of the central limit theorem, its average value is the required value with an uncertainty

$$\sigma^2_{<\Omega>} = \frac{1}{S}\int D_\sigma P_\sigma(\Omega_\sigma - <\Omega>)^2 \approx \frac{1}{S^2}\sum_s(\Omega_\sigma - <O>)^2. \tag{3.30}$$

It remains now to use a method for generating the field configurations. Generally one adopts the Metropolis, Rosenbluth, Rosenbluth, Teller and Teller algorithm (34).

The SMMC allows to compute strength functions. Given, in fact, the function

$$R_\Omega = \frac{Tre^{-\beta H}\Omega\Omega}{Tre^{-\beta H}} \ , \tag{3.31}$$

one obtains for large β

$$R_\Omega^\infty = \sum_i \frac{|\langle\Psi|\Omega|i\rangle|^2}{\langle\Psi|\Psi\rangle} \ , \tag{3.32}$$

where $\{|i\rangle\}$ is a complete set of eigenvectors of the Hamiltonian. The function R_Ω^∞ is then the sum of transition probabilities to the ground state, and its derivative are the operator momenta.

The problem which is encountered in following this approach is given by the need for W_σ to be real and semi-positive definite (sign problem). This is always true for boson systems, but for fermions this condition is fulfilled only by some schematic Hamiltonians. Moreover, while well suited to the ground state, the method is not able to provide detailed information on nuclear spectroscopy.

Even with this limitation, SMMC has proved to be a powerful and efficient tool for studying ground-state and thermal properties of medium-mass nuclei as well as electroweak nuclear properties such as Gamow-Teller strength distributions and the dipole giant resonance.

3.3 Truncation schemes

3.3.1 Quantum Monte Carlo Diagonalization

The Quantum Monte Carlo Diagonalization (QMCD) methods, (35), combines the stochastic and the diagonalization approach. Unlike the SMMC, which evaluates expectation values and strength functions, QMCD gives explicit eigenvectors, diagonalizing the Hamiltonian matrix. The difference with the other diagonalization approaches is in that the basis states are generated stochastically with a Monte Carlo run.

As with the SMMC, the QMCD exploits the fact the the imaginary-time evolution operator behaves as a filter which yields only the ground state for $\beta \to \infty$. The leading idea of QMCD can be easily understood for a toy model using the schematic Hamiltonian

$$H = \frac{1}{2}VO^2 \ . \tag{3.33}$$

One can then find for the evolution operator the expression

$$e^{-\beta H} = e^{-\beta\frac{1}{2}VO^2} = \sqrt{\frac{\beta|V|}{2\pi}}\int_{-\infty}^{\infty} d\sigma e^{-\frac{1}{2}\beta|V|\sigma^2}e^{-\beta h(\sigma)} \ , \tag{3.34}$$

where $h(\sigma) = |V|\sigma O$. This can be integrated numerically by MC sampling the quantity

$$e^{-\beta H} = e^{-\beta\frac{1}{2}VO^2} \sim \sqrt{\frac{\beta|V|}{2\pi}}\sum_\sigma^{(MC)} d\sigma e^{-\beta h(\sigma)} \ , \tag{3.35}$$

with the Gaussian probability weight

$$w_\sigma \propto e^{-\frac{1}{2}\beta|V|\sigma^2} \ . \tag{3.36}$$

The ground state, $|\Phi_g\rangle$, can then be written as

$$|\Phi_g\rangle \sim \sum_{\sigma}^{(MC)} e^{-\beta h(\sigma)}|\Phi_0\rangle \ , \tag{3.37}$$

The above wave function can be used to compute the ground state energy as in the previous section

$$\langle H\rangle = \frac{\langle\Phi_g|H|\Phi_g\rangle}{\langle\Phi_g|\Phi_g\rangle} \sim \frac{\langle\Phi_0|H\sum_\sigma^{(MC)} e^{-\beta h(\sigma)}|\Phi_0\rangle}{\langle\Phi_0|\sum_\sigma^{(MC)} e^{-\beta h(\sigma)}|\Phi_0\rangle}. \tag{3.38}$$

The main idea of QMCD is that $|\Phi_\sigma\rangle$ can be interpreted as a basis vector. Different values of σ generate different state vectors. One can therefore diagonalize the Hamiltonian in a space spanned by those states.

Suppose now that a set of state vectors is available. Then a new vector $|\Phi_\sigma\rangle$ is generated stochastically and added to the set. We diagonalize the Hamiltonian in this enlarged space. If the energy of the ground state is lowered appreciably, the vector is included in the basis. It is discarded otherwise. The iteration proceeds until the energy eigenvalue converges reasonably well.

For more than one eigenstate, one first determines the basis vectors for the lowest eigenstate. Once a reasonable convergence is attained, one can switch to the second lowest eigenstate. Keeping the basis vectors for the lowest eigenstate, one generates other candidates according to their contributions to the second lowest eigenvalue. In diagonalizing the Hamiltonian matrix, one merges the basis vectors for the lowest and those for the second lowest eigenstates, but uses the second eigenvalue for selecting the basis vectors for the second eigenstate. The selection proceeds until a reasonable convergence is reached for the second eigenvalue. By repeating this process, we can obtain higher eigenstates as well.

All the above considerations hold also for a more general Hamiltonian. In this case the ground state is

$$|\Phi_g\rangle = \sum_{\vec{\sigma}} |\Phi_{\vec{\sigma}}\rangle \ , \tag{3.39}$$

where

$$|\Phi(\vec{\sigma}\rangle \propto \prod_{n=1}^{N_t} e^{-\Delta\beta h(\vec{\sigma_n})}|\Phi_0\rangle \ , \tag{3.40}$$

and

$$\vec{\sigma} = \{\vec{\sigma_1}, \vec{\sigma_2}, \ldots, \vec{\sigma_{N_t}}\} \ , \tag{3.41}$$

are a set of random numbers defining the auxiliary fields.

QMCD is basically an importance sampling method which selects stochastically the basis states relevant to the diagonalization of the Hamiltonian. The random sampling selects only important basis vectors obtaining a drastic truncation of the SM space.

On the other hand, the basis states so generated are not orthogonal and form in general a redundant set. Moreover, they do not have the spin as good quantum number. Specific procedures have been developed to obviate at these shortcomings.

3.3.2 Density-Matrix Renormalization Group

The Density Matrix Renormalization Group (DMRG) was originally introduced by White (36) in the attempt to overcome the limitations of Wilson's renormalization group (RG) (37) in describing one-dimensional quantum lattice models. The new method was soon shown to be extremely powerful, producing extremely accurate results for the ground state energy of the Heisenberg S=1 chain.

The idea of RG theories in the context of quantum lattices is to start with a set of lattice sites and then to iteratively add to it subsequent sites until all have been treated. At each iteration, the dimension of the enlarged space increases as the product of the dimension of the initial subspace and that of the added site. The renormalization group procedure consists of reducing the enlarged space to the same dimension as the initial subspace and then transforming all operators to this new truncated basis (renormalization).

The DMRG differs from Wilson RG in the criterion adopted to implement the truncation. While the Wilson RG retains the lowest Hamiltonian eigenstates of the enlarged space, the DMRG uses a very different strategy, consisting in selecting those states with the largest eigenvalues of the reduced density matrix for the enlarged space in the presence of a medium.

The DMRG was recently extended to nuclei and proposed as a tool to large scale shell model calculations (38). Within this approach, one considers a block of m states, for instance a set of single particle and single hole states around the Fermi surface. Few other s states, like the nearby shells, are added forming an enlarge block B. The entire system - enlarged block + medium - is referred to as the superblock.

The Hamiltonian is diagonalized in the superblock, yielding the ground state wave function

$$|\Psi\rangle = \sum_{i=1,m\times s} \sum_{j=1,t} \Psi_{ij} |i\rangle_B |i\rangle_M \ . \tag{3.42}$$

where B denotes the states in the enlarged block, M the states in the medium and t the number of states in the medium.

One is now able to construct the reduced density matrix for the enlarged block in the ground state

$$\rho_{ij}^{(B)} = \sum_{k=1,t} \Psi_{ik}^* \Psi_{jk} \ , \tag{3.43}$$

with i and j running between 1 and $m \times s$. The density matrix is brought to diagonal form

$$\rho^{(B)} |u_\alpha >_B = \omega_\alpha^{(B)} |u_\alpha >_B \ . \tag{3.44}$$

Those eigenstates $|u_\alpha >_B$ with the largest eigenvalues $\omega_\alpha^{(B)}$ are the most important states of the enlarged block in the ground state of the superblock, i.e. of the system. One thus consider only the space spanned by the m states of the enlarged block with the largest density matrix eigenvalues.

The basic idea then is to systematically grow the system block by adding more and more shell to the updated blocks and then at each stage to truncate to the m most important states obtained in this way.

The first SM calculations based on the DMRG adopted an uncoupled m-scheme. This has the drawback that conserving angular momentum symmetry becomes difficult. To avoid this problem the use of an angular-momentum-preserving variant of the DMRG was proposed and applied to medium-mass nuclei with some success (39).

Chapter 4

The APL algorithm

The Lanczos algorithm is widely adopted, and very efficient, in finding the extremal eigenvalues and eigenvectors of the Hamiltonian matrices in nuclear Shell Model calculations. Its implementation, however, has to be treated with particular care, in order to avoid the arising of spurious solutions.

This chapter presents an iterative extremal algorithm, alternative to Lanczos, proposed few years ago (40). The method is stable, and easy to implement. It is also endowed with an importance sampling procedure, which allows an effective truncation of the SM space (41). The algorithm is as general as Lanczos, and can be proficiently used in other fields.

Section 4.1 presents the procedure for generating the lowest eigenstate. The convergence properties of the method are also discussed. Section 4.2 shows how the algorithm can be generalized so as to yield an arbitrary number of eigensolutions. Section 4.3 illustrates the importance sampling which can be coupled with the algorithm.

4.1 One-dimensional eigenspace

Let $\hat{A}$ be a self-adjoint operator. This is represented by a Hermitian matrix $A = \{a_{ij}\}$ in an orthonormal basis $\{| \, 1\rangle, | \, 2\rangle, \ldots, |j\rangle, \ldots, |N\rangle\}$. We assume, for simplicity, that the matrix is symmetric. We first outline the procedure for generating the lowest eigenstate of such a matrix.

4.1.1 The iterative process

The algorithm consists of several iteration loops. The first loop goes through the following steps :

1a) Start with the first two basis vectors and construct and diagonalize the 2×2 matrix

$$A_2^{(1)} \equiv \begin{pmatrix} \lambda_1^{(1)} & a_{12} \\ a_{12} & a_{22} \end{pmatrix}, \tag{4.1}$$

having put $A_1^{(1)} \equiv \lambda_1^{(1)} = a_{11}$.

1b) Extract the lowest eigenvalue $\lambda_2^{(1)}$ and the corresponding eigenvector

$$| \, \lambda_2^{(1)}\rangle = C_{2,1}^{(1)} \, | \, 1\rangle + C_{2,2}^{(1)} \, | \, 2\rangle, \tag{4.2}$$

for $j = 3, \ldots, N$,

1c) select the two vectors $\{|\lambda_{j-1}^{(1)}\rangle, |j\rangle\}$, construct and diagonalize the 2×2 matrix

$$A_j^{(1)} \equiv \begin{pmatrix} \lambda_{j-1}^{(1)} & b_j^{(1)} \\ b_j^{(1)} & a_{jj} \end{pmatrix} , \tag{4.3}$$

where

$$b_j^{(1)} = \langle \lambda_{j-1}^{(1)} \mid \hat{A} \mid j \rangle. \tag{4.4}$$

1d) Extract the lowest eigenvalue $\lambda_j^{(1)}$ and the corresponding eigenvector

$$\mid \lambda_j^{(1)} \rangle = C_{j,(j-1)}^{(1)} \mid \lambda_{j-1}^{(1)} \rangle + C_{j,j}^{(1)} \mid j \rangle, \tag{4.5}$$

end j.

The first loop just outlined yields an approximate eigenvalue and eigenvector

$$\begin{array}{rcl} E^{(1)} & \equiv & \lambda_N^{(1)} \\ \mid \psi^{(1)} \rangle & \equiv & |\lambda_N^{(1)}\rangle = C_{N,N-1}^{(1)} \mid \lambda_{N-1}^{(1)} \rangle + C_{N,N}^{(1)} |N\rangle \\ & = & \sum_{i=1}^{N} C_i^{(1)} \mid i \rangle \end{array} .$$

We now put

$$\lambda_0^{(2)} = \lambda_N^{(1)}, \qquad \mid \lambda_0^{(2)} \rangle = \mid \lambda_N^{(1)} \rangle , \tag{4.6}$$

and use the new *linear dependent* basis

$$\{|\lambda_0^{(2)}\rangle, |1\rangle, \ldots |j\rangle, \ldots |N\rangle\} , \tag{4.7}$$

to start a new iterative procedure. This goes through the following refinement loops:

for $n = 2, 3, \ldots$ till convergence

for $j = 1, 2, \ldots, N$

2a) Compute $b_j^{(n)} = \langle \lambda_{j-1}^{(n)} \mid \hat{A} \mid j \rangle$.

2b) Solve the eigenvalue problem in the generalized form

$$det \left\{ \begin{pmatrix} \lambda_{j-1}^{(n)} & b_j^{(n)} \\ b_j^{(n)} & a_{jj} \end{pmatrix} - \lambda \begin{pmatrix} 1 & C_{j-1,j}^{(n)} \\ C_{j-1,j}^{(n)} & 1 \end{pmatrix} \right\} = 0 .$$

The appearance of the metric matrix is to be noticed. It comes from the non orthogonality of the re-defined basis $\{|\lambda_{j-1}^{n}\rangle, |j\rangle\}$.

2c) Select the eigenvalue $\lambda_j^{(n)}$ and the corresponding eigenvector

$$\mid \lambda_j^{(n)} \rangle = p_j^{(n)} \mid \lambda_{j-1}^{(n)} \rangle + q_j^{(n)} \mid j \rangle , \tag{4.8}$$

with the appropriate normalization condition

$$\langle \lambda_j^{(n)} | \lambda_j^{(n)} \rangle = [p_j^{(n)}]^2 + [q_j^{(n)}]^2 + 2\, p_j^{(n)} q_j^{(n)} C_{j-1,j}^{(n)} = 1 , \tag{4.9}$$

end j

end n.

The n-th loop yields an approximate eigenvalue and eigenvector

$$\begin{array}{rcl} \lambda_N^{(n)} & \equiv & E^{(n)} \equiv \lambda_0^{(n+1)} \\ |\lambda_N^{(n)}\rangle & \equiv & \mid \psi^{(n)} \rangle \equiv |\lambda_0^{(n+1)}\rangle \end{array} .$$

4.1.2 Convergence properties

The iterative method just outlined converges to the extremal eigenvalue and the corresponding eigenvector of the matrix A.

In fact, the eigenvector obtained at the j-th step of the n-th iteration can be expressed in the form

$$|\Phi_j^{(n)}\rangle = p_j^{(n)}|\Phi_{j-1}^{(n)}\rangle + q_j^{(n)}|j\rangle \ , \tag{4.10}$$

where $p_j^{(n)}$ and $q_j^{(n)}$ fulfill the normalization condition

$$[p_j^{(n)}]^2 + [q_j^{(n)}]^2 + 2p_j^{(n)}q_j^{(n)}C_{j-1,j}^{(n)} = 1 \ . \tag{4.11}$$

The explicit form of the factors $p_j^{(n)}$ e $q_j^{(n)}$ is

$$q_j^{(n)} = \frac{|B_j^{(n)}|}{\left[(a_{jj}C_{j-1,j}^{(n)} - b_j^{(n)})^2 + 2C_{j-1,j}^{(n)}(a_{jj}K_{j-1,j}^{(n)} - b_j^{(n)})B_j^{(n)} + (B_j^{(n)})^2\right]^{1/2}} \ , \tag{4.12}$$

$$p_j^{(n)} = (a_{jj}C_{j-1,j}^{(n)} - b_j^{(n)})\frac{q_j^{(n)}}{B_j^{(n)}} \ , \tag{4.13}$$

where

$$B_j^{(n)} = (\lambda_{j-1}^{(n)} - \lambda_j^{(n)}) - C_{j-1,j}^{(n)}\left[(a_{jj} - \lambda_j^{(n)})(\lambda_{j-1}^{(n)} - \lambda_j^{(n)})\right]^{1/2} \ . \tag{4.14}$$

It is apparent from these relations that, if

$$|\ \lambda_{j-1}^{(n)} - \lambda_j^{(n)}\ | \rightarrow \ 0, \quad \forall j, \tag{4.15}$$

the sequence $|\ \psi^{(n)}\rangle$ has a limit $|\ \psi\rangle$, which is an eigenvector of the matrix A.

In fact, defining the residual vectors

$$|\ r^{(n)}\rangle = (\hat{A} - E^{(n)})\ \ |\ \psi^{(n)}\rangle, \tag{4.16}$$

a direct computation gives for their components

$$\begin{aligned} r_l^{(n)} \ &= \ p_N^{(n)}\left[(a_{ll} - \lambda_l^{(n)})(\lambda_{l-1}^{(n)} - \lambda_l^{(n)})\right]^{\frac{1}{2}} + q_N^{(n)}\left\{a_{lN} - \lambda_N^{(n)}\delta_{lN}\right\} \\ &- \ p_N^{(n)}\left\{(\lambda_{l-1}^{(n)} - \lambda_l^{(n)})\ K_{l,l-1}^{(n)} + (\lambda_{N-1}^{(n)} - \lambda_N^{(n)})\ K_{l,N-1}^{(n)}\right\}. \end{aligned} \tag{4.17}$$

In virtue of (4.15), the norm of the n-th residual vector converges to zero, namely $||\ r^{(n)}\ || \rightarrow 0$. Equation (4.15) gives therefore a necessary condition for the convergence of $|\ \psi^{(n)}\rangle$ to an eigenvector $|\ \psi\rangle$ of A, with a corresponding eigenvalue $E = lim\ E^{(n)}$.

Equation (4.15) is not only a necessary but also a sufficient condition for the convergence to the lowest or the highest eigenvalue of A. In fact, the sequence $\lambda_j^{(n)}$ is monotonic (decreasing or increasing, respectively), bounded from below or from above by the trace and therefore convergent.

The algorithm turns out to have a variational foundation. As one can easily verify by direct substitution, the derivative with respect to $\alpha_j^{(n)}(= q_j^{(n)}/p_j^{(n)})$ of the Rayleigh coefficient

$$\rho(\Phi_j^{(n)}) = \frac{\langle\Phi_j^{(n)}|\widehat{A}|\Phi_j^{(n)}\rangle}{\langle\Phi_j^{(n)}|\Phi_j^{(n)}\rangle} \ , \tag{4.18}$$

vanishes in correspondence of the the values 4.12 and 4.13 of $p_j^{(n)}$ and $q_j^{(n)}$. The algorithm is therefore equivalent to the optimal relaxation method (42). Being however formulated in terms of matrices, it can be generalized so as to produce a number of eigensolutions larger than one.

4.2 General method

4.2.1 Multi-dimensional eigenspace

We proceed just as in the one-dimensional case. Indeed, the first loop goes through the following steps:

1a) Start with $m(\geq v)$ basis vectors, construct and diagonalize the m-dimensional principal submatrix

$$A_1^{(1)} = \begin{pmatrix} a_{11} & a_{12} & \cdots & a_{1m} \\ \vdots & \vdots & \cdots & \vdots \\ \vdots & \vdots & \cdots & \vdots \\ a_{m1} & a_{m2} & \cdots & a_{mm} \end{pmatrix} , \tag{4.19}$$

1b) select the v lowest eigenvalues and corresponding eigenvectors

$$\begin{aligned} \Lambda_1^{(1)} &\equiv \{\lambda_1^{(1)}(1), \lambda_1^{(1)}(2), \ldots, \lambda_1^{(1)}(v)\} \\ \mid \Lambda_1^{(1)}\rangle &\equiv \{\mid \lambda_1^{(1)}(1)\rangle, \mid \lambda_1^{(1)}(2)\rangle, \ldots, \mid \lambda_1^{(1)}(v)\rangle\} \end{aligned} ,$$

for $k = 2, 3, \ldots, k_N$, where k_N are the steps necessary to exhaust the whole N-dimensional matrix,

1c) construct and diagonalize the matrix

$$A_k^{(1)} = \begin{pmatrix} \Lambda_{k-1}^{(1)} & B_k^{(1)} \\ B_k^{(1)}(T) & A_k^{(1)}(C) \end{pmatrix} , \tag{4.20}$$

where $\Lambda_k^{(1)}$ is a v-dimensional diagonal matrix

$$\Lambda_{k-1}^{(1)} = \begin{pmatrix} \lambda_{k-1}^{(1)}(1) & 0 & \ldots & 0 \\ 0 & \lambda_{k-1}^{(1)}(2) & \ldots & 0 \\ 0 & \ldots & \ldots & 0 \\ 0 & \ldots & 0 & \lambda_{k-1}^{(1)}(v) \end{pmatrix} , \tag{4.21}$$

and

$$A_k^{(1)}(C) = \{a_{ij}\} \quad (i, j = (k-1)p + 1, \ldots, kp) , \tag{4.22}$$

is a p-dimensional submatrix. The two submatrices are coupled by $B_k^{(1)}$ and its transpose, whose matrix elements are

$$b_{ij}^{(k)} = \langle \lambda_{(k-1)}^{(1)}(i) \mid \hat{A} \mid j\rangle , \tag{4.23}$$

where $i = 1, \ldots, v$; $j = (k-1)p + 1, \ldots, kp$,

1d) select the v lowest eigenvalues and corresponding eigenvectors

$$\begin{aligned} \Lambda_k^{(1)} &\equiv \{\lambda_k^{(1)}(1), \lambda_k^{(1)}(2), \ldots, \lambda_k^{(1)}(v)\} \\ \mid \Lambda_k^{(1)}\rangle &\equiv \{\mid \lambda_k^{(1)}(1)\rangle, \mid \lambda_k^{(1)}(2)\rangle, \ldots, \mid \lambda_k^{(1)}(v)\rangle\} \end{aligned} ,$$

end k

The first loop yields the v approximate eigenvalues and eigenvectors

$$\begin{array}{rcl} \Lambda_{k_N}^{(1)} & \equiv & \Lambda_0^{(2)} \equiv \{\lambda_{k_N}^{(1)}(1), \lambda_{k_N}^{(1)}(2), \ldots, \lambda_{k_N}^{(1)}(v)\} \\ \mid \Lambda_{k_N}^{(1)}\rangle & \equiv & \mid \Lambda_0^{(2)}\rangle \equiv \{\mid \lambda_{k_N}^{(1)}(1)\rangle, \mid \lambda_{k_N}^{(1)}(2)\rangle, \ldots, \mid \lambda_{k_N}^{(1)}(v)\rangle\} \end{array} .$$

Now the linearly dependent basis states $\mid \{\Lambda_0^{(2)}\rangle, |1\rangle, \ldots |N\rangle\}$ are the new entries for a new iteration loop.

This goes through the same steps as in the one-dimensional eigenspace with one essential modification. Each loop, in fact, can be viewed as the solution of the eigenproblem for the restriction $\hat{A}|_S$ of the operator $\hat{A}$ to a subspace defined by the span of the set of vectors $\mid i_p\rangle \equiv \{|\lambda_k^{(i)}(1)\rangle, \ldots, |\lambda_k^{(i)}(v)\rangle, \mid (k-1)p+1\rangle, \ldots, \mid kp\rangle\}$. Since this basis is no longer orthonormal, just as in the one-dimensional eigenspace, and may be even redundant, we have to solve an eigenvalue problem of general form. This is done most effectively through a Cholesky decomposition of the overlap matrix $\langle i_p \mid i'_p\rangle$.

With this modifications, the iteration loops proceed as the first one, generating a sequence of v vectors $\psi_1^{(i)}, \ldots, \psi_v^{(i)}$. The restriction of the operator $\hat{A}$ to these sets defines a sequence of diagonal matrices, whose non zero elements are the current eigenvalues $\lambda_1^{(i)}, \ldots, \lambda_v^{(i)}$. This monotonic sequence is certainly bounded from below and therefore convergent.

As proved and illustrated through typical numerical tests (40), the algorithm is robust, being numerically stable and converging always to the extremal eigenvalues. It yields ghost-free solutions and is also of easy implementation.

The efficiency and the convergence rate of the iterative procedure have been tested applying the methods to a five-point finite difference matrix arising from the two-dimensional Laplace equation (40), in terms of the norm of the residual vector at the n-th iteration, $||r^{(n)}||$. As shown in figure 4.1, the iterative procedure converges much faster in the multidimensional case. In fact, the convergence rate increases with the number ν of generated eigenvalues. In terms of number of iteration to reach the convergence, the algorithm is faster than Lanczos.

The speed of each iteration has now to be evaluated. This aspect is illustrated with more details in the next chapter. It is shown that the leading term, when dealing with the number of operations needed for each iteration, is the computation of the matrix element

$$b_{kj}^{(n-1)} = \langle \lambda_k^{(n-1)} \mid \hat{A} \mid j\rangle \ \ (k = 1, v) ,$$

which reduces to a row-by-column product, exactly as in the Lanczos method. In general, this procedure goes like O(N^2), but reduces to O(N) when handling sparse matrices.

The actual speed of a SM code, however, arises from the interaction of several factors. The machine, the implementation and the matrix elements computation are some of the critical points of the calculation. The algorithm proposed here is theoretically very fast, but there are still several improvements to do, in order to pass beyond the performances of the codes available nowadays .

4.3 Importance sampling

The importance sampling is naturally suggested by the structure of the algorithm. It goes through the following steps:

1a) Turn the m-dimensional principal submatrix $\{a_{ij}\}$ into diagonal and select the lowest ν eigenvalues $\lambda_1, \lambda_2, \ldots, \lambda_v$.

for $j = m+1, \ldots, N$

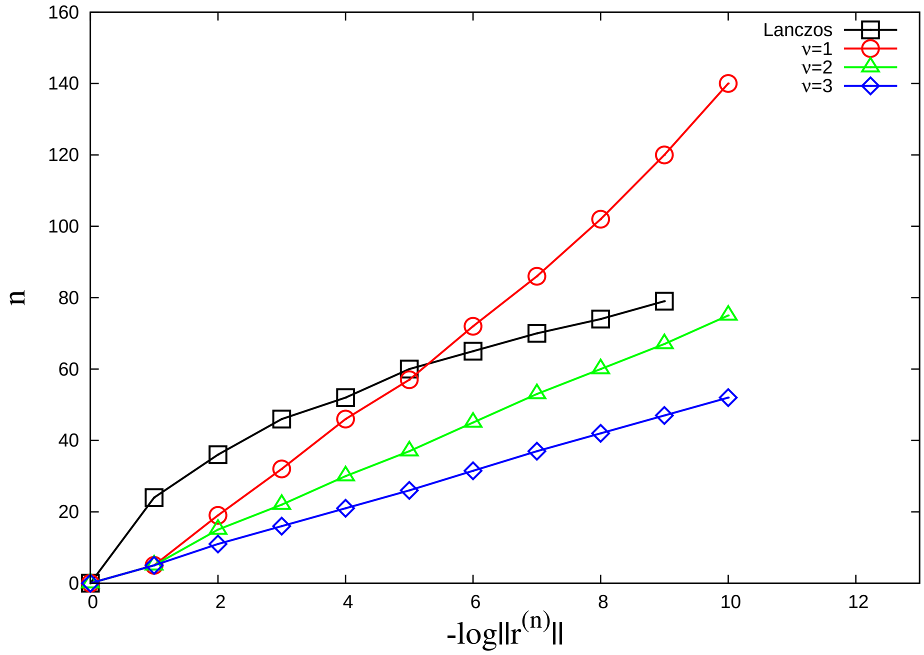

Figure 4.1: Convergence rate, in terms of the norm of the residual vector at the n-th iteration, of the algorithm applied to a finite difference matrix deduced from Laplace equation, for different numbers ν of generated eigenvalues (taken from (40)).

1b) diagonalize the $v+1$-dimensional matrix

$$A = \begin{pmatrix} \Lambda_v & \vec{b}_j \\ \vec{b}_j^T & a_{jj} \end{pmatrix} , \tag{4.24}$$

where $\vec{b}_j = \{b_{1j}, b_{2j}, \cdot, b_{vj}\}$.

1c) Select the lowest v eigenvalues $\lambda'_i, (i = 1, v)$ and accept the new state only if

$$\sum_{i=1,v} \mid \lambda'_i - \lambda_i \mid > \epsilon \ , \tag{4.25}$$

where ϵ is a positive number which can be chosen arbitrarily small. If the above condition is not fulfilled, the state is discarded and one restart from point 1b) with a new j.

end j

An equivalent, less time consuming sampling procedure is based on the method developed for deriving an exact non perturbative shell model Hamiltonian (9). The starting point is the similarity transformation

$$A' = \Omega^{-1} A \Omega \ , \tag{4.26}$$

where

$$\Omega = \begin{pmatrix} I_v & 0 \\ \vec{\omega} & I_Q \end{pmatrix} \ . \tag{4.27}$$

Here, I_v is the v-dimensional unit matrix and ω a v-dimensional vector. The transformed matrix has the following structure

$$A' = \begin{pmatrix} \Lambda_v + \vec{b}_j \otimes \vec{\omega} & \vec{b}_j \\ \vec{b}'_j & a_{jj} - \vec{\omega} \cdot \vec{b}_j \end{pmatrix} \ , \tag{4.28}$$

where

$$\vec{b}'_j = -(\vec{\omega} \cdot \vec{b}_j)\vec{\omega} - \vec{\omega}\Lambda_v + a_{jj}\vec{\omega} + \vec{b}^T_j \ . \tag{4.29}$$

One now imposes the decoupling condition

$$\vec{b}'_j = -(\vec{\omega} \cdot \vec{b}_j)\vec{\omega} - \vec{\omega}\Lambda_v + a_{jj}\vec{\omega} + \vec{b}^T_j = 0 \ . \tag{4.30}$$

Once the solution ω is obtained, the matrix element $a_{jj} - \vec{\omega} \cdot \vec{b}_j$ becomes an eigenvalue of the matrix A' and, therefore, of matrix A. Right multiplying Eq. (4.30) by $\vec{b}_j$, one obtains the dispersion relation

$$\vec{\omega} \cdot \vec{b}_j = -\sum_{i=1,v} \frac{b^2_{ij}}{a_{jj} - \lambda_i - \vec{\omega} \cdot \vec{b}_j} \ . \tag{4.31}$$

This admits $v+1$ solutions, corresponding to the $v+1$ eigenvalues of A. In correspondence of the lowest solution $(\vec{\omega} \cdot \vec{b}_j)_{min}$, we get the maximum eigenvalue

$$\lambda'_{max} = a_{jj} - (\vec{\omega} \cdot \vec{b}_j)_{min} \ . \tag{4.32}$$

The eigenvalues $\lambda_i \ , \ i = 1, \ldots, v$ separate at least in a weak sense the new eigenvalues $\lambda'_i \ , \ i = 1, \ldots, v+1$, namely

$$\lambda'_1 \leq \lambda_1 \leq \lambda'_2 \leq \lambda_2 \leq \ldots \leq \lambda'_v \leq \lambda_v \leq \lambda'_{max} \ . \tag{4.33}$$

Since

$$\sum_{i=1,v+1} \lambda'_i = \sum_{i=1,v} \lambda'_i + a_{jj} - (\vec{\omega} \cdot \vec{b}_j)_{min} = a_{jj} + \sum_{i=1,v} \lambda_i \ , \tag{4.34}$$

one has

$$\sum_{i=1,v} (\lambda'_i - \lambda_i) = (\vec{\omega} \cdot \vec{b}_j)_{min} \ . \tag{4.35}$$

The condition (4.25) is therefore equivalent to

$$(\vec{\omega} \cdot \vec{b}_j)_{min} > \epsilon \ . \tag{4.36}$$

The just outlined sampling procedure requires only the solution of the dispersion equation (4.31), which is of the type

$$f(z) = z \ , \tag{4.37}$$

and fulfills the condition

$$1 - df(z)/dz > 0 \ . \tag{4.38}$$

One can therefore easily solve it by using the Newton method of derivative. This alternative sampling procedure is not only rigorous but also more economical. It avoids, in fact, the $(N-v)-$fold iterated diagonalization of $v+1$ dimensional matrices.

An even simpler sampling is obtained by the perturbative criterion

$$\Delta\lambda_i = |\lambda'_i - \lambda_i| = \frac{b^2_j}{a_{jj} - \lambda_i} \ . \tag{4.39}$$

This last relation is of great relevance to the implementation of the importance sampling algorithm in the uncoupled m-scheme.

Chapter 5

Implementation of the algorithm in the m-scheme

As pointed out in Chapter 3, in going from the $j-j$ coupling to the unprojected m-scheme, the dimensions of the SM Hamiltonian matrix become soon very large. Thus, the implementation of the algorithm in such an uncoupled basis requires special care.

Let us consider a nucleus having n_π and n_ν valence protons and neutrons, respectively. The basis states are the eigenstates of the unperturbed Hamiltonian, H_0, and are denoted by

$$|i\rangle = |\alpha_{1_\pi} \ , \ \dots \ \alpha_{i_\pi} \ , \ \dots \ , \alpha_{n_\pi}\rangle|\alpha_{1_\nu} \ , \ \dots \alpha_{i_\nu} \ , \ \dots \ , \ \alpha_{n_\nu}\rangle \ , \tag{5.1}$$

where $\alpha_i = a_i m_i$ and $a_i = \{n_i l_i j_i\}$ are the quantum numbers of a particle in a shell . In the m-scheme, these states are classified according to their total magnetic quantum number

$$M = M_\pi + M_\nu \ , \tag{5.2}$$

where $M_\tau = m_{1_\tau} + \dots m_{i_\tau} + \dots m_{n_\tau}$.

In order to obtain an effective projection of the total angular momentum, it is convenient to adopt the modified Hamiltonian

$$H_J = H + c\left[\mathbf{J}^2 - J(J+1)\right]^2 \ , \tag{5.3}$$

where $\mathbf{J}$ is the total spin operator, J a given integer (or half-integer), and c a positive constant.

The structure of the Hamiltonian suggests to decompose the full space into several subspaces

$$\mathcal{H} = \mathcal{H}_0 \oplus \mathcal{H}_1 \cdots \oplus \mathcal{H}_k \cdots \oplus \mathcal{H}_F \ . \tag{5.4}$$

Each subspace $\mathcal{H}_k$ is composed of a set of partitions $\{n_i\}_k = \{a_1^{n_1} \ , \ \dots \ , \ a_i^{n_i} \ , \ \dots\}_k$, where $\sum_i n_i = p$. It is clearly invariant with respect to the total angular momentum operator, $\mathbf{J}$. The partitions in $\mathcal{H}_k$ differ from those in $\mathcal{H}_{k-1}$ by at most two single particle shells a_i. Given this particular structure, we can apply the APL algorithm in the following simplified manner.

We first diagonalize the Hamiltonian H_J in $\mathcal{H}_0$ obtaining v lowest eigenvalues $E_1^{(0)} \ , \ \dots \ , \ E_v^{(0)}$ and eigenvectors $\psi_1^{(0)} \ , \ \dots \ , \ \psi_v^{(0)}$ spanning a subspace Λ_0. These eigensolutions are exact in this subspace and have all the same spin J if the constant c is chosen so as to push the states with $J' \neq J$ up in energy.

Because of its two-body nature, the Hamiltonian couples the subspace Λ_0 to $\mathcal{H}_1$ only. It is, therefore, sufficient to diagonalize H_J in the subspace $\Lambda_0 \oplus \mathcal{H}_1$ to generate new updated eigenvalues $E_1^{(1)} \ , \ \dots \ , \ E_v^{(1)}$ and eigenvectors $\psi_1^{(1)} \ , \ \dots \ , \ \psi_v^{(1)}$, defining the subspace Λ_1 .

We proceed iteratively. Once the updated eigensolutions defining the subspace Λ_k are obtained, we diagonalize the Hamiltonian in the upgraded subspace $\Lambda_k \oplus \mathcal{H}_{k+1}$. We cover eventually the full space obtaining the exact v eigensolutions $\{E_i \ , \ \psi_i\}$.

A possible sketch of the iterative procedure is

$$\mathcal{H}_0 \Rightarrow \Lambda_0 \rightarrow \Lambda_0 \oplus \mathcal{H}_1 \Rightarrow \Lambda_1 \rightarrow \dots \Lambda_{k-1} \oplus \mathcal{H}_k \Rightarrow \Lambda_k \rightarrow \dots \Lambda_{F-1} \oplus \mathcal{H}_F \Rightarrow \Lambda_F \tag{5.5}$$

5.1 Numerical procedure

In order to be able to face the diagonalization of very large matrices as required in large scale shell model calculation, it is necessary to optimize the iterative process by reducing maximally the number of operations required at each iteration.

To this purpose, we observe that, at each k step, we need to construct and diagonalize a matrix

$$A = \begin{pmatrix} \Lambda_k & B_k \\ B_k^T & A_k \end{pmatrix} , \tag{5.6}$$

where Λ_k is a diagonal matrix, bearing on its diagonal the eigenvalues $\lambda_i^{(k-1)}$ of the previous step, B_k is a rectangular $\nu \times p$ block, whose matrix elements are given by $b_{ij} = \langle \Phi_i^{(k-1)} | \widehat{A} | j \rangle$, and A_k a square $p \times p$ matrix $a_{ij} = \langle i | \widehat{A} | j \rangle$.

There are, therefore, three time-consuming operations : calculating the block B, and diagonalizing the matrix and updating the eigenvectors,

$$|\Psi_i^{(k)}\rangle = \sum_{j=1}^{\nu} C_{ij}^{(k)} |\Psi_j^{(k-1)}\rangle + \sum_{m=1}^{p} D_{im}^{(k)} |m\rangle . \tag{5.7}$$

This can be written in the compact matrix form

$$\hat{\Psi}^{(k)} = \hat{C}^{(k)} \hat{\Psi}^{(k-1)} + \hat{D}^{(k)} \mathbf{m} . \tag{5.8}$$

The best known algorithm for finding all the eigenvalues and eigenvectors of an Hermitian matrix is due to Francis , (43) and (44), and is based on the QR decomposition, as discussed in appendix A. The number of operations required by the Francis's algorithm for a complete diagonalization increases as N^3. If p is the length of the iteration step, the matrix to diagonalize is $p + \nu$ dimensional, and the number of operations required for each iteration increases as $O((p + \nu)^3) \cdot (N/p)$. In order to have a linear dependence with N the length of the iteration step is to be chosen small. If it is taken of the order of hundreds, one gets approximately $O((p + \nu)^3) \cdot (N/p) \simeq O(p^2 N)$. The time needed to compute 5, 20, or even 30 extremal eigenvalues, is then comparable. This feature is particularly interesting for applications in low-energy nuclear spectroscopy.

On the other hand, in reducing the length of the iteration step, and then the time used for diagonalizing the corresponding matrix, the number of operations needed to update the eigenvectors increases. In fact, since at each step the cost for updating the eigenstate goes like $(N + p)$ for each vector, the total number is $(N + p) \cdot (N/p)$, which would be linear with N only diagonalizing the whole matrix ($p = N$) at once.

The issue can be solved by implementing the following procedure. In the one dimensional case, let us write

$$\Psi^{(k)} = C^{(k)} \Psi^{(k-1)} + \sum_{m=1}^{p} D_m^{(k)} |m\rangle = \left(\prod_{l=1}^{k} C^{(l)} \right) \left(\Psi^{(0)} + \sum_{m=1}^{p} \frac{D_m^{(k)}}{\prod_{l=1}^{k} C^{(l)}} |m\rangle \right) . \tag{5.9}$$

We can then retain the structure of the eigenvector, by storing separately the components $C^{(k)}$ of the previous vectors, $\Psi^{(0)}$, on the whole base, and the components of the new vectors, $\Psi^{(k)}$, on the p basis states normalized to $C^{(k)}$. The number of operations is then reduced to $2p + 1$ for each step, that is to $N \cdot (2p + 1)/p \simeq 2N$ in total.

This procedure can be straightforward extended to the general case. Recalling (5.7), the eigenvectors structure can be preserved by defining the $\nu \times \nu$ matrix $\hat{K}^{(k)} = \hat{C}^{(k)} \hat{K}^{(k-1)}$, and writing

$$\hat{\Psi}^{(k)} = \hat{K}^{(k)} \left(\hat{\Psi}^{(0)} + [\hat{K}^{(k)}]^{-1} \hat{D}^{(k)} \mathbf{m} \right) . \tag{5.10}$$

The matrix defined above is non-singular because it is linked to the convergence. In fact, as the $|\Psi_i\rangle$ vectors approach the matrix eigenvectors, $\hat{K}^{(k)}$ goes to the identity. The updating of the eigenvectors in the form (5.10) requires a smaller computation time.

We need, therefore, ν^3 operations for the matrix multiplication $\hat{K}^{(k)}\hat{D}^{(k-1)}$, $O(\nu^3)$ for the inversion of $\hat{D}^{(k)}$, and $p \cdot \nu^2$ for the product $[\hat{D}^{(k)}]^{-1}\hat{C}^{(k)}$. We have also to perform $p \cdot \nu$ sums. This means that the total number of operations is linear in N.

The last term to evaluate is the computation of the matrix elements b_{ij} of the non diagonal block B. This is in fact a matrix-by-vector product, for each of the ν solutions, and requires $O(N^2)$ operations. Dealing with sparse matrices, as in m-scheme SM, the number of operations scales to $b \cdot N$, where b is the sparsity of the matrix. This is again the dominant term, allowing the method to produce a very large number of eigensolutions without significant variation in the computation time.

Once the number of operations needed for one iteration of the algorithm has been estimated, one can try a first direct comparison with other extremal diagonalization methods. The Lanczos algorithm, and eventually its Arnoldi's generalization to Hermitian matrices, is considered a benchmark in the field .

A complete comparison would require not only an evaluation of the convergence properties. This kind of study is much more complicated from a mathematical point of view, and is still at a preliminary stage. A comparison of this kind has been attempted in the original work (40). The results seems to put the two methods on equal footing.

Strictly speaking, in terms of operation number our approach should be equivalent to that named after Lanczos. Of course, implementation plays a key role at this point, and the experience in the field has consequently its own weight. Another aspect is the parallelization of the related code, which has still to be attempted.

5.2 Importance sampling

The following step consists in searching for a reliable way of cutting the basis. This can be done by adapting the sampling procedure to the m-scheme. Let us fix a sequence of positive small numbers of decreasing values $\epsilon_1 > \cdots > \epsilon_k > \cdots > \epsilon_F$. Having generated the lowest ν eigenvectors Ψ_1 , ... , Ψ_ν in H_0 , we proceed as in the exact case, using the same scheme of 5.5 with one constraint. In going from $\mathcal{H}_{k-1}$ to $\mathcal{H}_k$, we pick up only the basis states $|j\rangle$ that fulfill the condition

$$\frac{|\langle j|H_J|\psi_i^{k-1}\rangle|^2}{a_{jj} - E_i^{k-1}} > \epsilon_k \ . \tag{5.11}$$

More specifically, in the first step ($k = 1$), the above condition selects a set of states $\{|j\rangle\}$ forming a subspace $\mathcal{H}_1(\epsilon_1) \in \mathcal{H}_1$. The eigenvalue problem is thus solved in $\Lambda_0 \oplus \mathcal{H}_1(\epsilon_1)$ yielding ν new eigensolutions $\{E_k^{(1)}(\epsilon_1)\ ,\ \psi_k^{(1)}(\epsilon_1)\}$ defining the subspace $\Lambda_1(\epsilon_1)$. We now explore the full subspace complementary to $\mathcal{H}_0 \oplus \mathcal{H}_1(\epsilon_1)$ and select all the states $|j\rangle$ that fulfill the condition 5.11 with ϵ_2 replacing ϵ_1. The states so selected span a subspace $\mathcal{H}_2(\epsilon_2) \in \mathcal{H}_1 \oplus \mathcal{H}_2$. The above procedure is iterated with updated eigensolutions and decreasing sampling values ϵ_k until the full space is covered.

A sketch of the sampling procedure is provided by the following sequence

$$\begin{array}{llll} \mathcal{H}_0 \Rightarrow \Lambda_0 & \stackrel{\epsilon_1}{\rightarrow} & \Lambda_0 \oplus \mathcal{H}_1(\epsilon_1) \Rightarrow \Lambda_1(\epsilon_1) & \stackrel{\epsilon_2}{\rightarrow} \ \ldots \\ \quad\ldots & \stackrel{\epsilon_F}{\rightarrow} & \Lambda_{F-1}(\epsilon_{F-1}) \oplus \mathcal{H}_F(\epsilon_F) \Rightarrow \Lambda_F(\epsilon_F) & \end{array} \ . \tag{5.12}$$

In the limit $\epsilon_F \rightarrow 0$, the exact solution is recovered, namely $\lim_{\epsilon_F\rightarrow 0} \Lambda_F(\epsilon_F) = \Lambda_F$, or, more explicitly,

$$\lim_{\epsilon_F \rightarrow 0} \{E_i(\epsilon_F)\ ,\ \psi_i(\epsilon_F)\} = \{E_i\ ,\ \psi_i\}\ , \tag{5.13}$$

where $\{E_i \ , \ \psi_i\}$ indicates the exact eigenvalues and eigenvectors. The sampling procedure is as stable as the algorithm. It yields, indeed, orthonormal eigenfunctions. These are obtained, at each step, by the diagonalization of a symmetric submatrix. The subspaces selected by the sampling are not strictly invariant with respect to J. The invariance, however, is restored as the sampling value ϵ becomes sufficiently small. In fact, all sampled eigenstates reach soon a good J.

The just outlined sampling process reminds of the Density Matrix Renormalization Group. As in the DMRG, our sampling goes through enlarging, immersing and truncating. On the other hand, it is more straightforward and is based on updating both energies and wavefunctions.

Chapter 6

Numerical applications: Large scale SM calculations

We will show in this chapter how the method can be applied for large scale SM calculations in medium-heavy nuclei. We will consider semimagic as well as neutron-proton open shell nuclei.

More specifically we will perform full shell model calculations for the semimagic ^{116}Sn and for a set of heavy Xe isotopes in the vicinity of the $N = 132$ shell closure. In both cases, we will adopt a model space defined by the valence nucleons within the $N = 4$ major shell, without the g9/2 shell and with the intruder state h11/2, and use a G matrix with core polarization derived from the CD-Bonn NN potential (19).

^{116}Sn, having $N_\nu = 16$ valence neutrons, is certainly the most challenging among the stable semimagic nuclei.

Concerning the Xe isotopes we will start with ^{134}Xe and end up with ^{130}Xe (45; 46). This nucleus is close to the borderlines of the possibilities of the available codes. In fact, to our knowledge, ours is the first large scale SM calculation in nuclei, like ^{132}Xe and ^{130}Xe, which depart from $N = 132$ shell closure.

We will test the convergence rate of the iterative sampling process by investigating both energy eigenvalues and $E2$ transitions. We will then present the spectra of all mentioned nuclei. It will be clear from a glance at these spectra that the method can produce a large number of levels for each angular momentum.

We will investigate also the $E2$ and $M1$ transitions and use them as a tool for determining the symmetry of the low-lying states in Xe isotopes with respect to the exchange of protons with neutrons, with special attention at the so called mixed symmetry (MS) states predicted in the interacting boson model (IBM) and discovered only a decade ago.

6.1 SM study of ^{116}Sn

In Sn isotopes, only valence neutrons come into play. They are confined within the valence space, made up of the $N = 4$ major shell, without the g9/2 state and with the intruder level h11/2. Since we are dealing with identical particles, the number of configurations to take into account is relatively small even though the sparsity of the Hamiltonian matrix is modest. In fact, in the most general case in which the overall magnetic quantum number of the SM basis states is $M = 0$, the largest configuration space in ^{116}Sn is composed of $n \simeq 1.6 \cdot 10^7$ Slater determinants.

We used the single particle energies shown in table 6.1 and borrowed from Ref.(47). As already mentioned, a G matrix derived from the CD-Bonn potential and renormalized by the coupling with the core excitations was used as effective potential. The $E2$ transition strengths were computed using the proton and neutron effective charges $e_p = 1.5$ and $e_n = 1$.

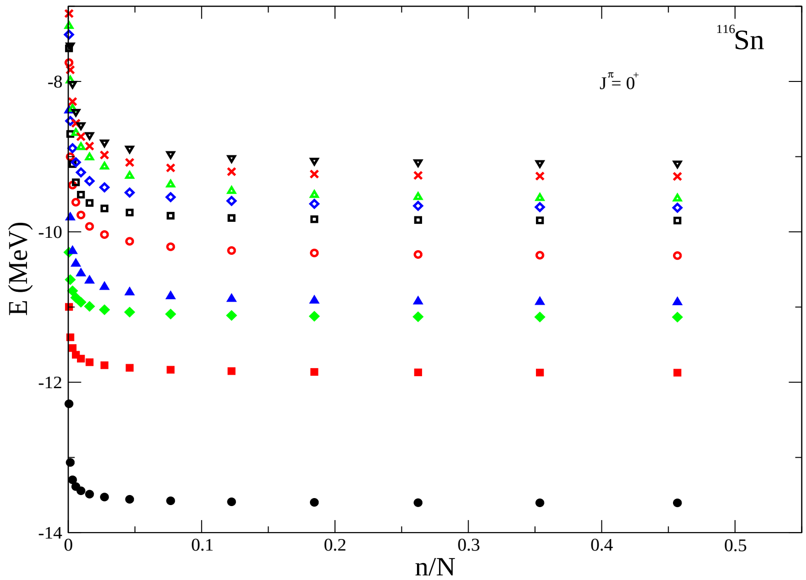

Figure 6.1: Energy behavior of the lowest $J = 0^+$ states in ^{116}Sn, plotted against the percentage of sampled states, n/N.

$(\mathrm{nlj})_\nu$	1d5/2	0g7/2	2s1/2	1d3/2	0h11/2
ϵ	0.00	0.08	2.45	2.55	3.20

Table 6.1: Neutron single particle energies (in MeV)

The preliminary step of the iterative process consists in choosing a possibly small subspace in order generate the first set of eigensolutions. An initial subspace $\mathcal{H}_0$ of dimensions $n_0 \simeq 50$ was sufficient to generate ten lowest eigenstates with good J. Once chosen $\mathcal{H}_0$, the iterative sampling procedure is applied using a sequence of decreasing ϵ values. The lowest $J = 0^+$ and $J = 2^+$ energy eigenvalues are plotted versus the fraction n/N of the basis states in Figs 6.1 and 6.2, respectively. It is seen that all the eigenvalues approach closely the exact values for less than 10% of the basis states.

Fig.6.3 shows that a rapid convergence is achieved also for the reduced probabilities of the $E2$ transitions between the lowest $J^\pi = 2^+$ and $J^\pi = 0^+$ states. The behavior of the $B(E2)$'s suggest a smooth behavior and a rapid convergence of the wave function, consistently with what was proved in Ref. (41).

The smooth convergence of both energies and strengths versus n/N makes highly reliable an extrapolation of the sequence of the physical observables produced by the iterative procedure to their exact values, even when the Hamiltonian matrix its too large and is beyond the capabilities of the method.

The calculated versus the experimental low-energy spectra of ^{116}Sn are shown in Fig.6.4. The agreement between SM and experimental levels is good, even if no effort was spent to reproduce the experimental data, apart from a proper choice of the single particle energies. In particular, there was no need of monopole corrections to the single particle energies, as commonly done in other approaches for several lighter nuclei (48).

The calculated spectrum is seen to be as rich as the experimental one. This result has been achieved without any special computational effort. Indeed, the algorithm would allow to generate many more states for each J^π.

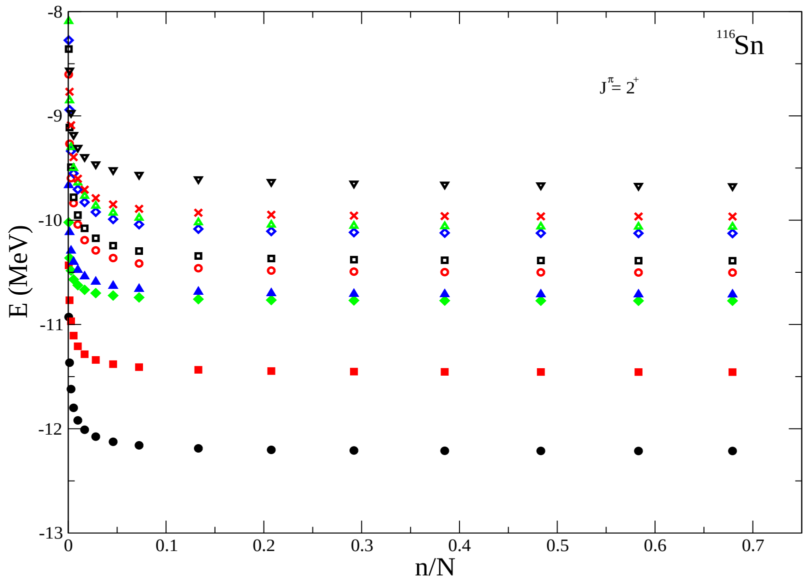

Figure 6.2: Energy behavior of the lowest $J = 2^+$ states in ^{116}Sn.

6.2 Study of Heavy Xenon isotopes

More challenging is the application of the method to proton-neutron open shell nuclei. In fact, if both valence protons and neutrons are to be taken into account, not only the implementing procedure becomes more involved but the dimensions of the Hamiltonian matrix grow rapidly with the number of nucleons.

Heavy Xe isotopes are taken here as ground test. We will see that the good convergence of the iterative procedure is confirmed also in this general case (45). Moreover, the spectra and electromagnetic strengths produced are in good agreement with experiments. Such a consistency allows us to investigate the microscopic structure of the low-lying states, especially in relation to their proton-neutron symmetry (46).

In fact, the reason why we focus our attention on Xe isotopes was dictated by the extensive experimental investigations carried out on these isotopes (49; 50; 51). Those studies focused mainly on the evolution with the number of valence neutrons of the so called mixed-symmetry (MS) states, whose existence was predicted within the IBM (52; 53; 54).

6.2.1 Symmetric and mixed symmetry states in the IBM

In the IBM, the low-energy properties are ascribed uniquely to correlations among proton and neutron pairs coupled to $L = 0$ and $L = 2$. These pairs are described as s and d bosons respectively. In the original formulation, the one dubbed IBM, no distinction is made between protons and neutrons. The states are therefore fully symmetric with respect to exchange of the boson operators.

In the IBM-2 proton and neutron bosons are distinct. New states therefore emerge. We can have, in fact, completely symmetric as well as mixed symmetry states with respect to the exchange of proton with neutron pairs.

For a quantitative description it is useful to introduce the F-spin quantum number, which is the boson counterpart of isospin. Proton and neutron bosons form a F-spin doublet with $F_3 = 1/2$ for protons and $F_3 = -1/2$ for neutrons. States with maximum F-spin, $F = F_{max}$, are completely symmetric with respect to proton-neutron exchange. The other states with $F < F_{max}$ have mixed symmetry (MS). Only MS states with $F = F_{max} - 1$ have been observed

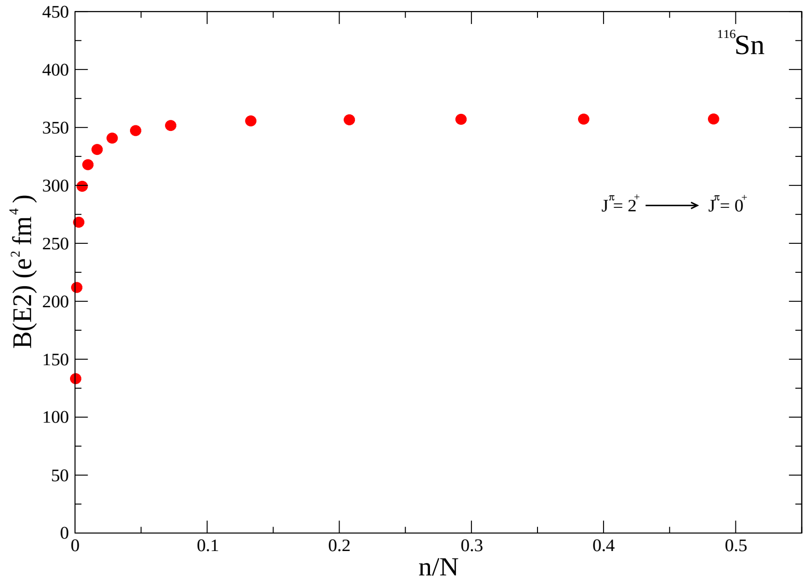

Figure 6.3: Reduced transition probabilities between the lowest $J = 2^+$ and $J = 0^+$ states in ^{116}Sn.

so far.

A clear picture of the structure of the IBM-2 states is gained in the so called Q-phonon scheme. We can define the one-boson symmetric and MS states as

$$\begin{array}{rcl} |2_S^+\rangle & \propto & Q_S|0_1^+\rangle \\ |2_m^+\rangle & \propto & Q_m|0_1^+\rangle \end{array} , \tag{6.1}$$

where $|0_1^+\rangle$ is a correlated ground state and

$$\begin{array}{rcl} Q_S & = & Q_\pi + Q_\nu \\ Q_m & = & Q_\pi - Q_\nu \end{array} , \tag{6.2}$$

are respectively the proton-neutron symmetric (F-scalar) and antisymmetric (F-vector) components of the boson quadrupole operator. Out of these operators we can construct two-boson symmetric and MS states

$$\begin{array}{rcl} |J_S^+\rangle & \propto & [Q_S \times Q_S]^J\,|0_1^+\rangle \\ |J_m^+\rangle & \propto & [Q_m \times Q_S]^J\,|0_1^+\rangle \end{array} , \tag{6.3}$$

The IBM $E2$ operator is composed of a sum of F-scalar and F-vector components

$$T(E2) = e_\pi Q_\pi + e_\nu Q_\nu = e_S Q_S + e_m Q_m \ , \tag{6.4}$$

where Q_S and Q_m are given by 6.2 and the charges are $e_S = (e_\pi + e_\nu)/2$ and $e_m = (e_\pi - e_\nu)/2$.

The $M1$ operator has a similar structure

$$T(M1) = g_\pi L_\pi + g_\nu L_\nu = g_S L_S + g_m L_m \ , \tag{6.5}$$

where

$$\begin{array}{rcl} L_S & = & L_\pi + L_\nu \\ L_m & = & L_\pi - L_\nu \end{array} , \tag{6.6}$$

and $g_S = (g_\pi + g_\nu)/2$ and $g_m = (g_\pi - g_\nu)/2$.

Strong F-scalar $E2$ transitions occur between states of the same proton-neutron symmetry and differing by one d bosons. The F-vector $E2$ operator couples weakly mixed symmetry to symmetric states differing by one d boson.

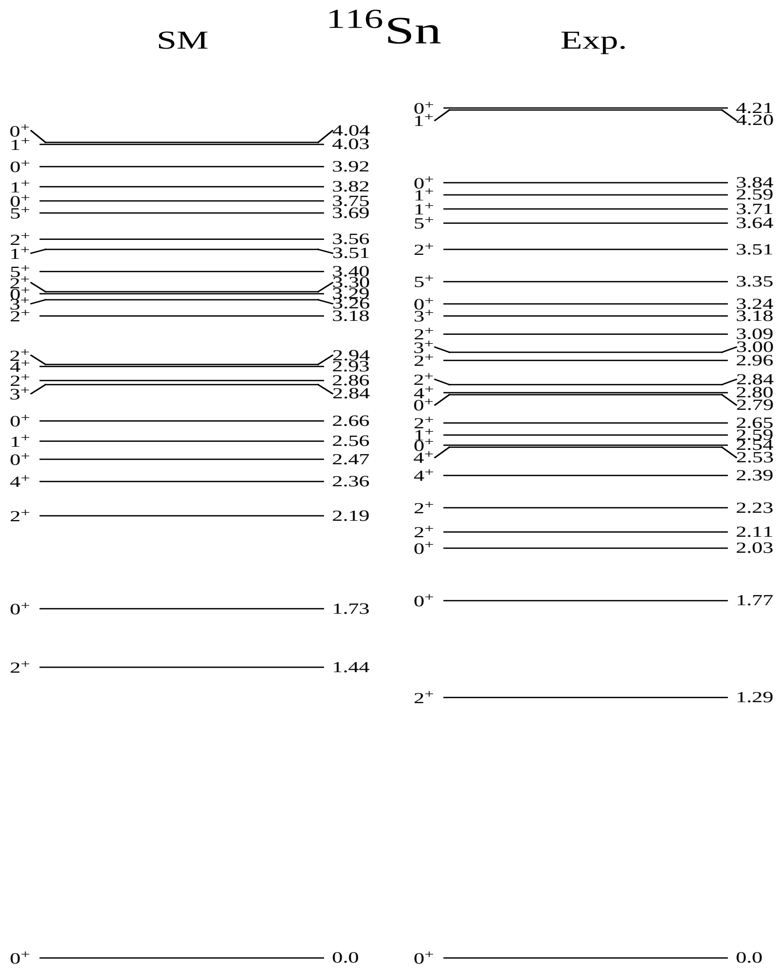

Figure 6.4: Shell Model (SM) and experimental low-energy spectra for ^{116}Sn.

The F-scalar $M1$ operator, being proportional to the total angular momentum does not promote any transition. The F-vector component, instead, connects mixed symmetry with symmetric states, both having the same number of d bosons. Its main action, in fact, is to transform an F-scalar into an F-vector quadrupole boson

$$\begin{array}{rcl} L_m|2_S^+\rangle & = & (L_\pi - L_\nu)Q_S|0_1^+\rangle = (L_\pi - L_\nu)(Q_\pi + Q_\nu)|0_1^+\rangle \\ & = & (L_\pi Q_\pi - L_\nu Q_\nu)|0_1^+\rangle \propto (Q_\pi - Q_\nu)|0_1^+\rangle \end{array} . \tag{6.7}$$

The above formula suggests that the MS states are the analogue of the scissors mode (55; 56), observed in most deformed nuclei and studied theoretically in many approaches, (57)(58).

How the measurement of the $E2$ and $M1$ transition strengths provides the fingerprints of F-spin symmetry is illustrated in Fig. 6.5.

Identifications of MS states in spherical or nearly spherical nuclei were reported in the 1980s (59; 60). They were observed unambiguously and copiously only in 1999 through an experiment on Mo isotopes (61). Since then, they were systematically identified and studied in several other nuclei in the vicinity of the shell closures $N = 50$ and $N = 82$. A review may be found in (62; 63). The reviews report also the theoretical investigations carried out within a restricted shell model scheme (64) and, more thoroughly, in the microscopic quasiparticle-phonon model (QPM) (65; 66).

Specific theoretical investigations of MS states in the vicinity of N=82 have been performed recently within the QPM (67; 68) and a large scale shell model approach (69). Because of the large amount of experimental data available, Xe isotopes offer the opportunity of studying the

Figure 6.5: Signatures of proton-neutron symmetric and MS states.

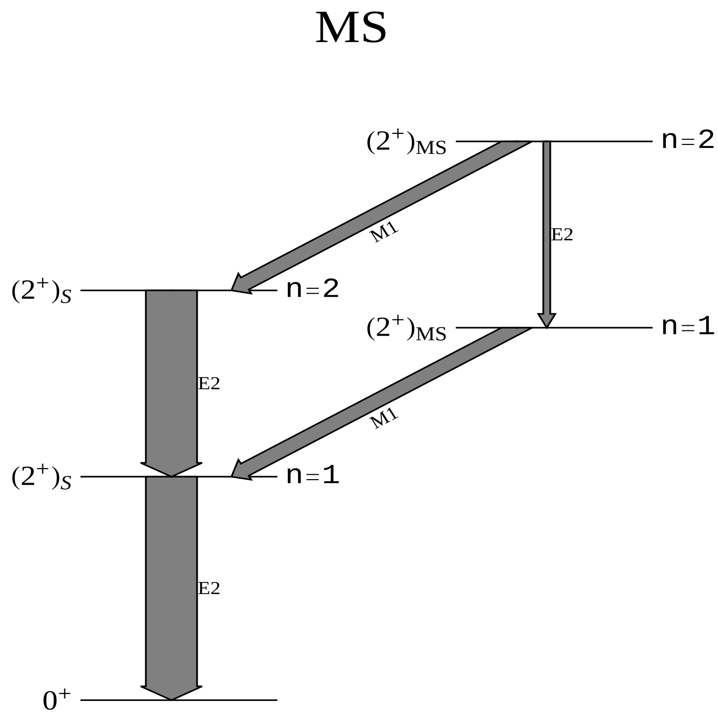

evolution of the MS states along a path which goes from pure vibrational to transitional and, eventually, deformed nuclei.

6.2.2 SM study of heavy Xe isotopes

We apply the sampling algorithm to the chain of even isotopes $^{134-130}$Xe. We first analyze the convergence properties of the iterative process and, then, perform a detailed investigation of the computed spectra and transition strengths in relation to the experimental data. We considered a scheme in which the protons are particles external to the $Z = 50$ core, while the neutrons are holes referred to the $N = 82$ core. We used the levels of ^{135}Xe as neutron single-hole energies. For the protons, we took the single particle energies adopted in Ref. (40) to study the spectra of ^{108}Sn and ^{133}Xe. Their values are given in Table 6.2.2.

Once again, a G-matrix derived from the CD-Bonn potential was taken as a two-body interaction. The G-matrix includes the core polarization contributions appropriate for the model space under consideration. We used the proton and neutron effective charges $e_p = 1.6$ and $e_n = 0.7$, respectively, for the $E(2)$ strengths and a spin gyromagnetic quenching factor $g_s = 0.5$ for the $M(1)$ transition probabilities.

$(\mathrm{nlj})_\pi$	2d5/2	1g7/2	3s1/2	2d3/2	1h11/2
ϵ_p	0.00	0.2	2.2	2.3	2.9
$(\mathrm{nlj})_\nu^{-1}$	$(2d3/2)^{-1}$	$(3s1/2)^{-1}$	$(1h11/2)^{-1}$	$(1g7/2)^{-1}$	$(2d5/2)^{-1}$
ϵ_h	0.00	0.2885	0.5266	1.1315	1.2604

Table 6.2: Single proton-particle and neutron-hole energies (in MeV)

^{132}Xe					
$J_i^\pi = 0_1^+$			$J_i^\pi = 2_1^+$		
$(n/N)_k$	J^π_{samp}	E_k	$(n/N)_k$	J^π_{samp}	E_k
0.107	0.024	-2.628	0.082	2.007	-1.848
0.154	0.014	-2.682	0.119	2.004	-1.933
0.214	0.008	-2.712	0.166	2.002	-1.980
0.288	0.004	-2.729	0.224	2.001	-2.007
0.377	0.003	-2.738	0.296	2.0004	-2.022
0.479	0.001	-2.744	0.383	2.0005	-2.032
0.590	0.0006	-2.747	0.485	2.0002	-2.038
^{130}Xe					
$J_i^\pi = 0_1^+$			$J_i^\pi = 2_1^+$		
$(n/N)_k$	J^π_{samp}	E_k	$(n/N)_k$	J^π_{samp}	E_k
0.012	0.131	-1.371	0.016	2.027	-0.710
0.020	0.099	-1.678	0.028	2.021	-1.099
0.033	0.071	-1.930	0.046	2.017	-1.442
0.052	0.052	-2.130	0.073	2.010	-1.705
0.079	0.036	-2.281	0.107	2.004	-1.816

Table 6.3: Convergence rate of the energies (in MeV) in ^{130}Xe and ^{132}Xe.

Convergence of the sampling process and results

For the study of the convergence of the sampling procedure we consider some selected levels and transitions of ^{132}Xe and ^{130}Xe. The dimensions of their Hamiltonian matrices are $N \simeq 3.7 \times 10^7$ for ^{132}Xe and $N \simeq 0.8 \times 10^9$ for ^{130}Xe.

Preliminary to the iterative procedure is the choice of the initial subspace $\mathcal{H}_0$ (see Eq.5.12). Its dimensions n_0 increase with the number of eigenstates of good J we intend to generate. To yield up to ten eigenstates, the space dimensions required are of the order $n_0 \sim 100$.

Having chosen $\mathcal{H}_0$, we could start the iterative sampling procedure 5.12 with decreasing values of ϵ_k. Each ϵ_k determines uniquely the dimension n_k of the Hamiltonian matrix to be diagonalized.

In the case of ^{132}Xe, the iterative procedure can be easily pursued until the full space is covered. We stopped, however, the sampling at $\sim 70\%$ of the basis states.

For ^{130}Xe, we were forced to stop the sampling at $\sim 10\%$. Proceeding further is possible but too time consuming on a desktop. Thus, the sampling will produce reliable results only in case of fast convergence.

As shown in Fig. 6.6 for ^{132}Xe, about 10% of the basis states are enough to lead the $J^\pi = 0^+$ and $J^\pi = 2^+$ eigenvalues to convergence. Indeed, the $J^\pi = 0^+$ absolute energies E_k decrease by 65 keV in going from $n/N \sim 0.115$ to $n/N \sim 0.59$ (Table 6.3).

The spectrum converges much faster. Indeed, the energy difference $E(0_2^+) - E(0_2^+)$ changes by ~ 10 keV when we move from $n/N \sim 0.08$ to $n/N \sim 0.46$.

The same convergence rate is found for the levels of ^{130}Xe (Figs. 6.7 and Table 6.3). Indeed, the fraction of states considered ($\sim 10\%$) is enough to bring the energy eigenvalues to the plateau. On the ground of the analysis made for ^{132}Xe, the energies obtained here may differ from the asymptotic values ($n/N = 1$) by at most 100 keV or by $10 \div 20$ keV, when referred to the ground state.

All the corresponding eigenstates have good J. As shown in Table 6.3, even with about 10% of the basis states, the J values coincide with the exact ones up to the second or third

Figure 6.6: Convergence rate of the lowest $J^\pi = 0^+$ and $J^\pi = 2^+$ eigenvalues in ^{132}Xe.

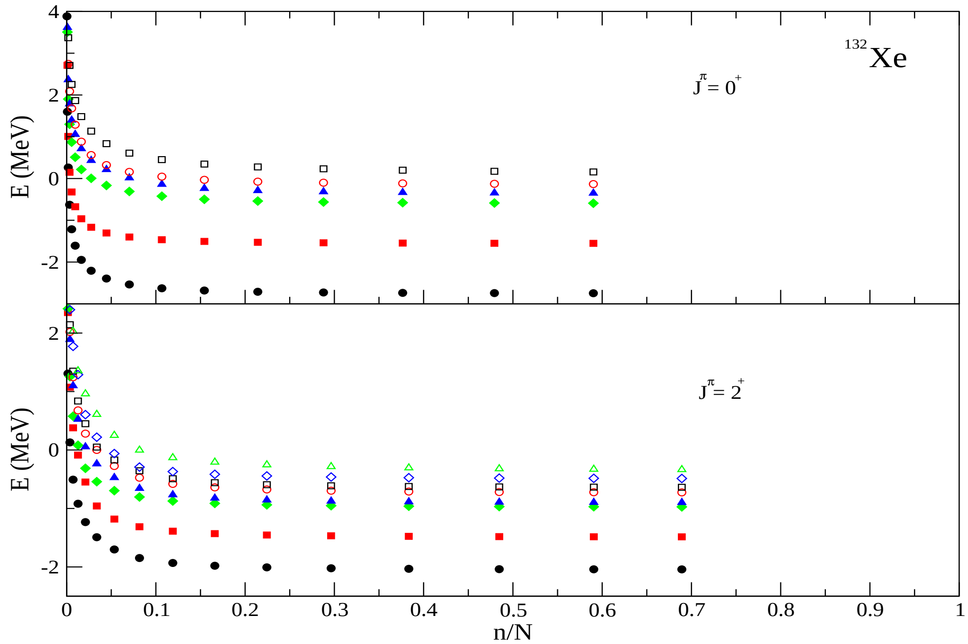

decimal digit.

Thus, although the subspaces selected according to the sampling criterion 5.11 are not strictly J-invariant, the invariance is eventually restored by a relatively small fraction of basis states.

As shown in Fig. 6.8, we obtain a good convergence of the strengths of the $E(2)$ transitions to the ground state. In ^{132}Xe , the $E(2)$ strengths reach their saturated values for $n/N \sim 0.1$. In going from $n/N \sim 0.11$ to $n/N \sim 0.59$, the strengths increases from $B(E2) \sim 22.23$ W.u. to $B(E2) \sim 22.8$ W.u., a $\sim 2\%$ increment.

The same convergence rate is obtained for the $B(E2)$ values in ^{130}Xe. The values obtained for $n/N \sim 0.11$ may be smaller than the asymptotic one by $\sim 2\%$ - 3%.

The convergence properties, however, deteriorate when we consider the transitions between excited states. In ^{132}Xe, the $2_2^+ \rightarrow 2_1^+$ $E2$ transition strength reaches the plateau with a relatively small fraction of states (Fig. 6.9). The convergence is, instead, poor for the $2_3^+ \rightarrow 2_1^+$ $M1$ transition. Analogous convergence properties are found for the other transitions.

The above results suggest that $\sim 10\%$ of the sampled states are not sufficient to produce for ^{130}Xe converging strengths. Explicit calculations have, indeed, confirmed that the $E2$ and, especially, the $M1$ transition strengths do not reach convergence. We have, therefore, to conclude that, in ^{130}Xe, the sampling yields reliable values only for the SM spectrum and the $2_1^+ \rightarrow 0_1^+$ $E2$ transition strength.

Analysis of the results

The convergence analysis states clearly the domain of applicability of the algorithm. In our specific case, we must confine our analysis to ^{132,134}Xe and to the energy levels of ^{130}Xe. Experimental versus theoretical spectra are shown in Figs. 6.10 and 6.11.

In all isotopes, the theoretical spectrum is in fairly good agreement with experiments, especially in the low-energy sector. The upper sector is in general more compressed than the experimental one. This includes some levels with uncertain spin assignment (70).

Of comparable quality are the results on the $E2$ and $M1$ transitions in ^{132,134}Xe. As shown

Table 6.4: Experimental and SM $B(E2)$ (W.u.) in $^{132-134}$Xe. The isoscalar $B_{IS}(E2)$ and isovector $B_{IV}(E2)$ strengths are also given.

^{A}Xe	$J_i \rightarrow J_f$	B(E2)		$B_{IS}(E2)$	$B_{IV}(E2)$
		EXP	SM		
^{134}Xe	$2_1^+ \rightarrow 0_1^+$	15.3(11)	15.0	9.97	0.29
	$2_2^+ \rightarrow 0_1^+$	0.74(5)	0.51	0.14	0.41
	$2_3^+ \rightarrow 0_1^+$	0.72(7)	0.31	0.04	3.14
	$2_4^+ \rightarrow 0_1^+$	0.63(6))	0.09	0.07	0.0
	$2_5^+ \rightarrow 0_1^+$		0.02	0.01	0.23
	$2_2^+ \rightarrow 2_1^+$	20(2)	14.8	9.39	0.50
	$2_3^+ \rightarrow 2_1^+$	0.56(4)	1.83	1.65	0.08
	$2_4^+ \rightarrow 2_1^+$	0.14(1)	0.11	0.01	0.24
	$2_5^+ \rightarrow 2_1^+$		0.57	0.41	0.00
	$2_6^+ \rightarrow 2_1^+$		5.04	2.41	1.05
	$4_1^+ \rightarrow 2_1^+$	11.6(8)	15.4		
^{132}Xe	$2_1^+ \rightarrow 0_1^+$	23.0(15)	22.8	17.70	0.02
	$2_2^+ \rightarrow 0_1^+$	0.056(7)	0.072	0.00	0.21
	$2_3^+ \rightarrow 0_1^+$	0.67(18)	0.16	0.01	1.32
	$2_4^+ \rightarrow 0_1^+$	0.20(3)	0.03	0.07	1.06
	$2_5^+ \rightarrow 0_1^+$		0.003	0.18	1.50
	$2_2^+ \rightarrow 2_1^+$	29.4(46)	28.8	22.37	0.02
	$2_3^+ \rightarrow 2_1^+$	1.14(73)	2.68	2.17	0.02
	$2_4^+ \rightarrow 2_1^+$	$\leq$3.1(9)	1.71	2.18	0.75
	$2_4^+ \rightarrow 2_2^+$	$\leq$32(12)	0.04	0.32	0.02
	$2_5^+ \rightarrow 2_1^+$		0.51	0.12	0.10
	$4_1^+ \rightarrow 2_1^+$	29.5(45)	30.55		
	$4_2^+ \rightarrow 2_1^+$		1.89		
	$4_2^+ \rightarrow 2_2^+$		6.74		

Table 6.5: Experimental and theoretical $B(M1)$ (μ_n^2) in $^{132-134}$Xe. The orbital strengths are also shown .

^{A}Xe	$J_i \rightarrow J_f$	B(M1)		B_{orb} (M1)
		EXP	SM	
^{134}Xe	$2_2^+ \rightarrow 2_1^+$	0.015(1)	0.024	0.0
	$2_3^+ \rightarrow 2_1^+$	0.30(2)	0.20	0.28
	$2_4^+ \rightarrow 2_1^+$	0.041(3)	0.008	0.00
	$2_5^+ \rightarrow 2_1^+$		0.097	0.00
	$\sum_i B_i(M1, 2_i^+ \rightarrow 2_1^+) =$	0.36	0.33	0.28
^{132}Xe	$2_2^+ \rightarrow 2_1^+$	0	0	0.00
	$2_3^+ \rightarrow 2_1^+$	0.22(6)	0.07	0.08
	$2_4^+ \rightarrow 2_1^+$	0	0.04	0.05
	$2_5^+ \rightarrow 2_1^+$		0.14	0.13
	$2_6^+ \rightarrow 2_1^+$	0	0.10	0.01
	$\sum_i B_i(M1, 2_i^+ \rightarrow 2_1^+) =$	0.22(6)	0.35	0.27

Figure 6.7: Convergence rate of the lowest $J^\pi = 0^+$ and $J^\pi = 2^+$ eigenvalues in ^{130}Xe.

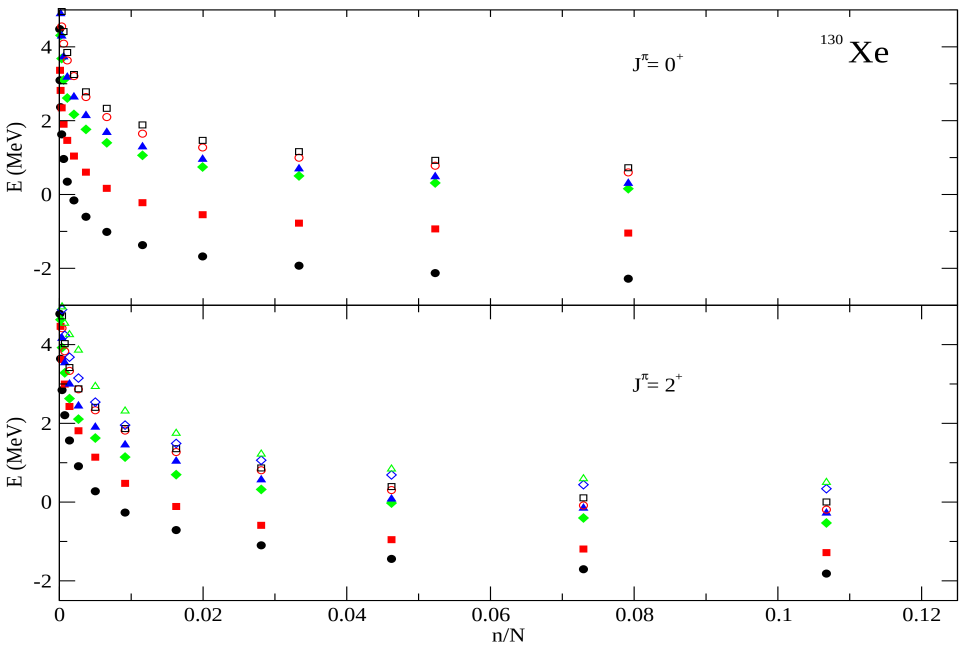

in Figs. 6.12 and Table 6.4, the $E2$ transitions are consistent with the experiments. The SM $2_i^+ \rightarrow 0_1^+$ peaks are close to the experimental ones. Good is also the agreement between SM and experimental strengths of the $2_i^+ \rightarrow 2_1^+$ transitions in ^{132}Xe. Small discrepancies are observed in ^{134}Xe, where the SM $2_i^+ \rightarrow 0_1^+$ transition strength is slightly more fragmented than the experimental one.

The SM 2_1^+ collects by far the largest strength of the $E2$ transitions to the ground state. Table 6.4 shows that this transition is isoscalar indicating that the SM 2_1^+ corresponds to the IBM symmetric one-boson 2^+ or, in microscopic terms, to the QPM isoscalar one-phonon quadrupole vibrational mode.

The residual $2_i^+ \rightarrow 0_1^+$ $E2$ strength is collected by the 2_3^+ state in ^{134}Xe (Table 6.4). The isovector nature of the $2_3^+ \rightarrow 0_1^+$ qualifies the SM 2_3^+ as the counterpart of the IBM MS one-boson 2^+ or the isovector one-phonon quadrupole mode.

In ^{132}Xe, the isovector strength is shared by at least three 2^+ states. Thus, the correspondence with the IBM MS one-boson 2^+ cannot be established unambiguously.

The other SM 2^+ states are coupled very weakly to the ground state. They, therefore, describe two-boson (or two-phonon in QPM) excitations. In all nuclei, only the 2_2^+ is strongly collective and corresponds to a proton-neutron symmetric two-boson state. It is, in fact, strongly coupled to the 2_1^+ by the isoscalar $E2$ operator (Table 6.4). The others states have appreciable two-phonon components. They are weakly collective so that it is not easy to guess their symmetry.

On the other hand, it is not mandatory to state a correspondence with all IBM states. In fact, not all the SM states are collective. Moreover, given the microscopic nature of SM, it is natural to expect that the $E2$ strength, collected by a single IBM MS state, gets fragmented and shared by several SM states. It is also worth to point out that the F-spin is not a good quantum number in SM. The correspondence is made more problematic by the fact that, in SM, the transitions occur between $T \neq 0$ states, so that two states with the same T may be coupled by both isoscalar and isovector components.

The results on the $M1$ response are more controversial. As shown in Figs. 6.13 and Table 6.5, the measured $M1$ strength is concentrated mostly, if not solely, on a single 2^+ state, while

Figure 6.8: Convergence properties of $B(E2, 2^{+}1 \rightarrow 0_1^{+})$ in ^{130}Xe and ^{132}Xe.

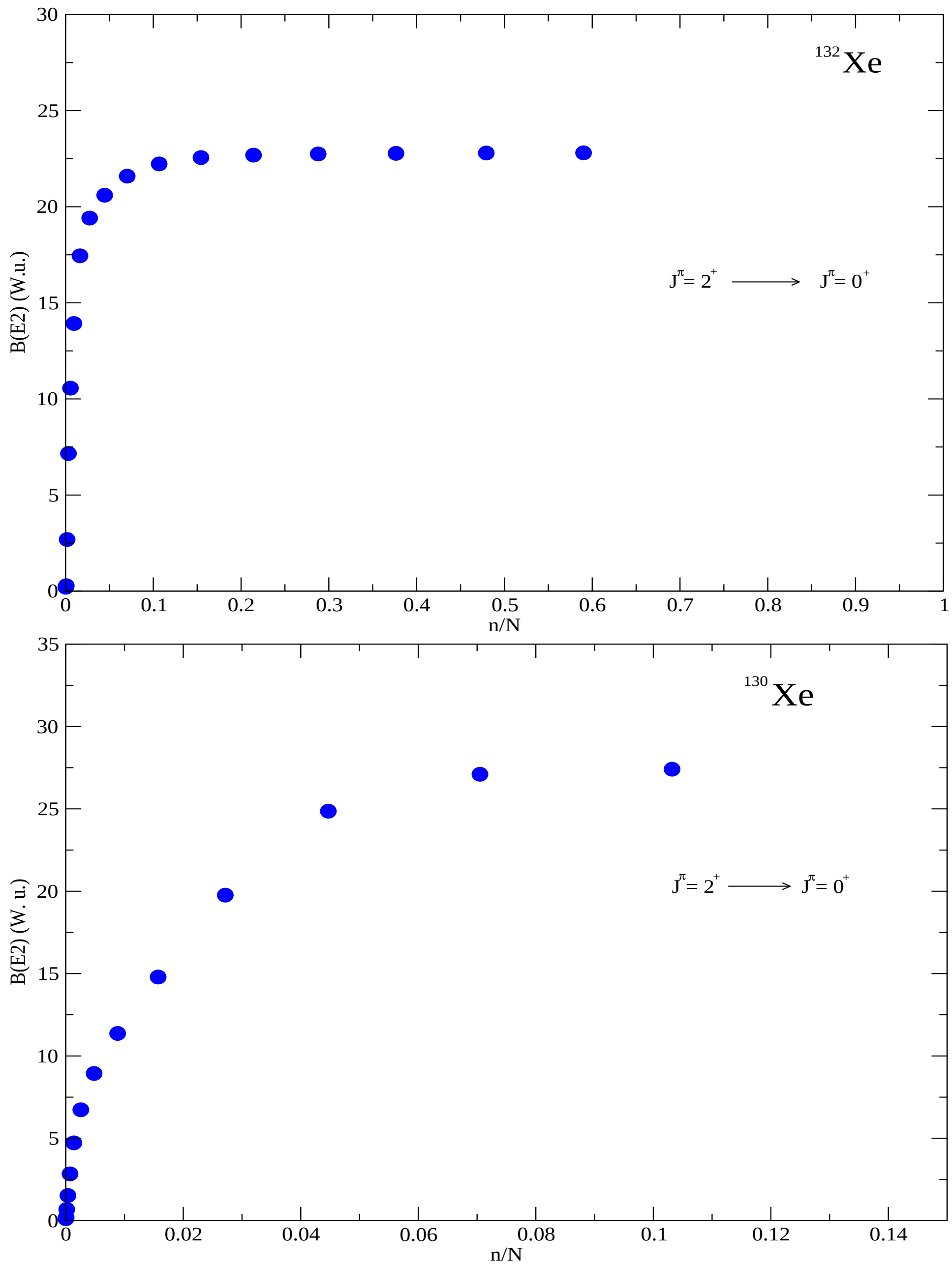

Figure 6.9: Convergence properties of $B(E2, 2_2^+ \rightarrow 2_1^+)$ and $B(M1, 2_3^+ \rightarrow 2_1^+)$ in ^{132}Xe.

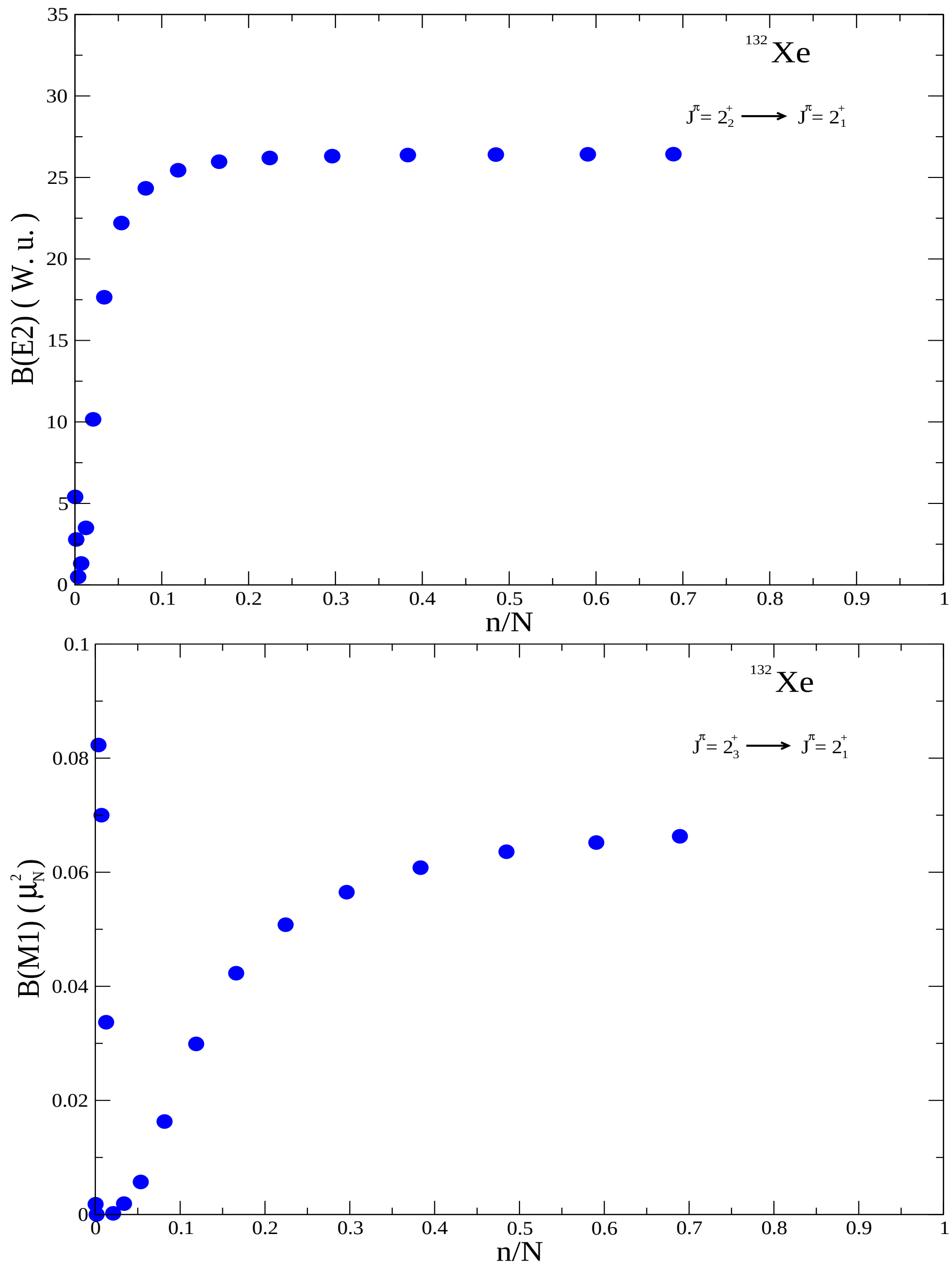

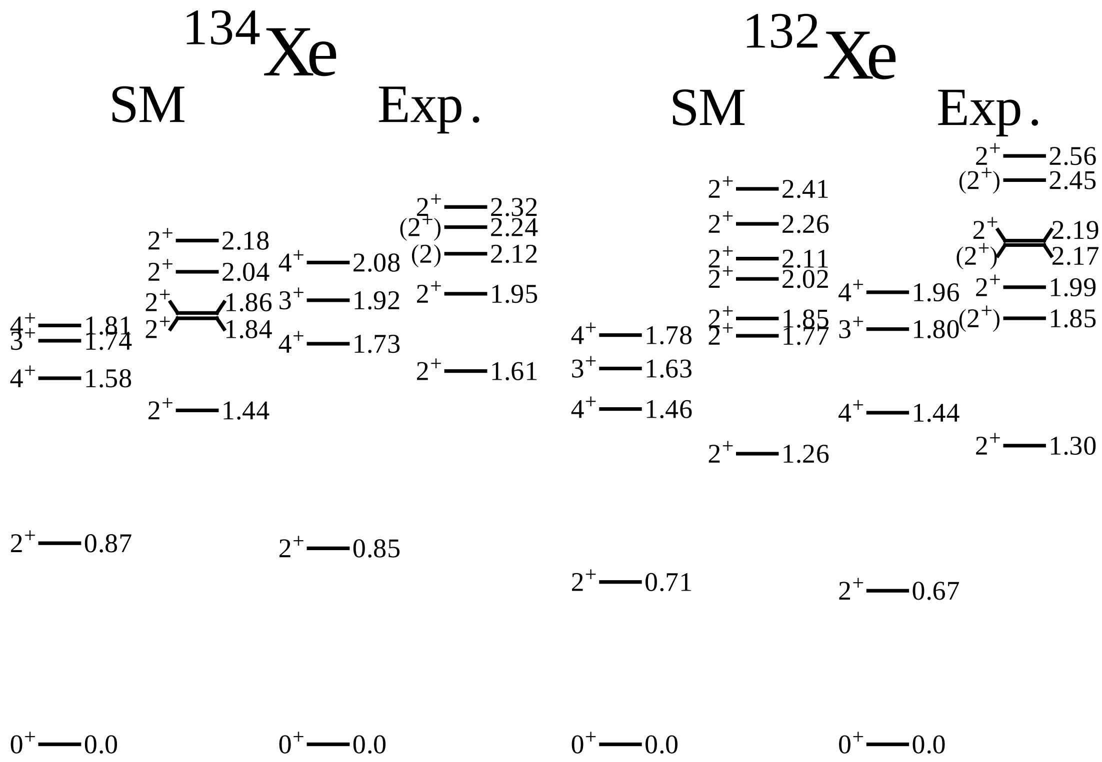

Figure 6.10: Experimental versus calculated ^{134}Xe and ^{132}Xe spectra.

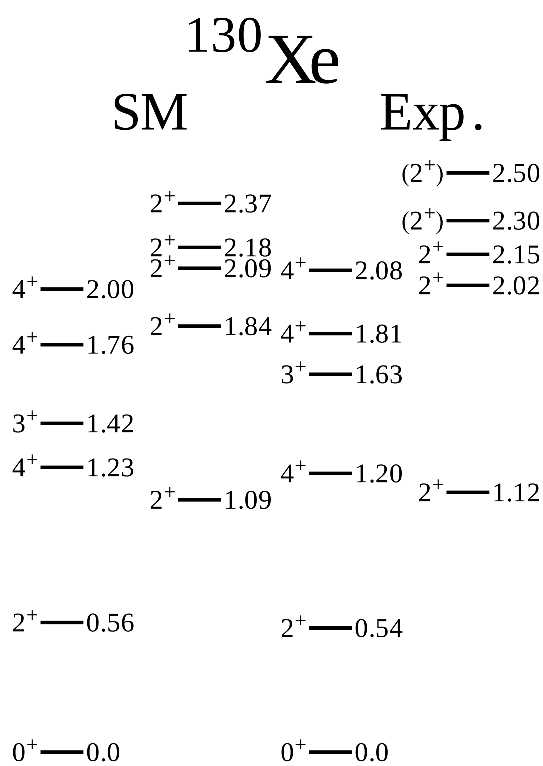

Figure 6.11: Experimental versus calculated ^{130}Xe spectra.

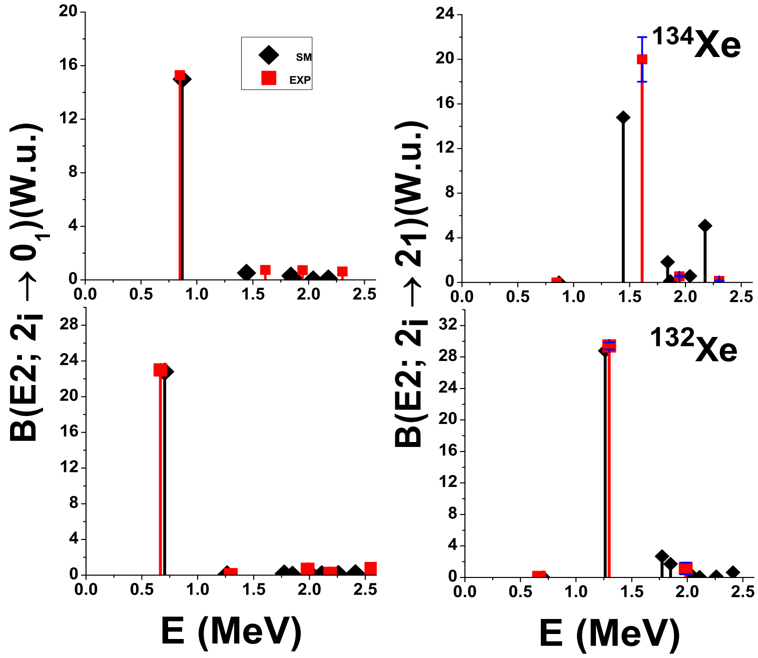

Figure 6.12: Experimental and calculated $E2$ strength distribution in $^{132-134}$Xe.

the SM strength is fragmented to some extent, especially in ^{132}Xe. It is, in fact, distributed among few 2^+ states, all clustered around a pronounced peak, lying close to the experimental one.

It is interesting to notice that, in ^{134}Xe, the orbital strength is entirely concentrated on the 2^+_3 and coincides practically with the measured one. In ^{132}Xe , all transitions are almost purely orbital except for the one involving the 2^+_6 and promoted by the spin component. If we exclude this transition, the total SM strength is within the errors of the experimental value.

It is not easy to identify the origin of such a fragmentation. Both $M1$ and isovector $E2$ transitions probe small pieces of the wave function. Moreover, the $M1$ transition strengths are the outcome of the competitive action between spin and orbital components. The occurrence of a spin transition in the range of interest suggests that a better insight would be gained if the SM space could be enlarged so as to include the spin-orbit partners of the g7/2 proton and h11/2 neutron single particle states. Unfortunately, the dimensions of such an enlarged SM space would become prohibitive.

6.3 Concluding remarks

In summary, the implementation of the importance sampling algorithm in the m-scheme offers significant advantages with respect to the old formulation in the $j-j$ coupled scheme. In fact, it makes straightforward the calculation of the Hamiltonian matrix, a great advantage since the algorithm requires to update the Hamiltonian matrix at each step of the iterative process. It exploits the sparsity of the Hamiltonian matrix which leads to an effective truncation of the shell model space.

Unfortunately, although both the number of operations and execution time grow linearly with the dimensions N of the Hamiltonian matrix, the importance sampling procedure becomes too time consuming, at least on a desktop, as the dimensions of the Hamiltonian matrix ap-

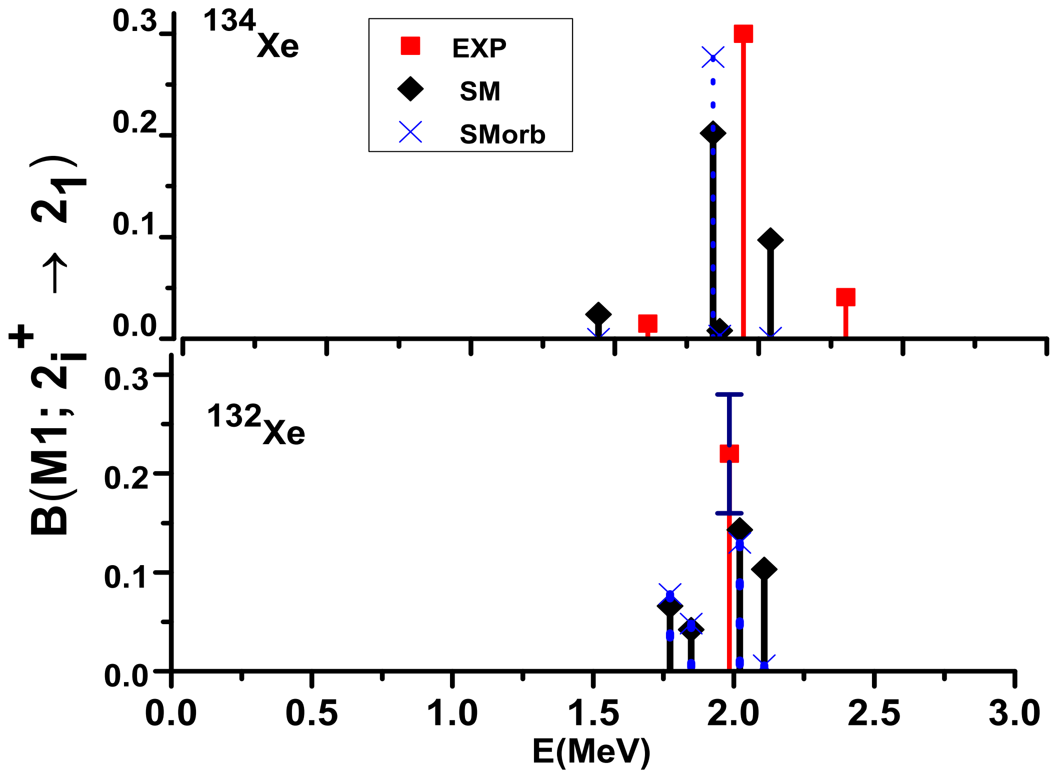

Figure 6.13: Experimental and calculated $M1$ strength distribution in $^{130-134}$Xe.

proach $N \sim 10^9$. It follows that, in nuclei like ^{130}Xe, the method is able to sample up to 10% of the basis states. This fraction of states is sufficient to bring to convergence the energy levels but not the strengths of the $E2$ and, especially, the $M1$ transitions among excited states.

Thus, the implementation of the algorithm is very far from reaching the performances of codes like Antoine. We have two possible complementary routes for trying to enlarge its domain of applicability. A possible way is to try to find out a sampling criterion which exploits more efficiently the sparsity of the Hamiltonian matrix. A more meaningful progress may be obtained by elaborating a parallel version of the code, if feasible. Such a parallelization should, hopefully, reduce drastically the execution time.

For the nuclei at reach, the method yields at once an arbitrary number of orthogonal eigenstates with a given J. It offers therefore a rather broad picture of their spectroscopic properties and a useful key for disclosing the nature of the low-lying states in these nuclei.

An illustrative example is offered here by the $^{132-134}$Xe isotopes. The results obtained are in fairly good agreement with the data. This is quite remarkable, since we use a unique set of single particle energies for all isotopes and an unmodified realistic two-body potential. The spectra as well as the $E2$ and $M1$ transitions are generally consistent with the experiments. Their analysis allows to determine the collectivity and the proton-neutron symmetry of the low-lying states. Some discrepancies concerning mainly the $M1$ transitions remain. Curing them is a quite challenging task, since the $M1$ transitions probe very small pieces of the wave function. Taking them into account might require an enlargement of the shell model space which is far from being feasible in our SM scheme.

PART TWO

Collective Models

Chapter 7

From semiclassical to microscopic approaches to collective excitations

The Tamm-Dancoff (TDA) and its generalization, the Random Phase Approximation (RPA) offer an elegant, physically transparent, microscopic description of collective excitations in nuclei (71; 72). They describes not only the global properties of the giant resonances but explain in part their fine structure by accounting for the decay of the collective mode to single-particle levels (Landau damping) (73). The two approaches, however, cannot account for anharmonic features such as the collisional damping, responsible for the so called spreading width, and are unable to describe multiphonon excitations.

Multiphonon collective modes in nuclei were predicted already within the Bohr-Mottelson model (74). Their evidence, however, has grown considerably in the last two decades. At low energy, fluorescence scattering experiments have detected low-lying double-quadrupole, double-octupole and mixed quadrupole-octupole multiplets in nearly spherical heavy nuclei (75; 76; 77). At high energy, a number of different reactions have established the existence of a double giant dipole resonance (78; 79).

Multiphonon excitations and their inherent anharmonicities were widely studied within the interacting Boson model (IBM) of Arima and Iachello (52; 53; 54) in its proton-neutron version (IBM2). The (IBM2) (53) came out to be a precious tool for systematics analysis of the low-energy spectra throughout the whole periodic table. It is able to classify the states according to their symmetry and to show how the gross properties of nuclei evolve as one moves from spherical to transitional and, eventually, well deformed regions. Because of its phenomenological nature, however, the IBM2 cannot unveil the fine structure of collective modes. These need to be studied in approaches that consider explicitly the nucleonic degrees of freedom.

To this purpose, Boson expansion techniques have been implemented under some Fermion-Boson mapping prescription (80; 81; 82). These expansion yield RPA to lowest order (72). IBM itself can be viewed as a phenomenological realization of a Fermion-Boson mapping (83). Unfortunately, all Boson series converge poorly and, therefore, have been of limited applicability. Nonetheless, the Fermion-Boson mapping idea inspires most of the microscopic approaches in use.

The nuclear field theory (74; 84) and the QPM (85) are two well known examples. The first has been especially suitable for characterizing the anharmonicities of the vibrational spectra and the spreading widths of the giant resonances, while the QPM has been extensively adopted for the study of the fine structure of multiphonon excitations (65; 66; 86; 87).

Much less exploited are other microscopic multiphonon approaches based on the iterative solution of equations of motion (88; 89).

Moving along the lines of these latter approaches, a new equation of motion method (90) has been developed, which generates iteratively a basis of multiphonon states, built out of phonons constructed in the Tamm-Dancoff approximation. The basis so obtained is highly correlated and makes much easier the task of diagonalizing the nuclear Hamiltonian.

Here, we first outline the RPA as well as the Tamm-Dancoff (TDA) approximation pointing out their harmonic character. We, then, give a very brief account of the QPM, analyzing its virtues and limitations.

7.1 Semiclassical approach to collective modes

In macroscopic models one first singles out a collective coordinate α_λ, of multipolarity λ, describing for instance a proton-neutron relative displacement ($\lambda = 1$) or a quadrupole ($\lambda = 2$) or octupole ($\lambda = 3$) shape vibrations (74) .

One, then, defines a conjugate momentum π_λ, and writes an harmonic oscillator (HO) Hamiltonian in terms of these coordinates

$$H = \frac{1}{2B_\lambda}\Pi_\lambda + \frac{1}{2}C_\lambda \alpha_\lambda \ . \tag{7.1}$$

It is more conveniently to express the collective coordinates in term of the phonon creation, $O^\dagger_\lambda$, and annihilation, O_λ, operators obtaining

$$H = \omega_\lambda O^\dagger_\lambda O_\lambda \ , \tag{7.2}$$

where $\omega_\lambda = \sqrt{C_\lambda / B_\lambda}$ is the energy of the mode. In such a form, it is immediate to derive the eigenvalue equation

$$[H, O^\dagger_\lambda] = \hbar\omega_\lambda O^\dagger_\lambda \ . \tag{7.3}$$

The HO vacuum $|0\rangle$ defines the nuclear ground state. The collective mode is described by a single state, the first excited HO state $|\lambda\rangle = O^\dagger_\lambda|0\rangle$, of energy ω_λ, which collects the whole strength of the collective coordinate α_λ.

This purely harmonic model can only account qualitatively for the gross features of nuclear collective excitations. Indeed, the collective HO Hamiltonian is not immediately related to the nuclear Hamiltonian H. Nonetheless, collective and microscopic approaches are intimately correlated (74).

7.2 Particle-hole formalism

It is useful to write the nuclear Hamiltonian

$$H = H_0 + \hat{V} \ , \tag{7.4}$$

in the second quantized form. We get

$$H_0 = \sum_i \epsilon_i a^\dagger_i a_i \ , \tag{7.5}$$

where ϵ_i are the single-particle energies and

$$\hat{V} = \frac{1}{4}\sum_{ijkl} V_{ijkl} a^\dagger_i a^\dagger_j a_l a_k \ , \tag{7.6}$$

where $V_{ijkl} =< kl\hat{V}|ij$ are the antisymmetrized matrix elements of the nucleon-nucleon two-body potential. The $a^\dagger_i$ (a_i)are the creation (annihilation) particle operators with respect to the physical vacuum.

We now assume that the single-particle energies have been obtained self-consistently in the Hartree-Fock (HF) approximation. Let us consider the lowest unperturbed eigenstates $|\rangle$

$$H_0|\rangle = E_0^{(0)}|\rangle \ , \tag{7.7}$$

of energy $E_0^{(0)} = \sum_{h=1}^{F} \epsilon_h$. Thus the HF state $|\rangle$ correspond to the filling of the lowest single particle shells up to the Fermi energy ϵ_F.

The action on $|\rangle$ yields

$$\begin{array}{rclr} a_p|\rangle & = & 0 \ , & \epsilon_p > \epsilon_F \ , \\ b_h|\rangle & = & a^\dagger_{\bar{h}}|\rangle = 0 \ , & \epsilon_h < \epsilon_F \ . \end{array} \tag{7.8}$$

The above relations define the HF state $|\rangle$ as the particle-hole (ph) vacuum. In fact, we can define particle ($|p\rangle$) and hole ($|h^{-1}\rangle$) states with respect to HF reference state through the relations

$$\begin{array}{rcl} |p\rangle & = & a^\dagger_p|\rangle \ , \\ |h^{-1}\rangle & = & b^\dagger|\rangle = a_{\bar{h}}|\rangle \ . \end{array} \tag{7.9}$$

They are both eigenstates of H_0, with energies ϵ_p and $-\epsilon_h$ with respect to the HF ground energy $E_0^{(0)}$.

7.3 Tamm-Dancoff approximation

The TDA consists, basically, in solving the nuclear SM eigenvalue problem

$$H|\lambda\rangle = (H_0 + V)|\lambda\rangle = E_\lambda|\lambda\rangle \ , \tag{7.10}$$

in a restricted space spanned by ph states

$$|p(h)^{-1}\rangle = a^\dagger_p a_{\bar{h}}|\rangle \ . \tag{7.11}$$

By projecting Eq. (7.10) into the ph subspace, one obtains the eigenvalue equation

$$\sum_{p'h'} A(ph\ ;\ p'h')\ c^\lambda(p'h') = \omega_\lambda c^\lambda(ph) \ , \tag{7.12}$$

where

$$\omega_\lambda = E_\lambda - E_0^{(0)} \ , \tag{7.13}$$

is the energy of the TDA eigenstate λ with respect to the HF unperturbed energy $E_0^{(0)}$.

The matrix A has the simple expression

$$A(ph\,;\,p'h') = \delta_{pp'}\delta_{hh'}(\epsilon_p - \epsilon_{\bar{h}}) + V_{p'\bar{h}\bar{h}'p} \ , \tag{7.14}$$

where

$$V_{p'\bar{h}\bar{h}'p} = \langle p'(h')^{-1}|\hat{V}|p(h)^{-1}\rangle = \langle p'\bar{h}|V|\bar{h}'p\rangle \ , \tag{7.15}$$

are the matrix elements of the two-body potential $\hat{V}$, in its second quantized form (7.6), and the $|p(h)^{-1}\rangle$ states are given by Eq. (7.11). It can be represented graphically by the vertices shown in Fig. 7.1. TDA amounts to the sum of an infinite number of diagrams, as illustrated in Fig. 7.2.

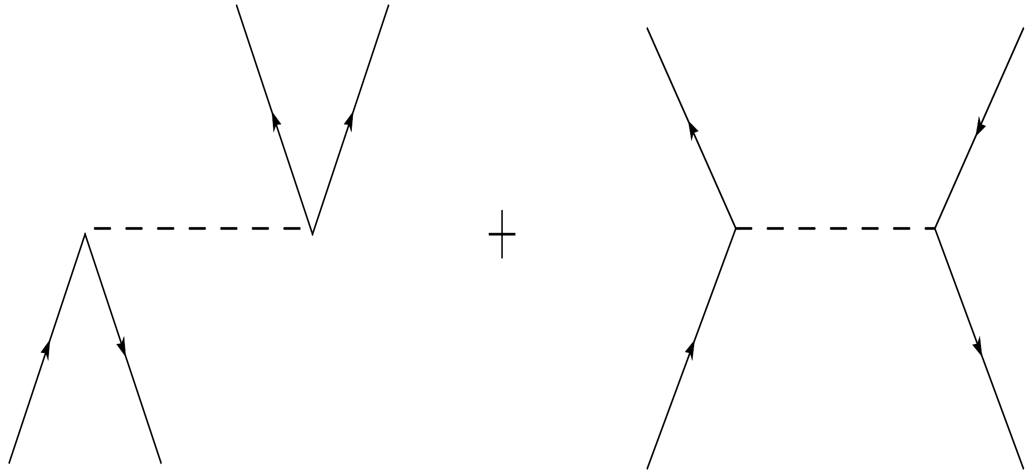

Figure 7.1: TDA vertices.

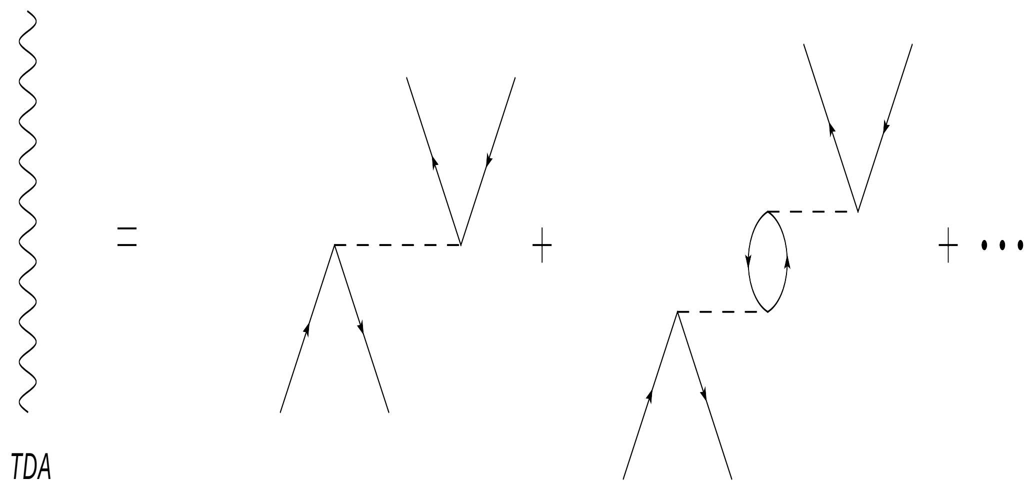

Figure 7.2: TDA series.

The transition amplitudes predicted within this approximation are easily derived. For a one-body operator

$$\hat{W} = \sum_{rs} W_{rs} a_r^\dagger a_s \ , \tag{7.16}$$

where $W_{rs} = \langle s|W|r\rangle$, one obtains

$$\langle\lambda|\hat{W}|\rangle = \sum_{ph} c_{ph}^\lambda W_{ph} \ . \tag{7.17}$$

It is easy to verify that the non energy weighted sum rule is fulfilled

$$\sum_\lambda |\langle\lambda|\hat{W}|\rangle|^2 = \sum_{ph} |W_{ph}|^2 \ . \tag{7.18}$$

For open shell nuclei, the quasiparticle formalism has to be used. In such a scheme the *ph* basis states are replaced by the quasiparticle states

$$|rs\rangle = \alpha_r^\dagger \alpha_s^\dagger |0\rangle \ , \tag{7.19}$$

where $\alpha_r^\dagger$ creates a quasiparticle with quantum numbers r out of the BCS vacuum $|0\rangle$. By simple algebraic manipulations one obtains the TDA eigenvalue equations

$$\sum_{r<s}\Big[\delta_{rq}\delta_{st}(E_r+E_s)+\langle qt|\mathcal{V}|rs\rangle\Big]c_{qt}^{(\lambda)}=\hbar\omega c_{rs}^{(\lambda)}\ , \tag{7.20}$$

where

$$\begin{array}{rcl}\langle qt|\mathcal{V}|rs\rangle & = & V_{rsqt}\left(u_ru_su_qu_t+v_rv_sv_qv_t\right)\\ & & -V_{r\bar{q}\bar{s}t}\left(v_qu_tu_rv_s+v_tu_qu_sv_r\right)\\ & & +V_{r\bar{t}\bar{s}q}\left(v_tu_qu_rv_s+v_tu_qu_sv_r\right)\end{array}\ . \tag{7.21}$$

The TDA eigenstates are then given by

$$|\lambda\rangle=\sum_{r<s}c_{rs}^{(\lambda)}|rs\rangle=\sum_{r<s}c_{rs}^{(\lambda)}\alpha_r^\dagger\alpha_s^\dagger\,, \tag{7.22}$$

and the transition amplitudes for a one-body operator W (7.16) become

$$\langle\lambda|\hat{W}|\rangle=\sum_{rs}c_{rs}^{\lambda}W_{rs}(u_rv_s+\tau u_sv_r)\ , \tag{7.23}$$

where $\tau=+(-)$ for time-even(odd) operators.

7.4 The Random Phase Approximation

The RPA is a generalization of TDA. This method was originally introduced by Bohm and Pines (91) for studying the plasma oscillations of the electron gas. The term Random Phase Approximation referred to the neglect of the coupling between plasma vibrations of different momenta.

The RPA generalization appears straightforward if we consider the TDA eigenvalue equations 7.10 as a result of a projection into the ph subspace of the harmonic oscillator (HO)-like equation

$$[H,O_\lambda^\dagger]|\rangle=\omega_\lambda O_\lambda^\dagger|\rangle\ , \tag{7.24}$$

where $|\rangle$ is the HF vacuum, and

$$O_\lambda^\dagger=\sum_{ph}X_{ph}^{(\lambda)}(\lambda)a_p^\dagger a_{\bar{h}}\ , \tag{7.25}$$

is the TDA phonon operator.

This (HO)-like form of the eigenvalue equation can be generalized by replacing the unperturbed ph vacuum $|\rangle$ with the lowest true eigenstate of the full Hamiltonian H, namely the nuclear ground state $|0\rangle$. The phonon operators O_λ and $O_\lambda^\dagger$ have to satisfy the new conditions

$$O_\lambda|0\rangle=0\ ,\qquad |\lambda\rangle=O_\lambda^\dagger|0\rangle. \tag{7.26}$$

Under the above constraints, the phonon operators O_λ and $O_\lambda^\dagger$ satisfy the following HO-like equations

$$\Big[H,O_\lambda^\dagger\Big]\,|0\rangle\ =\ \omega_\lambda O_\lambda^\dagger|0\rangle=(E_\lambda-E_0)O_\lambda^\dagger|0\rangle\ . \tag{7.27}$$

The RPA eigenvalue problem, as in the case of TDA, is formulated in a space spanned by ph states. These, however, can be generated either by creating or destroying a ph pair from

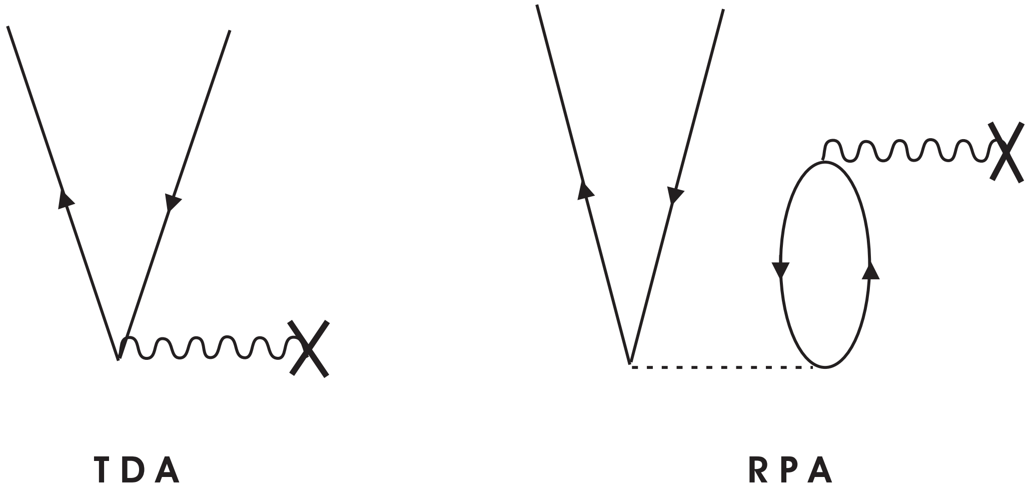

Figure 7.3: Excitation mechanism in TDA and RPA.

the ground state, where $n(ph)$ states in addition to the HF ph vacuum are present. This is illustrated in Fig. 7.3. Thus, the phonon operators have the general form

$$O^\dagger_\lambda = \sum_{ph} \left[Y^{(\lambda)}_{ph} a^\dagger_p a_{\bar{h}} - Z^{(\lambda)}_{ph} a^\dagger_{\bar{h}} a_p \right] . \tag{7.28}$$

The explicit eigenvalue equations are obtained by expanding the commutator in Eq.(7.27) and linearizing the resulting expression. It is necessary, at this stage, to make the so called quasi-Boson-approximation (QBA). This is the basic approximation of RPA and consists in using the Hartree-Fock vacuum, $|\rangle$, instead of the correlated one $|0\rangle$, to actually compute the quantities

$$\begin{array}{lcl} \langle 0|a^\dagger_p a_{p'}|0\rangle & \sim & \langle |a^\dagger_p a_{p'}|\rangle = 0, \\ \langle 0|a^\dagger_h a_{h'}|0\rangle & \sim & \langle |a^\dagger_h a_{h'}|\rangle = \delta_{hh'} \end{array} . \tag{7.29}$$

Under this approximation, one obtains

$$\begin{pmatrix} A & B \\ B^* & A^* \end{pmatrix} \begin{pmatrix} Y \\ Z \end{pmatrix} = \hbar\omega \begin{pmatrix} I & 0 \\ 0 & -I \end{pmatrix} \begin{pmatrix} Y \\ Z \end{pmatrix} , \tag{7.30}$$

where A is nothing but the TDA matrix (7.14) and B takes into account the correlations of the ground state

$$B_{ph,p'h'} = \langle ph^{-1}p'h'^{-1}|V|0\rangle \simeq \langle ph^{-1}p'h'^{-1}|V|\rangle = V_{pp'\bar{h}\bar{h}'} . \tag{7.31}$$

This is represented by the diagram in Fig. 7.4. Thus, RPA implicitly sums an infinite number of perturbative terms. A typical one is represented diagrammatically in Fig. 7.5.

The RPA states $|\lambda\rangle = O^\dagger_\lambda|0\rangle$ are orthonormalized according to

$$\langle\lambda|\lambda'\rangle = \langle 0|O_\lambda O^\dagger_{\lambda'}|0\rangle = \langle 0|[O_\lambda,\, O^\dagger_{\lambda'}]|0\rangle \cong \langle|[O_\lambda, O^\dagger_{\lambda'}]|\rangle \ = \delta_{\lambda\lambda'} , \tag{7.32}$$

yielding

$$\sum_{ph} [Y^*_{\lambda'}(ph)Y_\lambda(ph) - Z^*_\lambda(ph)Z_\lambda(ph)] = \delta_{\lambda\lambda'}. \tag{7.33}$$

In the above equations, use has been made of the QBA .

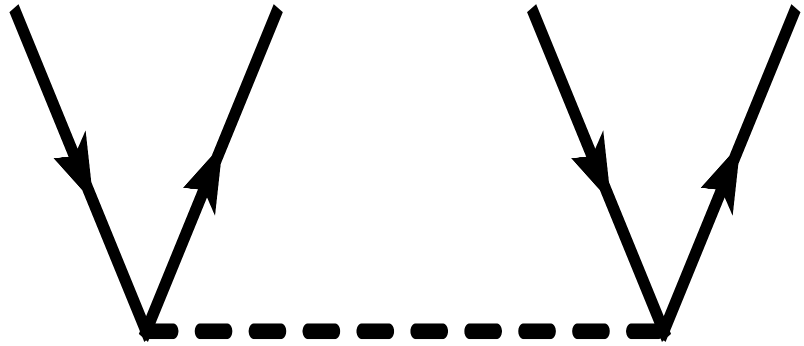

Figure 7.4: Diagrammatic representation of 7.31.

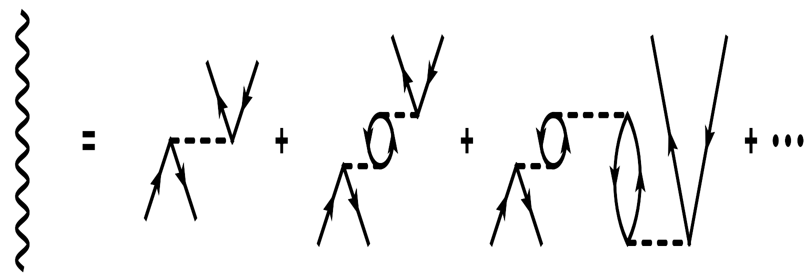

Figure 7.5: Diagrams contributing to a RPA phonon.

The same approximation is used to compute the transition amplitudes for a generic one-body operator W obtaining

$$\langle\lambda|W|0\rangle = \langle 0|[O_\lambda,\, W]|0\rangle \cong \langle|[O_\lambda,\, W]|\rangle = \sum_{ph}(Y_{ph}^{(\lambda)*}W_{ph} + Z_{ph}^{(\lambda)*}W_{hp})\ . \tag{7.34}$$

It can be proved (92) that the energy weighted sum rule is fulfilled

$$\sum_\lambda \omega_\lambda|\langle\lambda|W|0\rangle| = \frac{1}{2}\langle|[W,[H,\, W]]|\rangle = \sum_{ph}(\epsilon_p - \epsilon_h)|W_{ph}|^2. \tag{7.35}$$

Notice that, in the left-hand side, the true ground state appears, while, in the right-hand side, the true ground state is replaced by the HF state $|\rangle$.

For open shell nuclei, the RPA has to be formulated in the quasiparticle formalism. In this quasiparticle random-phase approximation (QRPA), the phonon operators, defined in 7.28, are expressed in term of quasiparticle creation and annihilation operators

$$O_\lambda^\dagger = \sum_{r<s}\left[Y_\lambda(rs)\alpha_r^\dagger\alpha_s^\dagger - Z_\lambda(rs)\alpha_s\alpha_r\right]\ , \tag{7.36}$$

$$O_\lambda = \sum_{r<s}\left[Y_\lambda^*(rs)\alpha_s\alpha_r - Z_\lambda^*(rs)\alpha_r^\dagger\alpha_s^\dagger\right]\ . \tag{7.37}$$

A procedure analogous to the one adopted in the ph case yields an eigenvalue equation identical to 7.30, but with

$$A_{rs,qt} = \begin{array}{l} V_{rsqt}\left(u_r u_s u_q u_t + v_r v_s v_q v_t\right) \\ -V_{r\bar{t}\bar{s}t}\left(v_q u_t u_r v_s + v_t u_q u_s v_r\right) \\ +V_{r\bar{t}\bar{s}q}\left(v_t u_q u_r v_s + v_q u_t u_s v_r\right) \end{array} , \tag{7.38}$$

$$B_{rs,qt} = \begin{array}{l} -V_{rs\bar{q}\bar{t}}\left(u_r u_s v_q v_t + v_r v_s u_q u_t\right) \\ +V_{rq\bar{s}\bar{t}}\left(u_r v_s u_q v_t + v_r u_s v_q u_t\right) \\ -V_{rt\bar{s}\bar{q}}\left(u_r v_s v_q u_t + v_r u_s u_q v_t\right) \end{array} . \tag{7.39}$$

RPA has many nice features. It fulfills, for instance, the energy weighted sum rule for one-body operators and accounts, to some extent, for the correlations of the ground state. This, however, is accomplished in the quasi-boson approximation. Thus RPA can be considered reliable only when the ground state correlations are small as is the case of collective excitations in spherical nuclei in proximity of shell closure or in well deformed nuclei. It breaks down in nuclei which are soft toward deformation. In those nuclei, the RPA equations become singular yielding vanishing or complex eigenvalues.

A prescription for avoiding the QBA is given in the so called renormalized RPA (93) and consists in computing the particle and hole occupation numbers using a correlated ground state rather than the HF *ph* vacuum. Due to this prescription, the eigenvalue equations are free of singularities.

TDA does not account for ground state correlations and fulfills the non energy weighted sum rule but not the energy-weighted sum. It is, on the other hand, exact and yields always stable eigenvalue equations, free of singularities.

In any case, neither TDA or RPA, even in its renormalized version, are suited for describing multiphonon spectra and their anharmonic features. They are anchored in the *ph* space and, therefore, do not allow many-particle-many-hole excitations, responsible for the fragmentation of the giant resonances and for multiphonon excitations.

7.5 Beyond TDA and RPA

In order to study these complex excitations, it is necessary to enlarge the space so as to include at least two-particle two-hole ($2ph$) states. This extension has been achieved in the small amplitude vibrational limit and is known as second RPA (SRPA). The SRPA equations were derived first by Sawicki (94) and later by Yannouleas et al. (95; 96) using the equation of motion method of Rowe (97). Their solution in finite nuclei is quite problematic and therefore approximations have to be made.

The most drastic approximation is to neglect the mutual coupling among two-particle two-hole states (2p2h) (98; 99). This is also done in a recent calculation using a potential derived by the Unitary Correlation Method (UCOM) (100) and applied to ^{16}O ^{40}Ca and ^{90}Zr.

A more refined approximation consists in replacing one *ph* pair with a correlated state (RPA phonon) thereby obtaining a particle-phonon coupling (74; 101; 102; 103; 104).

Based on this approximation is a relativistic extension of Migdal's theory, which exploits the Green function techniques to enlarge the configuration space beyond the *ph* space underlying RPA (105; 106; 107). This enlarged space covers two-quasiparticle configurations plus states obtained by coupling the two-quasiparticle configurations with low-lying QRPA phonons. This relativistic quasiparticle random-phase approximation (RQRPA) plus phonon coupling (PC) was applied successfully to the giant dipole resonance (GDR) and the pygmy giant resonance in spherical open shell nuclei (108; 109; 110).

A further progress has been made in recent SRPA calculation using a Skyrme force (111), where the interaction between $2p2h$ states is partly taken into account.

All the above approaches include up to $2ph$ or $2qp$ configurations and, therefore, are suited to describe the fragmentation of collective modes rather than the multiphonon excitations. This is accomplished only in the quasiparticle phonon model (QPM) (85).

The QPM adopts a two-body Hamiltonian which is a sum of several separable multipole-multipole potentials. Due to this simplifying assumption, the QPM is able to cover a very large configuration space and to include up to three phonon basis states.

The intrinsic Hamiltonian has the form

$$H = H_{sp} + V_{pair} + V_M^{ph} + V_{SM}^{ph} + V_M^{pp} \ , \tag{7.40}$$

where H_{sp} is a one-body Hamiltonian, V_{pair} the monopole pairing, V_M^{ph} and V_{SM}^{ph} are respectively sums of separable multipole and spin-multipole interactions acting in the particle-hole channel, and V_M is the sum of particle-particle multipole pairing potentials.

The QPM procedure goes through several steps. One starts with performing a quasiparticle RPA calculation 7.36 using a Hamiltonian composed of a sum of separable multipole pieces. Once the QRPA phonons are generated, it is possible to express the Hamiltonian into the phonon form

$$H_{QPM} = \sum_{i\mu} \omega_{i\lambda} O^\dagger_{i\lambda\mu} O_{i\lambda\mu} + H_{\nu q} \ , \tag{7.41}$$

where the first term is the unperturbed phonon Hamiltonian and $H_{\nu q}$ is a phonon-coupling piece. The phonon Hamiltonian is diagonalized in a space spanned by states composed of one, two, and three QRPA phonons, so that the eigenfunction have the structure

$$\begin{aligned} \Psi_\nu &= \textstyle\sum_i C_i O^\dagger_\nu(i)|0\rangle + \sum_{\substack{\lambda_1 \\ \lambda_2}} C^\nu_{\lambda_1\lambda_2} \left[O^\dagger_{\lambda_1} \times O^\dagger_{\lambda_2}\right]_\nu |0\rangle \\ &+ \textstyle\sum_{(\lambda_1\lambda_2)\mu\lambda_3} C^\nu_{(\lambda_1\lambda_2)\mu\lambda_3} \left[\left(O^\dagger_{\lambda_1} \times O^\dagger_{\lambda_2}\right)_\mu \times O^\dagger_{\lambda_3}\right]_\nu |0\rangle \end{aligned} \ . \tag{7.42}$$

Because of its flexibility and handiness, the QPM is the multiphonon approach most widely adopted for microscopic systematic studies of low and high energy spectroscopic properties.

One of the problems to be faced in the QPM is the determination of the Hamiltonian parameters. Systematic analysis have determined different sets of parameters in different mass regions.

Another problem is connected with the fact that, like the SRPA, the QPM relies on the quasiboson approximation and, therefore, is valid in the small amplitude limit.

In summary, the QPM is a precious tool for investigating the fine structure of collective modes, but has a phenomenological character and is valid in the vicinity of shell closures or in well deformed nuclei.

Chapter 8

Equation of Motion Phonon Model

Recently, a new method has been proposed (90), which is known as the *Equation of Motion Phonon Model* (EPMP). The method generates iteratively a multiphonon basis in which the nuclear eigenvalue problem is solved for a Hamiltonian of general form.

The method does not rely on any approximation and, therefore, has the same accuracy of the shell model. With respect to SM, it is well suited to the investigation of collective modes at low and high excitation energy.

8.1 Equations of Motion Phonon Model in the particle-hole scheme

We start considering a two-body Hamiltonian in the second quantized form

$$H = \sum_i \epsilon_i a_i^\dagger a_i + \frac{1}{4}\sum_{ijkl} V_{ijkl}\, a_i^\dagger a_j^\dagger a_l a_k \ , \tag{8.1}$$

where ϵ_i are the single-particle energies, V_{ijkl} the antisymmetrized matrix elements of the nucleon-nucleon interaction, and $a_i^\dagger$ (a_i) the creation (annihilation) particle operators with respect to the physical vacuum, $|0\rangle$. We want to solve the eigenvalue problem

$$H|\Psi_\nu\rangle = E_\nu|\Psi_\nu\rangle \ , \tag{8.2}$$

for the nuclear Hamiltonian, within a Hilbert space, which is the direct sum of n-phonon subspace

$$\mathcal{H} = \sum_{n=0,N} \oplus \mathcal{H}_n \ . \tag{8.3}$$

We intend to construct n-phonon states $|n\,;\,\alpha\rangle$ fulfilling the following orthogonality conditions

$$\begin{array}{rcl} \langle n'\,;\,\beta|n\,;\,\alpha\rangle & = & \delta_{nn'}\delta_{\alpha\beta} \\ \langle n'\,;\,\beta|a_p^\dagger a_h|n\,;\,\alpha\rangle & = & \delta_{n'(n+1)}\langle n+1\,;\,\beta|a_p^\dagger a_h|n\,;\,\alpha\rangle \\ \langle n'\,;\,\beta|a_{p_1}^\dagger a_{p_2}|n\,;\,\alpha\rangle & = & \delta_{n'n}\langle n\,;\,\beta|a_{p_1}^\dagger a_{p_2}|n\,;\,\alpha\rangle \\ \langle n'\,;\,\beta|a_{h_1}^\dagger a_{h_2}|n\,;\,\alpha\rangle & = & \delta_{n'n}\langle n\,;\,\beta|a_{h_1}^\dagger a_{h_2}|n\,;\,\alpha\rangle \end{array} \ . \tag{8.4}$$

The above relations yield the identity decomposition

$$I = \sum_n P_n \ , \tag{8.5}$$

where

$$P_n = \sum_\alpha |n\,;\,\alpha\rangle\langle n\,;\,\alpha| \ . \tag{8.6}$$

Let us now assume that the states $|n\,;\,\alpha\rangle$ in the $(n-1)$-phonon subspace are known. This assumption is certainly fulfilled since we know the 1-phonon TDA states $|\lambda\rangle$. Our goal is to find the vectors belonging to the n-phonon subspace $\mathcal{H}_n$, in term of the $(n-1)$-phonon states

$$|n\,;\,\beta\rangle = \sum_{\lambda\alpha} C^{\beta}_{\lambda\alpha}(n) O^{\dagger}_{\lambda}|n-1\,;\,\alpha\rangle, \tag{8.7}$$

where

$$O^{\dagger}_{\lambda} = \sum_{ph} c^{\lambda}_{ph} a^{\dagger}_{p} a_{\bar{h}}\ , \tag{8.8}$$

are the TDA phonon operators. We now require that the n-phonon states bring the Hamiltonian to diagonal form within the n-phonon subspace

$$\langle n\,;\,\beta|H|n\,;\,\alpha\rangle = \delta_{\alpha\beta} E^{(n)}_{\alpha}\ . \tag{8.9}$$

In order to achieve this result, we start from the equations of motion

$$\langle n\,;\,\beta|\left[H, O^{\dagger}_{\lambda}\right]|n-1\,;\,\alpha\rangle = \left(E^{(n)}_{\beta} - E^{(n-1)}_{\alpha}\right) X^{\beta}_{\lambda\alpha}(n)\ , \tag{8.10}$$

where

$$X^{\beta}_{\lambda\alpha}(n) = \langle n\,;\,\beta|O^{\dagger}_{\lambda}|n-1\,;\,\alpha\rangle = \sum_{ph} c^{\lambda}_{ph}\langle n\,;\,\beta|a^{\dagger}_{p}a_{h}|n-1\,;\,\alpha\rangle\ . \tag{8.11}$$

These are the equations to be solved. The commutator in the left-hand side can be expanded as

$$\begin{array}{rcl} \langle n\,;\,\beta|\left[H, O^{\dagger}_{\lambda}\right]|n-1\,;\,\alpha\rangle & = & \sum_{ph} c^{\lambda}_{ph}\Big[(\epsilon_p - \epsilon_h)\langle n\,;\,\beta|a^{\dagger}_{p}a_{h}|n-1\,;\,\alpha\rangle \\ & + & \frac{1}{2}\sum_{ijk} V_{ijpk}\langle n\,;\,\beta|a^{\dagger}_{i}a^{\dagger}_{j}a_{k}a_{h}|n-1\,;\,\alpha\rangle \\ & + & \frac{1}{2}\sum_{ijk} V_{ihkj}\langle n\,;\,\beta|a^{\dagger}_{p}a^{\dagger}_{i}a_{j}a_{k}|n-1\,;\,\alpha\rangle\Big] \end{array}\ . \tag{8.12}$$

Rearranging the creation and annihilation operators, the terms in the sum are either linear in $\langle n\,;\,\beta|a^{\dagger}_{p}a_{h}|n-1\,;\,\alpha\rangle$, or of the form $\langle n\,;\,\beta|a^{\dagger}_{p}a_{h}a^{\dagger}_{i}a_{j}|n-1\,;\,\alpha\rangle$.

The terms of the latter form are linearized by making use of the identity decomposition (8.5) and (8.6). We get

$$\begin{array}{rcl} \langle n\,;\,\beta|a^{\dagger}_{p}a_{h}a^{\dagger}_{i}a_{j}|n-1\,;\,\alpha\rangle & = & \sum_{n'}\langle n\,;\,\beta|a^{\dagger}_{p}a_{h}P_{n'}a^{\dagger}_{i}a_{j}|n-1\,;\,\alpha\rangle \\ & = & \langle n\,;\,\beta|a^{\dagger}_{p}a_{h}P_{n-1}a^{\dagger}_{i}a_{j}|n-1\,;\,\alpha\rangle \\ & = & \sum_{\gamma}\langle n\,;\,\beta|a^{\dagger}_{p}a_{h}|n-1\,;\,\gamma\rangle\langle n-1\,;\,\gamma|a^{\dagger}_{i}a_{j}|n-1\,;\,\alpha\rangle \\ & = & \sum_{\gamma}\langle n\,;\,\beta|a^{\dagger}_{p}a_{h}|n-1\,;\,\gamma\rangle\rho^{(n-1)}_{\alpha\gamma}(ij) \end{array}\ , \tag{8.13}$$

where

$$\rho^{(n-1)}_{\alpha\gamma}(ij) = \langle n-1\,;\,\gamma|a^{\dagger}_{i}a_{j}|n-1\,;\,\alpha\rangle\ , \tag{8.14}$$

are the matrix elements of the particle ($i=p, j=p'$) and hole ($i=h, j=h'$) density operators between $(n-1)$-phonon states.

By inverting Eq. (8.8) we get

$$\langle n\,;\,\beta|a^{\dagger}_{p}a_{h}|n-1\,;\,\alpha\rangle = \sum_{\lambda} c^{\lambda}_{ph} X^{\beta}_{\lambda\alpha}(n). \tag{8.15}$$

The equations of motion (8.10) become now the eigenvalue equations

$$\sum_{\gamma\lambda'} A^{(n)}(\lambda\alpha\ ;\ \lambda'\gamma)\ X^{\beta}_{\lambda'\gamma}(n) = E^{(n)}_{\beta}\ X^{\beta}_{\lambda\alpha}(n)\ , \tag{8.16}$$

in the unknown amplitudes $X^{\beta}_{\lambda\alpha}$ (Eq. (8.11)).

The matrix A has the physically transparent phonon structure

$$A^{(n)}(\lambda\alpha\ ;\ \lambda'\gamma) = \Big(E_\lambda + E_\alpha\Big)\delta_{\alpha\gamma}\delta_{\lambda\lambda'} + \mathcal{V}_{\lambda\alpha\,;\,\lambda'\gamma}\ , \tag{8.17}$$

where E_λ and E_α are the energies of the TDA phonon, $|\lambda\rangle$, and of the $(n-1)$-phonon states, $|(n-1),\alpha\rangle$, and the term $\mathcal{V}$ takes into account the interaction between them.

One may notice the formal analogy with the *ph* TDA eigenvalue Eqs.(7.12, 7.14). This analogy is even closer for $n = 2$ as illustrated in Figs. 8.1 and 8.2. Indeed, in this case, one goes from the TDA to the EMPM equation by replacing the *ph* energies $\epsilon_p - \epsilon_h$ with the two phonon energies $E_\lambda + E_{\lambda'}$ (Fig. 8.1) and the *ph* two-body potential $V_{ph'hp'}$ with the phonon-phonon potential $\mathcal{V}_{\lambda\alpha\,;\,\lambda'\gamma}$ (Fig. 8.2). The matrix elements of this phonon-phonon

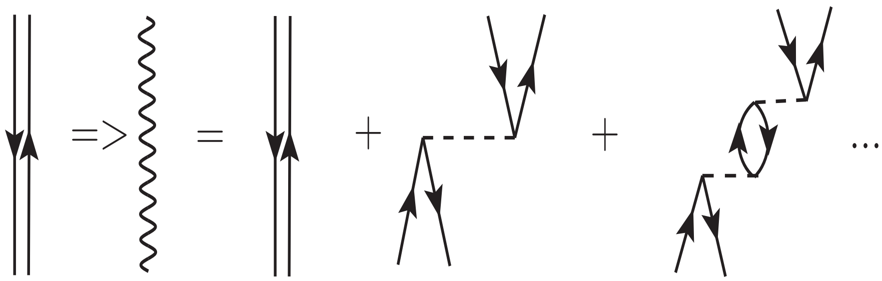

Figure 8.1: From particle-hole to (TDA) phonons

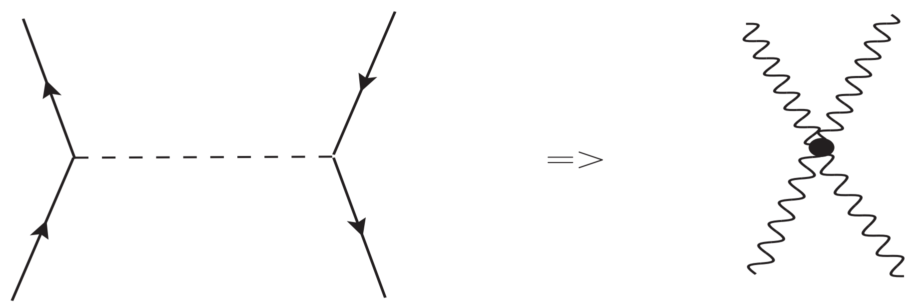

Figure 8.2: From *ph* to phonon-phonon vertices

potential are given by

$$\mathcal{V}_{\lambda\alpha\,;\,\lambda'\gamma} = \sum_{rs} \mathcal{V}_{\lambda\lambda'}(rs)\rho^{(n-1)}_{\alpha\gamma}(rs)\ , \tag{8.18}$$

where the label r and s are either particle ($r = p_1, s = p_2$) or hole ($r = h_1, s = h_2$) states. The potential appearing in the above equation is given by

$$\mathcal{V}_{\lambda\lambda'}(p_1p_2) = \frac{1}{2}\sum_{pp'} \rho_{\lambda\lambda'}(p'p)V_{p'p_1pp_2} + \sum_{hh'} \rho_{\lambda\lambda'}(hh')V_{hp_1h'p_2}\ , \tag{8.19}$$

$$\mathcal{V}_{\lambda\lambda'}(h_1h_2) = \sum_{pp'} \rho_{\lambda\lambda'}(p'p)V_{p'h_1ph_2} + \frac{1}{2}\sum_{hh'} \rho_{\lambda\lambda'}(hh')\,V_{hh_1h'h_2}\ , \tag{8.20}$$

where

$$\rho_{\lambda\lambda'}(pp') = \langle\lambda'|a^\dagger_p a_{p'}|\lambda\rangle = \sum_h c^{\lambda}_{p'h} c^{\lambda'}_{ph} , \quad (8.21)$$

$$\rho_{\lambda\lambda'}(hh') = \langle\lambda'|a^\dagger_h a_{h'}|\lambda\rangle = -\sum_p c^{\lambda}_{ph} c^{\lambda'}_{ph'} , \quad (8.22)$$

are the 1-phonon (TDA) density matrices.

The eigenvalue equations 8.16 contain only quantities defined within the $(n-1)$-phonon subspace. They can, therefore, be solved iteratively starting from the Tamm-Dancoff $n = 1$ phonon space. These equations, however, would yield redundant solution due to the impossibility of enforcing the Pauli principle between the TDA $O^\dagger_\lambda$ and the $(n-1)$-phonon states. In order to eliminate this redundancy, a general eigenvalues problem has to be formulated, starting from 8.16.

To this purpose, we insert the expression (8.7) of the state $|n\ ;\ \beta\rangle$ in the formula (8.11), giving the amplitude $X^{\beta}_{\lambda\alpha}(n)$, obtaining

$$X^{\beta}_{\lambda\alpha}(n) = \langle n\,;\,\beta|O^\dagger_\lambda|n-1\,;\,\alpha\rangle = \sum_{\lambda'\gamma} C^{\beta}_{\lambda'\gamma}(n) D^{(n)}(\lambda\alpha\ ;\ \lambda'\gamma) , \quad (8.23)$$

where

$$\mathcal{D}(\lambda\alpha\ ;\ \lambda'\gamma) = \langle n-1\ ;\ \gamma|O_{\lambda'}O^\dagger_\lambda|n-1\ ;\ \alpha\rangle , \quad (8.24)$$

is the overlap or metric matrix. Inserting this new formulas of the amplitudes $X^{\beta}_{\lambda\alpha}(n)$ into the equations of motion (8.16), we get the eigenvalue problem in a general form

$$\sum_{\lambda'\gamma\lambda"\gamma'} A(\lambda\alpha, \lambda'\gamma)\mathcal{D}_\beta(\lambda'\gamma, \lambda"\gamma')C^{\beta}_{\lambda"\gamma'} = E_\beta \sum_{\lambda'\gamma} \mathcal{D}_\beta(\lambda\alpha, \lambda'\gamma)C^{\beta}_{\lambda'\gamma} , \quad (8.25)$$

or, in short

$$HC = (A\mathcal{D})C = E\mathcal{D}C . \quad (8.26)$$

The metric matrix $\mathcal{D}$ is given by

$$D_{\alpha\beta}(\lambda;\lambda') = \delta_{\lambda\lambda'}\delta_{\alpha\beta} + \sum_\gamma X^{(\alpha)}_{\lambda'\gamma}(n-1)X^{(\beta)}_{\lambda\gamma}(n-1) - \sum_{rs} \rho_{\lambda\lambda'}(rs)\rho^{(n-1)}_{\alpha\beta}(rs) , \quad (8.27)$$

where the density matrices are given by Eqs. (8.21) for $n = 1$, and by the following relation

$$\rho^{(n)}_{\alpha\beta}(rs) = \sum_{\gamma\delta\lambda\lambda'} C^{(\alpha)}_{\lambda\gamma}(n)X^{(\beta)}_{\lambda'\delta}(n)\Big[\delta_{\gamma\delta}\rho_{\lambda\lambda'}(rs) + \delta_{\lambda\lambda'}\rho^{(n-1)}_{\gamma\delta}(rs)\Big] , \quad (8.28)$$

in the n-phonon case. These recursive formulas allow us to compute all the quantities appearing in the n-phonon eigenvalue equations in terms of those determined in the $(n-1)$-phonon subspace.

Now, we are able to design a procedure for extracting a set of linear independent states from the original N_r redundant vectors. Rather than using the traditional method based on the diagonalization of (112), we resort to the Cholesky decomposition, described in the appendix A. The latter has been preferred, since scales faster with the dimensions of $\mathcal{D}$.

This method selects a basis of linear independent states $\{O^\dagger_\lambda\ |n{-}1;\ \alpha\rangle\}$ spanning the physical subspace of the correct dimensions $N_n < N_r$ and, thus, enables us to construct a $N_n \times N_n$ non singular matrix $\mathcal{D}_n$. By left multiplication in the N_n-dimensional subspace we get from Eq. (8.26)

$$\left[\mathcal{D}^{(-1)}_n(\mathcal{A}\,\mathcal{D})_n\right] C = EC . \quad (8.29)$$

This equation determines only the coefficients $C^{(\beta)}_{\lambda\alpha}$ of the N_n-dimensional physical subspace. The remaining redundant $N_r - N_n$ coefficients are undetermined and, therefore, can be safely put equal to zero. The eigenvalue problem is thereby solved exactly.

We can now generate iteratively, with no approximations, a basis of n-phonon states, with $n = 1, 2, \cdots$. In such a basis, the Hamiltonian assumes the simple form given by Fig. 8.3. We have $n = 1, 2, \cdots$ diagonal blocks, each block corresponding to a subspace with a given number n of phonons. We have now to compute the terms which couple subspaces with different numbers of phonons, having in mind that only subspaces differing by at most two phonons are coupled by a two-body Hamiltonian.

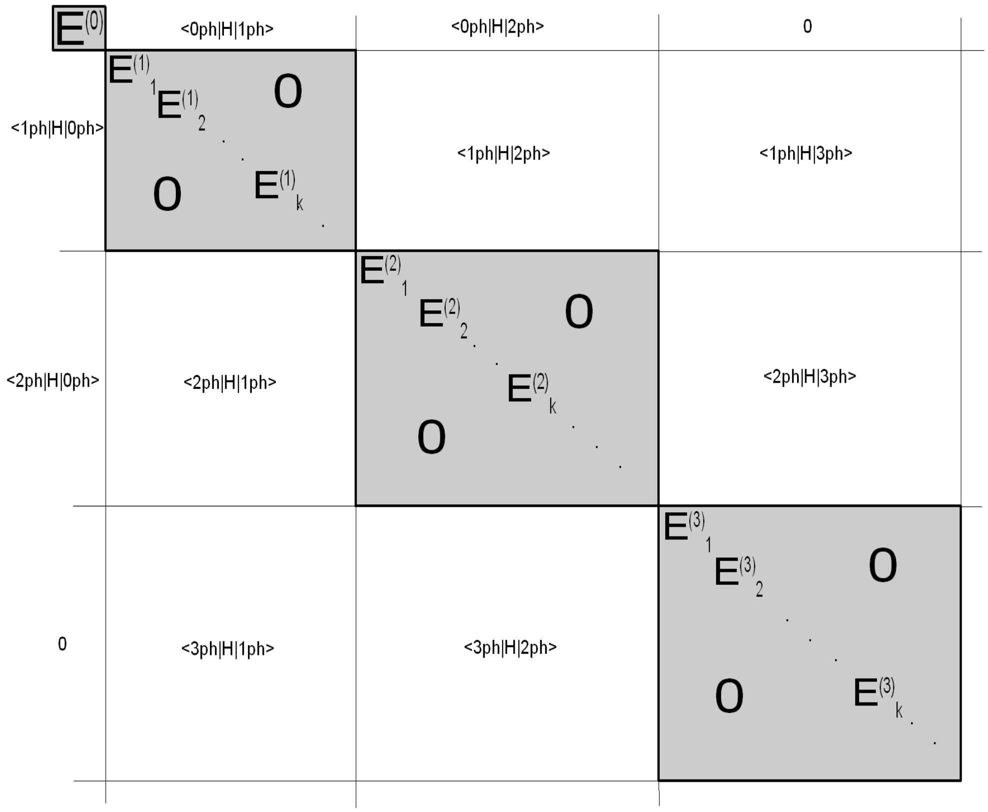

Figure 8.3: Hamiltonian matrix in the multiphonon basis.

The matrix elements between n and $(n-1)$-phonon states are given by

$$H_{\alpha_{n-1}\beta_n} = \langle n;\beta|\, H\, |n-1;\alpha\rangle = \sum_{\lambda\gamma} \mathcal{V}_{\alpha\gamma}(\lambda) X^{\beta}_{\lambda\gamma}(n) \; , \tag{8.30}$$

where

$$\mathcal{V}_{\alpha\gamma}(\lambda) = \frac{1}{2}\sum_{rs} V_{rs}(\lambda)\rho^{(n-1)}_{\alpha\gamma}(rs) \; , \tag{8.31}$$

and

$$V_{rs}(\lambda) = \sum_{ph} V_{prhs} c^{\lambda}_{ph} \; . \tag{8.32}$$

On the other hand, for the coupling between n and $(n-2)$-phonons, one finds

$$H_{\alpha_{n-2}\beta_n} = \langle n;\beta\,|\, H\, |n-2;\alpha\rangle = \frac{1}{4}\sum_{\lambda\lambda'\gamma} \mathcal{V}(\lambda\lambda') \;\; X^{\beta}_{\lambda\gamma}(n) \;\; X^{\gamma}_{\lambda'\alpha}(n-1) \; , \tag{8.33}$$

whit

$$\mathcal{V}(\lambda\lambda') = \sum_{php_1h_1} V_{pp_1hh_1} c^{\lambda}_{ph} c^{\lambda'}_{p_1h_1} \ . \tag{8.34}$$

The two coupling terms may be represented by the vertices of Figs. 8.4. Thus, the EMPM accounts explicitly, and not virtually as in RPA, for the ground state correlations (Fig. 8.5).

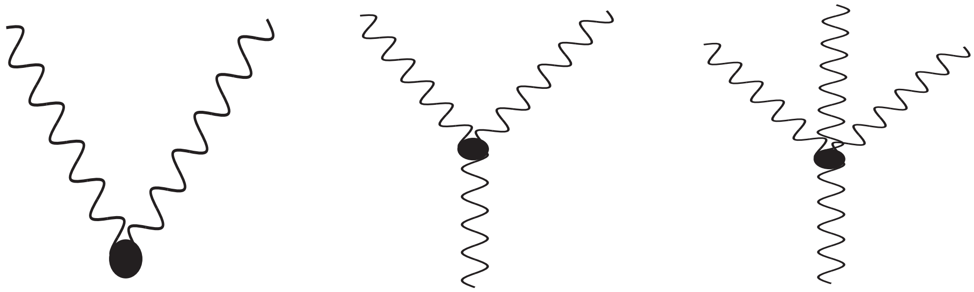

Figure 8.4: Phonon coupling vertices.

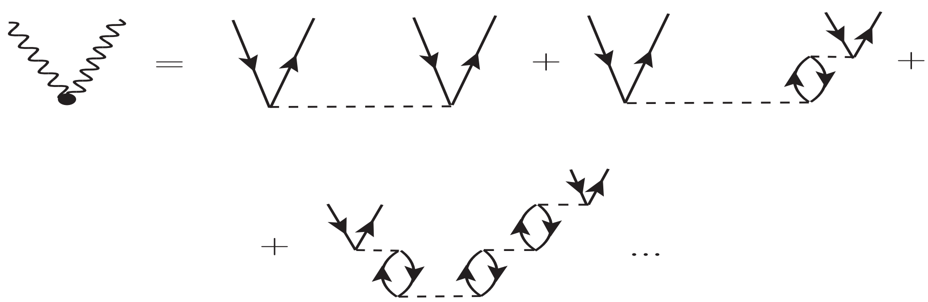

Figure 8.5: Ground state correlations in lowest order in the phonon-phonon interaction

The Hamiltonian can be diagonalized in the full space, yielding the eigenvectors

$$|\Psi_\nu\rangle = \sum_{n\alpha} C^{\nu}_{\alpha} |n \ ; \ \alpha\rangle, \tag{8.35}$$

where the basis states $|n \ ; \ \alpha\rangle$ are given by Eq. (8.7). Using these wave functions, we can compute the transition amplitudes of the one-body operator

$$\mathcal{M}(\lambda) = \sum_{kl} \mathcal{M}_{kl}(\lambda) a^{\dagger}_{k} a_l \ , \tag{8.36}$$

obtaining

$$\mathcal{M}(\lambda, i \to f) = \langle \Psi_{\nu_f} \mid \mathcal{M}(\lambda) \mid \Psi_{\nu_i} \rangle = \sum_{n_i\alpha_i n_f\beta_f} C^{(\nu_i)}_{n_i\alpha_i} C^{(\nu_f)}_{n_f\beta_f} \tag{8.37}$$

$$\times \quad \left[\sum_{k_\lambda} \mathcal{M}_{k_\lambda}(\lambda) \left(\delta_{n_i,(n_f-1)} X^{(\beta_f)}_{\lambda\alpha_i}(n_f) + \delta_{n_i,(n_f+1)} X^{(\alpha_i)}_{\lambda\beta_f}(n_i) \right) + \delta_{n_i,n_f} \sum_{rs} \mathcal{M}_{rs}(\lambda) \rho^{(n_i)}_{\alpha_i\beta_f}(rs) \right] ,$$

where

$$\mathcal{M}_{k_\lambda}(\lambda) = \langle \psi_{k_\lambda\lambda} \mid \mathcal{M}(\lambda) \mid 0 \rangle = \sum_{ph} c_{k_\lambda\lambda}(ph) \mathcal{M}_{ph}(\lambda) \ , \tag{8.38}$$

are the TDA transition amplitudes and $\mathcal{M}_{rs}(\lambda) = \langle s|\mathcal{M}|s\rangle$ is the particle-particle or hole-hole transition matrix elements.

8.2 EMPM in the quasi-particle formalism

In order to extend the method to open shell nuclei, we move from the the particle-hole (ph) to the quasiparticle (qp) formalism by making use of the Bogoliubov transformation. The transformed Hamiltonian becomes

$$H = H_0 + H_{11} + H_{22} + H_{31} + H_{40} + H_{13} + H_{04} \ , \tag{8.39}$$

where

$$\begin{aligned}
H_{11} &= \sum_k E_k \alpha^\dagger_k \alpha_k \ , \\
H_{22} &= \sum_{k_1k_2k_3k_4} H^{22}_{k_1k_2k_3k_4} \alpha^\dagger_{k_1}\alpha^\dagger_{k_2}\alpha_{k_4}\alpha_{k_3} \ , \\
H_{31} &= \sum_{k_1k_2k_3k_4} H^{31}_{k_1k_2k_3k_4} \alpha^\dagger_{k_1}\alpha^\dagger_{k_2}\alpha^\dagger_{k_4}\alpha_{k_3} \ , \\
H_{40} &= \sum_{k_1k_2k_3k_4} H^{40}_{k_1k_2k_3k_4} \alpha^\dagger_{k_1}\alpha^\dagger_{k_2}\alpha_{k_4}\alpha^\dagger_{k_3} \ .
\end{aligned} \tag{8.40}$$

The remaining terms H_{13} and H_{04} are Hermitian conjugates of H_{31} and H_{40}, respectively. The first term is the quasiparticle one-body operator with energies E_k. The other pieces are given by ($k_1 < k_2$, $k_3 < k_4$)

$$\begin{aligned}
H^{22}_{k_1k_2k_3k_4} &= V_{k_1k_2k_3k_4}\Big[u_{k_1}u_{k_2}u_{k_3}u_{k_4} + v_{k_1}v_{k_2}v_{k_3}v_{k_4}\Big] - V_{k_1\bar{k}_3\bar{k}_2k_4}\Big[u_{k_1}v_{k_2}v_{k_3}u_{k_4} + u_{k_2}v_{k_1}u_{k_3}v_{k_4}\Big] \\
&-V_{k_1\bar{k}_4\bar{k}_2k_3}\Big[u_{k_1}v_{k_2}u_{k_3}v_{k_4} + u_{k_2}v_{k_1}v_{k_3}u_{k_4}\Big] \ , \\
H^{31}_{k_1k_2k_3k_4} &= V_{k_1k_2k_3\bar{k}_4}u_{k_1}u_{k_2}u_{k_3}v_{k_4} - \frac{1}{2}\Big[V_{k_1\bar{k}_3\bar{k}_2\bar{k}_4}u_{k_1}v_{k_2}v_{k_3}v_{k_4} - V_{k_2\bar{k}_3\bar{k}_1\bar{k}_4}u_{k_2}v_{k_1}v_{k_3}v_{k_4}\Big] \ , \\
H^{40}_{k_1k_2k_3k_4} &= V_{k_1k_2\bar{k}_3\bar{k}_4}u_{k_1}u_{k_2}v_{k_3}v_{k_4} \ .
\end{aligned} \tag{8.41}$$

As in the ph formalism, we start from the equations of motions

$$\langle n\,;\,\beta|\left[H, O^\dagger_\lambda\right]|n-1\,;\,\alpha\rangle = \left(E^{(n)}_\beta - E^{(n-1)}_\alpha\right) X^\beta_{\lambda\alpha}(n) \ , \tag{8.42}$$

where the TDA phonon operators are now

$$O^\dagger_\lambda = \sum_{r<s} c^\lambda_{rs}\alpha^\dagger_r\alpha^\dagger_r \ . \tag{8.43}$$

By following a procedure analogous to the one adopted for the ph case, we get the eigenvalue equations

$$\sum_{\lambda'\gamma\lambda"\gamma'} A(\lambda\alpha,\lambda'\gamma)\mathcal{D}_\beta(\lambda'\gamma,\lambda"\gamma')C^\beta_{\lambda"\gamma'} = E_\beta\sum_{\lambda'\gamma}\mathcal{D}_\beta(\lambda\alpha,\lambda'\gamma)C^\beta_{\lambda'\gamma} \ , \tag{8.44}$$

where

$$A(\lambda\alpha,\lambda'\gamma) = (E_\lambda + E_\alpha)\delta_{\lambda\lambda'}\delta_{\alpha\gamma} + \sum_{rs}\mathcal{V}_{\lambda\lambda'}(rs)\rho^{(n-1)}_{\alpha\gamma}(rs) \ . \tag{8.45}$$

The phonon-phonon two-body potential has the expression

$$\mathcal{V}_{\lambda\lambda'}(rs) \ = \ \sum_{i<j,l<m} c_\lambda(ij)c_{\lambda'}(lm)\rho_{\lambda\lambda'}(rs)\Big[\delta_{rj}\mathcal{V}(lmsi) - \delta_{ri}\mathcal{V}_{22}(lmsj)\Big] \ , \tag{8.46}$$

where

$$\begin{aligned}\mathcal{V}(lmij) &= V_{lmij}\Big[u_iu_ju_lu_m + v_iv_jv_lv_m\Big] \\ &\quad -V_{\bar{l}i\bar{m}j}\Big[v_iu_ju_lv_m + v_ju_iu_mv_l\Big] + V_{l\bar{j}\bar{m}i}\Big[v_ju_iu_lv_m + v_iu_ju_mv_l\Big] . \end{aligned} \tag{8.47}$$

The above eigenvalue equations are solved iteratively to generate the n-phonon $(n = 1, 2, \cdots)$ basis states. These are used to compute the phonon-phonon coupling terms.

In this case, the matrix elements between n and $(n-1)$-phonon states are given by

$$\begin{aligned}H_{\alpha_{n-1}\beta_n} &= \langle n;\beta|\, H\, |n-1;\alpha\rangle = \langle n;\beta|\, H_{31}\, |n-1;\alpha\rangle = \\ &= \sum_{\lambda\gamma}\mathcal{H}_{\alpha\gamma}(\lambda)X^{(n)}_{\gamma\beta}(\lambda),\end{aligned} \tag{8.48}$$

where

$$\mathcal{H}_{\alpha\gamma}(\lambda) = \sum_{r<sqt} H^{(31)}_{rsqt}c_\lambda(rs)\rho^{(n-1)}_{\alpha\gamma}(tq) , \tag{8.49}$$

and

$$H^{(31)}_{rsqt} = V_{rsq\bar{t}}u_ru_su_qv_t - \frac{1}{2}\Big[V_{r\bar{q}\bar{s}\bar{t}}u_rv_sv_qv_t - V_{s\bar{q}\bar{r}\bar{t}}u_sv_rv_qv_t\Big] . \tag{8.50}$$

The matrix elements between n and $(n-2)$-phonon states have instead the simple form

$$\begin{aligned}H_{\alpha_{n-2}\beta_n} &= \langle n;\beta\,|\, H\, |n-2;\alpha\rangle = \langle n;\beta\,|\, H_{40}\, |n-2;\alpha\rangle = \\ &= \sum_{\lambda\lambda'\gamma}\mathcal{V}(\lambda\lambda')\;\; X^{(n)}_{\gamma\beta}(\lambda)\;\; X^{(n-1)}_{\alpha\gamma}(\lambda') ,\end{aligned} \tag{8.51}$$

where

$$\mathcal{V}(\lambda\lambda') = -\sum_{r<sq<t} H^{40}_{rsqt}c_\lambda(rs)c_{\lambda'}(qt) , \tag{8.52}$$

and

$$H^{40}_{rsqt} = V_{rs\bar{q}\bar{t}}u_ru_sv_qv_t . \tag{8.53}$$

Now, the full Hamiltonian can be diagonalized yielding eigenstates of the form (8.35). These wavefunctions can be used to compute the transition amplitudes

$$\begin{aligned}\mathcal{M}(\lambda, i\to f) &= \langle\Psi_{\nu_f}\mid\mathcal{M}(\lambda)\mid\Psi_{\nu_i}\rangle \\ &= \sum_{n_in_f\alpha_i\beta_f} C^{(\nu_i)}_{n_i\alpha_i}C^{(\nu_f)}_{n_f\beta_f}\langle n_f\beta_f|\mathcal{M}_\lambda|n_i\alpha_i\rangle ,\end{aligned} \tag{8.54}$$

of the one-body operator

$$\mathcal{M}(\lambda) = \sum_{kl}\mathcal{M}_{kl}(\lambda)a^\dagger_k a_l . \tag{8.55}$$

This operator, expressed in terms of qp operators, becomes

$$\begin{aligned}\mathcal{M}(\lambda) &= \sum_{kl}\mathcal{M}_{kl}(\lambda)\Big(u_kv_l\alpha^\dagger_k\alpha^\dagger_{\bar{l}} + v_ku_l\alpha_{\bar{k}}\alpha_l\Big) \\ &+ \sum_{kl}\mathcal{M}_{kl}(\lambda)\Big(u_ku_l\alpha^\dagger_k\alpha_l + v_kv_l\alpha_{\bar{k}}\alpha^\dagger_{\bar{l}}\Big) .\end{aligned} \tag{8.56}$$

After some algebraic manipulations, analogous to the ones made in the ph scheme, we obtain

$$\begin{aligned}
\mathcal{M}(\lambda, i \to f) &= \sum_{a n_i \alpha_i \beta_f} C^{(\nu_i)}_{n_i \alpha_i} \Big[\mathcal{M}_{0a}(\lambda) C^{(\nu_f)}_{n_i+1 \beta_f} X^{(n_i+1)}_{\alpha_i \beta_f}(\lambda) - \mathcal{M}_{a0}(\lambda) C^{(\nu_f)}_{n_i-1 \beta_f} X^{(n_i)}_{\beta_f \alpha_i}(\lambda) \Big] \\
&+ \sum_{n_i \alpha_i \beta_f} C^{(\nu_i)}_{n_i \alpha_i} C^{(\nu_f)}_{n_i \beta_f} \sum_{rs} \mathcal{M}_{rs}(\lambda) \Big(u_r u_s - \tau v_r v_s \Big) \rho^{(n_i)}_{\alpha_i \beta_f}(rs) \; . \qquad (8.57)
\end{aligned}$$

The structure is quite similar to the transition amplitudes 8.38 derived for the ph phonons.

8.3 EMPM in the coupled scheme

The eigenvalue equations keep a simple form even when we move to the coupled $j - j$ scheme. In such a scheme we have

$$H = H_0 + V \; , \qquad (8.58)$$

where

$$\begin{aligned}
H_0 &= \sum_r [r]^{1/2} \epsilon_r \Big(a^\dagger_r \times b_r \Big)^0 , \qquad (8.59) \\
V &= -\frac{1}{4} \sum_{ijkl\Gamma} [\Gamma]^{1/2} V^\Gamma_{rsqt} \Big[\Big(a^\dagger_r \times a^\dagger_s \Big)^\Gamma \times \Big(b_q \times b_t \Big)^\Gamma \Big]^0 , \qquad (8.60)
\end{aligned}$$

where $[\Gamma] = 2\Gamma + 1 = (2J_\Gamma + 1)$ and

$$V^\Gamma_{rsqt} = \langle qt, \Gamma | V | rs, \Gamma \rangle - (-)^{r+s-\Gamma} \langle qt\Gamma | V | sr, \Gamma \rangle \; . \qquad (8.61)$$

It is useful to write the two-body potential in the recoupled form

$$V = \sum_{r<sq<t\sigma} [\sigma]^{1/2} F^\sigma_{rsqt} \Big[\Big(a^\dagger_r \times b_s \Big)^\sigma \times \Big(a^\dagger_q \times b_t \Big)^\sigma \Big]^0 , \qquad (8.62)$$

where

$$F^\sigma_{rsqt} = \sum_\Gamma [\Gamma] (-)^{r+t-\sigma-\Gamma} W(rsqt; \sigma\Gamma) V^\Gamma_{rqst} \; , \qquad (8.63)$$

and $W(rsqt; \sigma\Gamma)$ are Racah coefficients.

We discuss only the method in the quasiparticle formalism, which contains the particle-hole scheme as a particular case. We, then, start with the equations of motion

$$\langle n, \beta \mid \Big\{ \Big[H, O^\dagger_\lambda \Big] \times \mid n-1, \alpha \rangle \Big\}^\beta = \Big(E^{(n)}_\beta - E^{(n-1)}_\alpha \Big) \langle n, \beta \mid \Big\{ O^\dagger_\lambda \times \mid n-1, \alpha \rangle \Big\}^\beta . \qquad (8.64)$$

The qp phonon operator is now

$$O^\dagger_{\lambda\mu} = \sum_{rs} c^\lambda_{rs} \zeta_{rs} (\alpha^\dagger_r \times \alpha^\dagger_s)^\lambda_\mu , \qquad (8.65)$$

where $\zeta_{rs} = [1 + \delta_{rs}]^{1/2}$. Using the Wigner Eckart theorem, we get

$$\langle n, \beta \parallel [H, O^\dagger_\lambda] \parallel n-1, \alpha \rangle = \Big(E^{(n)}_\beta - E^{(n-1)}_\alpha \Big) \langle n, \beta \parallel O^\dagger_\lambda \parallel n-1, \alpha \rangle . \qquad (8.66)$$

The procedure to be followed is similar to the uncoupled case. It is, however, more involved since one has to make a massive use of the Racah algebra. The final result is the eigenvalue equation

$$\sum_{\lambda'\gamma\lambda"\gamma'} A(\lambda\alpha,\lambda'\gamma)\mathcal{D}_\beta(\lambda'\gamma,\lambda"\gamma')C^\beta_{\lambda"\gamma'} = E_\beta \sum_{\lambda'\gamma} \mathcal{D}_\beta(\lambda\alpha,\lambda'\gamma)C^\beta_{\lambda'\gamma} \, , \tag{8.67}$$

where

$$A(\lambda\alpha,\lambda'\gamma) = (E_\lambda + E_\alpha)\delta_{\lambda\lambda'}\delta_{\alpha\gamma} + \sum_\sigma W(\beta\lambda'\alpha\sigma;\gamma\lambda)\mathcal{V}^\sigma_{\lambda\alpha,\lambda'\gamma} \ . \tag{8.68}$$

The phonon-phonon potential is given by

$$\mathcal{V}^\sigma_{\lambda\alpha,\lambda'\gamma} = \sum_{at}^{(\pi)} \mathcal{V}^\sigma_{\lambda\lambda'}(at)\rho_{\alpha\gamma}([a\times t]_\sigma)) \, , \tag{8.69}$$

where

$$\mathcal{V}^\sigma_{\lambda\lambda'}(at) = -[\lambda\lambda'\sigma]^{1/2}(-)^{\lambda+\lambda'+\sigma}\sum_{abrs} W(\lambda' b\sigma a;t\lambda)\zeta_{ab}\zeta_{rs}c^\lambda_{ab}c^{\lambda'}_{rs}\mathcal{V}^{\lambda'}_{rstb} \, , \tag{8.70}$$

and

$$\begin{aligned}\mathcal{V}^{\lambda'}_{rstb} &= V^{\lambda'}_{rstb}\Big(u_r u_s u_t u_b + v_r v_s v_t v_b\Big) \\ &+ F^{\lambda'}_{rstb}\Big(u_r v_s v_t u_b + v_r u_s u_t v_b\Big) - (-)^{t+b-\lambda'}F^{\lambda'}_{rsbt}\Big(u_r v_s u_t v_b + v_r u_s v_t u_b\Big) \, , \end{aligned} \tag{8.71}$$

and the metric matrix is given by

$$\begin{aligned}\mathcal{D}^{(\beta)}(\alpha\lambda;\alpha'\lambda') &= \Big[\langle n-1,\alpha' \mid \times O_{\lambda'}\Big]_{(\alpha'\lambda')\beta}\Big[O^\dagger_\lambda \times \mid n-1'\alpha\rangle\Big]_{(\alpha\lambda)\beta} \\ &= \delta_{\lambda\lambda'}\delta_{\alpha\alpha'} + \sum_\gamma W(\alpha'\lambda\lambda'\alpha;\gamma\beta)X^\alpha_{\gamma\lambda'}(n-1)X^{\alpha'}_{\gamma\lambda}(n-1) \\ &- (-)^{\alpha+\beta+\lambda}\sum_\sigma W(\lambda'\lambda\alpha'\alpha;\sigma\beta)\sum_{rs}\rho^{(\tau)}_{\lambda\lambda'}\big([r\times s]_\sigma\big)\rho^{(\tau)}_{\alpha'\alpha}\big([r\times s]_\sigma\big)_{(n-1)} \, , \end{aligned} \tag{8.72}$$

The n-phonon density matrices ($n>1$) in this formalism take the form

$$\begin{aligned}&\rho^{(n)}_{\alpha\alpha'}\big([r\times s]_\sigma\big) = \langle n;\alpha' \parallel \Big[\alpha^\dagger_r \times \beta_s\Big]_\sigma \parallel n;\alpha\rangle \\ &= [\alpha]^{1/2}\sum_{\lambda\lambda'\gamma}\rho_{\lambda\lambda'}\big([r\times s]_\sigma\big)\, W(\alpha'\sigma\gamma\lambda;\alpha\lambda')C^{(\alpha)}_{\lambda\gamma}(n)\, X^{(\alpha')}_{\lambda'\gamma}(n) \\ &+[\alpha]^{1/2}\sum_{\gamma\gamma'\lambda}(-)^{\alpha-\alpha'+\gamma-\gamma'}W(\alpha'\sigma\lambda\gamma;\alpha\gamma')C^{(\alpha)}_{\lambda\gamma}(n)\, X^{(\alpha')}_{\lambda\gamma'}(n)\rho^{(n-1)}_{\gamma\gamma'}\big([r\times s]_\sigma\big) \, . \end{aligned} \tag{8.73}$$

In case of $n=1$, we clearly have the simplified expression

$$\begin{aligned}\rho_{\lambda\lambda'}([r\times s]^\sigma) &= \langle\lambda' \parallel \Big(\alpha^\dagger_r\times\beta_s\Big)^\sigma \parallel \lambda\rangle \\ &= [\lambda\lambda'\sigma]^{1/2}\sum_t \zeta^{-1}_{ts}c^\lambda_{ts}\zeta^{-1}_{tr}c^{\lambda'}_{tr}W(\lambda' t\sigma s;r\lambda). \end{aligned} \tag{8.74}$$

We have now all the ingredients to solve the eigenvalue equations (8.67) for the n-phonon subspace and, therefore, to generate the multiphonon basis in the $qp\ j-j$ coupled scheme.

In order to complete the program of solving the eigenvalue problem in the full multiphonon space, we have to compute the matrix elements between phonon states with different numbers of phonon. For the $(n-1)$-n coupling we have

$$\begin{aligned} H_{\alpha_{n-1}\beta_n} &= \langle n;\beta|\,H\,|n-1;\alpha\rangle = \\ &= [\beta]^{-1}\sum_{\sigma\gamma}(-)^{\beta+\gamma+\sigma}\mathcal{V}^{\sigma}_{\alpha\gamma}X^{(\beta)}_{\sigma\gamma}(n)\ , \end{aligned} \tag{8.75}$$

where

$$\mathcal{V}^{\sigma}_{\alpha\gamma} = \sum_{tq}\mathcal{V}^{\sigma}_{tq}(\pi)\rho^{(n-1)}_{\alpha\gamma}([t\times q]^{\sigma})\ , \tag{8.76}$$

and

$$\mathcal{V}^{\sigma}_{tq}(\pi) = \sum_{rs}^{(\pi)} c^{\sigma}_{rs}(\pi)\zeta_{rs}V^{\sigma}_{rstq}\big(u_r u_s v_t u_q - v_r v_s u_t v_q\big)\ . \tag{8.77}$$

The $(n-2)$-n coupling term is given also in this case by a simpler formula

$$\langle n,\beta|H|n-2,\alpha\rangle = [\beta]^{-1}\sum_{i_\sigma k_\sigma\sigma\gamma}(-)^{\beta+\gamma+\sigma}X^{\beta}_{(i_\sigma\sigma)\gamma}(n)X^{\gamma}_{(k_\sigma\sigma)\alpha}(n-1)\mathcal{V}_{\sigma}(i_\sigma k_\sigma)\ , \tag{8.78}$$

where

$$\mathcal{V}_{\sigma}(i_\sigma k_\sigma) = \sum_{rstq}^{\pi}\zeta_{rs}\zeta_{tq}V^{\sigma}_{rstq}c^{i\sigma}_{rs}c^{k\sigma}_{tq}u_r u_s v_t v_q\ . \tag{8.79}$$

Now, the full Hamiltonian matrix can be constructed and brought to diagonal form. The eigenstates have the same form as in the $m-$scheme, namely

$$|\Psi_\nu\rangle = \sum_{n\alpha}C^{\nu}_{\alpha}|n\ ;\ \alpha\rangle, \tag{8.80}$$

to be used for the calculation of the transition amplitudes.

In the coupled scheme the one-body operator has the form

$$\mathcal{M}(\lambda\mu) = \frac{1}{[\lambda]^{1/2}}\sum_{rs}\langle r\parallel F_\lambda\parallel s\rangle\Big[a^\dagger_r\times b_s\Big]_{\lambda\mu}\ , \tag{8.81}$$

which, in terms of qp, becomes

$$\begin{aligned} \mathcal{M}(\lambda\mu) &= -\frac{1}{[\lambda]^{1/2}}\sum_{r\le s}\langle r\parallel F_\lambda\parallel s\rangle(u_r v_s+\tau u_s v_r)\zeta^{2}_{rs}\Big[\alpha^\dagger_r\times\alpha^\dagger_s\Big]_{\lambda\mu} \\ &+ \frac{1}{[\lambda]^{1/2}}\sum_{r\le s}\langle r\parallel F_\lambda\parallel s\rangle(v_r u_s+\tau u_r v_s)\zeta^{2}_{rs}\Big[\beta_r\times\beta_s\Big]_{\lambda\mu} \\ &+ \frac{1}{[\lambda]^{1/2}}\sum_{rs}\langle r\parallel F_\lambda\parallel s\rangle(u_r u_s-\tau v_r v_s)\Big[\alpha^\dagger_r\times\beta_s\Big]_{\lambda\mu}\ . \end{aligned} \tag{8.82}$$

Making use of the expression (8.80) of the total wavefunction, we obtain the transition amplitudes

$$\langle f J_f \parallel \mathcal{M}(\lambda) \parallel i J_i \rangle = \sum_{n_i \beta_i n_f \beta_f} C_{J_f}^{(f)}(n_f \beta_f) C_{J_i}^{(i)}(n_i \beta_i) \langle n_f; \beta_f J_f \parallel \mathcal{M}(\lambda) \parallel n_i; \beta_i J_i \rangle \ , \tag{8.83}$$

where

$$\begin{aligned}
&\langle n_f; \beta_f J_f \parallel\mid \mathcal{M}(\lambda) \parallel n_i; \beta_i J_i \rangle = [\lambda]^{-1/2} \\
&\times \Big[\delta_{n_f n_i} \sum_{rs} \langle r \parallel \mathcal{M}(\lambda) \parallel s \rangle (u_r u_s - \tau v_r v_s) \rho_{\beta_i \beta_f}^{(n_i)} \left([r \times s]_\lambda \right) \\
&\quad + \sum_k \mathcal{M}_{(k\lambda)} \Big(\delta_{n_f (n_i+1)} X_{\beta_i \beta_f}^{(n_f)}(k\lambda) + \delta_{n_f (n_i-1)} (-)^{J_f - J_i + \lambda} X_{\beta_f \beta_i}^{(n_i)}(k\lambda) \Big) \Big] \ ,
\end{aligned} \tag{8.84}$$

and

$$\begin{aligned}
\mathcal{M}_{(k\lambda)} &= \langle k\lambda \parallel \mathcal{M}(\lambda) \parallel 0 \rangle = \\
&= \sum_{r \leq s} c_{rs}^{(\beta_f \lambda)} \langle r \parallel F_\lambda \parallel s \rangle \zeta_{rs} (u_r v_s + \tau u_s v_r) \ ,
\end{aligned} \tag{8.85}$$

are the TDA transition amplitudes.

Chapter 9

Numerical implementation

In this chapter, the practical implementation of the Equation of Motion Phonon Model method is presented. We will work in the $j-j$ coupled scheme, and will refer to the formulas in the quasiparticle formalism. In fact, the *ph* expressions can be seen as a particular case of *qp* ones.

The calculation goes through several steps. First, one has to perform the following preliminary operations :

i. Solve the TDA eigenvalue equations (7.20) ($n = 1$) and obtain the eigenvalues E_λ and the eigenstates $\mid \lambda\rangle$ in terms of the expansion coefficients $c_\lambda(ph)$.

ii. Compute the density matrix $\rho_{\lambda\lambda'}(kl)$ using Eq. (8.74).

iii. Compute the matrix elements of the renormalized interaction $\mathcal{V}_{\lambda\lambda'}$ given by Eqs. (8.70).

The quantities E_λ, $\rho_{\lambda\lambda'}(kl)$ and $\mathcal{V}_{\lambda\lambda'}$ are the input for the iterative procedure.

for $n = 2, 3, \cdots$

- **i.** Using $\rho^{(n-1)}$ and $X(n-1)$, compute the metric matrix $\mathcal{D}$ of Eq. (8.72).
- **ii.** Perform the Cholesky decomposition of $\mathcal{D}$, to extract the linear independent $O^\dagger_\lambda|(n-1),\alpha\rangle$ states, and the corresponding reduced metric matrix, $\mathcal{D}_n$.
- **iii.** Using E_λ, $\rho^{(n-1)}$ and $\mathcal{V}$, compute the matrix $\mathcal{A}$ (8.68).
- **iv.** Construct the inverse matrix $\mathcal{D}_n^{-1}$ and perform the matrix multiplication $\mathcal{D}_n^{-1}(AD)_n$.
- **v.** Solve the generalized eigenvalue problem (8.29) for the n-phonon subspace.
- **vi.** Compute the density matrix $\rho^{(n)}$ through Eq. (8.73).

end n

It must be stressed that no approximations have been made in generating such a multiphonon basis. On the other hand, the number of redundant states increases very rapidly with the number of phonons. Though eliminated at the end of the process, they enter in the recursive formulas defining the different quantities contained in the matrices A and $\mathcal{D}$. This has the effect of slowing down considerably the procedure if we keep all the basis states. One possibility for a future development of the method is to investigate whether only the most collective TDA phonons $\mid \lambda\rangle$ contribute, in order to truncate severely the dimension of the other n-phonon subspaces.

Once generated, the multiphonon basis can be used to complete the construction of the Hamiltonian by computing the non diagonal matrix elements (8.75) and (8.78). The full Hamiltonian eigenvalue problem can then be solved, yielding the eigenvectors of Eq. (8.80)

9.1 Spurious states

As in any microscopic approach, we have to face the problem of the occurrence of spurious admixtures in the multiphonon basis induced by the center of mass (CM) motion. Moreover, since we adopt the BCS quasiparticle formalism, we have to remove additional spuriosity due the non conservation of the particle number.

9.1.1 Elimination of the center of mass motion

A longstanding and not entirely solved problem, appearing systematically in microscopic calculations, is the removal of the center of mass (CM) motion. This problem was first studied by Elliot and Skyrme in (113) and is caused by the SM mean field potential which breaks the translational invariance of the nuclear Hamiltonian. Thus the eigenstates of the SM Hamiltonian contain in general spurious components of CM excitation.

Elliot and Skyrme have shown that the problem is solvable exactly if, in a SM calculation, the unperturbed Hamiltonian H_0 is a purely harmonic oscillator Hamiltonian (113). In such a case one can easily decompose H_0 into an intrinsic and a CM pieces

$$H_0 = H_{intr} + H_{CM} \ , \tag{9.1}$$

where

$$\begin{aligned} H_{intr} &= \sum_{ij}[\frac{1}{2mA}(\vec{p}_i - \vec{p}_j)^2] + \frac{1}{2}mA\omega^2 \sum_{ij} (\vec{r}_i - \vec{r}_j)^2 \ , \\ H_{CM} &= \frac{\vec{P}^2}{2Am} + \frac{1}{2}mA\omega^2 \vec{R}^2 \ . \end{aligned} \tag{9.2}$$

Thus, the eigenfunctions factorize as follow

$$\Psi(\vec{q}, \vec{R}) = \phi_\mu^{intr.}(\vec{q})\phi_N^{CM}(\vec{R}) \ , \tag{9.3}$$

where $\vec{q}$ stands for all the intrinsic coordinates. The physical states are the ones in which the CM is kept in the ground state $\phi_N^{CM}(\vec{R})$.

When we include the two-body part V of the nuclear Hamiltonian, we need to tag the CM excited states. To this purpose, one considers the Hamiltonian

$$H_g = H + H_g^{(CM)} \ , \tag{9.4}$$

where

$$\begin{aligned} H &= H_{intr} + V \ , \\ H_g^{(CM)} &= gH^{(CM)} \ , \end{aligned} \tag{9.5}$$

and g is a positive number. The eigenvalue equation, for such an Hamiltonian, is

$$H\Psi_{\nu N} = \left[H + H_g^{(CM)}\right]\Psi_{\nu N} = E_{\nu N}\Psi_{\nu N} \ , \tag{9.6}$$

with eigenvalues

$$E_{\nu N} = E_\nu + \frac{g}{A}\hbar\omega\left(N + \frac{3}{2}\right) \ , \tag{9.7}$$

and eigenfunctions

$$\Psi_{\nu N} = \psi_\nu \Phi_N \ . \tag{9.8}$$

For a sufficiently large value of g, the CM excited states are well separated in energy from those corresponding to intrinsic excitations only. We can therefore keep only the states in which the CM is in the ground state

$$\Psi_{\nu 0} = \psi_\nu \Phi_0 \; . \tag{9.9}$$

This prescription was proposed by Palumbo (114) and applied by Glockner and Lawson (115) to the Shell Model. The procedure, however, works only approximately when the spin-orbit and l^2 terms are added to the harmonic oscillator Hamiltonian.

Moreover, referring the SM basis states to a fixed frame, in order to get the factorization of the wavefunction in the form given by Eq. (9.8) it is necessary to use a complete set of basis states up to a given major shell N. If, for instance, we consider unperturbed excitations up to 3-$\hbar\omega$, all SM states up to $N = 3$ must be included. Only the use of such a complete set of states guaranties the factorization of the eigenstates into an intrinsic and a CM components.

This constraint is overcome in the EMPM, where the CM spurious mode can be disposed of in the preliminary stage of TDA.

In TDA, in fact, the separation of the CM from the intrinsic motion is achieved, exactly in light and approximately in heavy nuclei, no matter how large is the ph space. Let us, in fact, express $H_g^{(CM)}$ in terms of nucleon coordinates

$$H_g^{(CM)} = \sum_i h_i^{(c.m.)} + \sum_{i<j} v_{ij}^{(c.m.)} \; , \tag{9.10}$$

where

$$h_i^{(c.m.)} = \frac{1}{2m_{c.m.}} p_i^2 + \frac{1}{2} m_{c.m.} \omega_{c.m.}^2 r_i^2 \; , \tag{9.11}$$

$$v_{ij}^{(c.m.)} = \frac{1}{m_{c.m.}} \mathbf{p}_i \cdot \mathbf{p}_j + m_{c.m.} \omega_{c.m.}^2 \mathbf{r}_i \cdot \mathbf{r}_j \; , \tag{9.12}$$

having defined

$$m_{c.m.} = \frac{A}{g} m \; , \qquad \omega_{c.m.} = \frac{g}{A} \omega \; . \tag{9.13}$$

The first piece (9.11) is a one-body term which renormalizes the single-particle energies and can be ignored. The second one (9.12) is a separable dipole-dipole potential. The corresponding TDA matrix is then

$$A(ph; p'h') = [\epsilon_p - \epsilon_h]\, \delta_{hh'} \delta_{pp'} \; + V_{p'\bar{h}\bar{h}'p} \; + V^{(g)}_{p'\bar{h}\bar{h}'p} \; , \tag{9.14}$$

where

$$V^{(g)}_{p'\bar{h}\bar{h}'p} = 2 \frac{g-1}{A} m\omega^2 \sum_\mu \Big[\langle p \mid x_\mu \mid \bar{h} \rangle \langle \bar{h}' \mid x_{\bar{\mu}} \mid p' \rangle - \langle p \mid x_\mu \mid \bar{p}' \rangle \langle \bar{h}' \mid x_{\bar{\mu}} \mid \bar{h} \rangle \Big] \; . \tag{9.15}$$

The above formula shows that the dipole operator can couple only 1-$\hbar\omega$ ph states in the direct channel. The exchange term contributes only in the presence of spin-orbit intruders. Thus, in light nuclei, the ph states of energy higher than 1-$\hbar\omega$ are not affected by the CM Hamiltonian.

In heavy nuclei, few ph states can be coupled by the exchange terms. Thus, in these nuclei, the removal of the CM motion, according to the prescription outlined above, can be achieved only approximately.

On the other hand, at the level of Tamm-Dancoff, one can resort to a simpler method, which is valid in general. Let us observe, in fact, that in TDA the center of mass wavefunction has the structure

$$\Phi_1 = \mathcal{N} \vec{R} |0\rangle \; , \tag{9.16}$$

where $\mathcal{N}$ is a normalization factor. We can therefore construct a *ph* basis orthogonal to the spurious component, Φ_1, with the Gram-Schmidt procedure. Passing to this base, we obtain TDA phonons not contaminated by the CM motion. This states will be used in building the multiphonon states of the EMPM, which thereby result free of CM spuriosity.

The extent of CM contaminations can be quantified computing the strength

$$B(R) = | < \lambda|\Phi_1 > |^2 = \mathcal{N}^2| < \lambda|\vec{R}|0 > |^2 \; . \tag{9.17}$$

This quantity is plotted in Figs. 9.1, for TDA calculation in ^{20}O. When the CM motion is

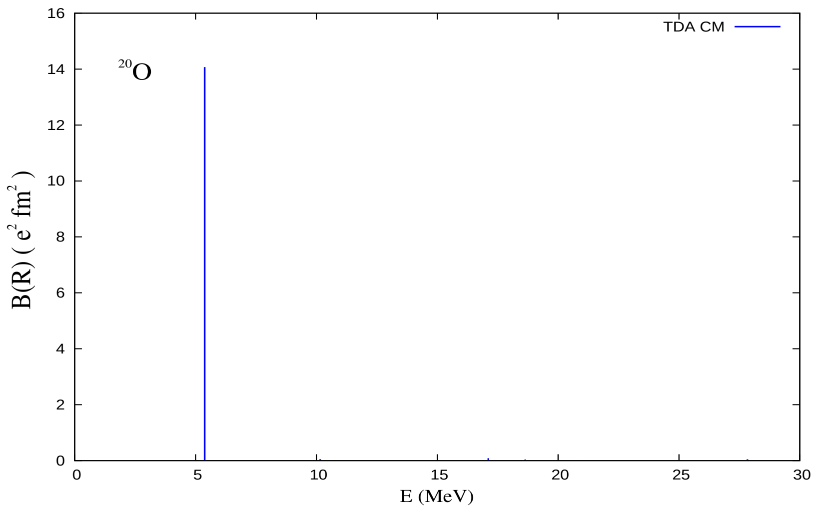

Figure 9.1: Center of mass translational strength in a TDA calculation for ^{20}O.

not removed, one gets a huge peak corresponding to the excitation of the CM and other small peaks whose height gives an indication of the CM contamination in each TDA state. These spurious peaks disappear when the CM is removed by one of the mentioned prescriptions.

The CM motion can be removed also in RPA, if a HF basis is adopted (72). In such a case, in fact, the CM mode fall at zero energy and, therefore, can be removed. It is to be said, however, that the CM energy goes to zero only if a huge *ph* space is adopted (116), which is not the case in most calculations. It is then safer to resort to the mentioned methods even in RPA.

9.1.2 Removal of the number operator spuriosity

The Gram-Schmidt orthogonalization procedure has been also adopted to eliminate the spurious admixtures originated from the breaking of the number of particle symmetry. The BCS quasiparticle vacuum is not an eigenstate of the particle number operator $\hat{n} = \sum_i a_i^\dagger a_i$. It follows that $\hat{n}$ couples the TDA two-quasiparticle basis states to the BCS vacuum. In order to eliminate this contamination we construct the normalized spurious state

$$|\Phi_0\rangle = \frac{1}{N_0}\hat{n}|0\rangle = \frac{1}{N_0}\sum_a C_a \mathcal{A}^\dagger(aa0)|0\rangle = \frac{1}{N_0}\sum_a C_a|a^2 0\rangle \; , \tag{9.18}$$

where

$$|a^2 0\rangle = \frac{1}{(2)^{1/2}}\left(\alpha_a^\dagger \times \alpha_a^\dagger\right)^{J=0}|0\rangle \; , \tag{9.19}$$

are the two-quasiparticle states coupled to $J = 0$, N_0 is the normalization constant and

$$C_a = (2(2a+1))^{1/2}\, u_a v_a \; . \tag{9.20}$$

We use a Schmidt orthogonalization to generate $n-1$ $\{|\Phi_i\rangle\}$ states, orthogonal to the spurious component, $|\Phi_0\rangle$

$$
\begin{aligned}
|\Phi_0\rangle &= \tfrac{1}{N_0(1)} \textstyle\sum_{i=1}^{n} C_i |a_i^2 0\rangle \ , \\
|\Phi_1\rangle &= \tfrac{1}{N_0(1)N_0(2)} \left[N_0^2(2)|a_1^2 0\rangle - \textstyle\sum_{i=2}^{n} C_1 C_i |a_i^2 0\rangle\right] \ , \\
|\Phi_2\rangle &= \tfrac{1}{N_0(2)N_0(3)} \left[N_0^2(3)|a_2^2 0\rangle - \textstyle\sum_{i=3}^{n} C_2 C_i |a_i^2 0\rangle\right] \ , \\
\cdots &= \cdots \ , \\
|\Phi_{n-1}\rangle &= \tfrac{1}{N_0(n-1)N_0(n)} \left[N_0^2(n)|a_{n-1}^2 0\rangle - C_{n-1} C_n |a_n^2 0\rangle\right] \ ,
\end{aligned}
\tag{9.21}
$$

with

$$
N_0(k) = \left(\sum_{i=k}^{n} C_i^2\right)^{1/2} \ . \tag{9.22}
$$

As for the CM case, the states belonging to this base are free of spuriosity and allows the construction of multiphonon states which are not contaminated. Even here, a quantitative estimate of the qp spurious admixtures is provided by the strength

$$
B(N) = | < \lambda|\hat{n}|0 > |^2 \ , \tag{9.23}
$$

which has several peaks corresponding to the TDA basis states, if the spuriosity is not removed.

9.2 Nuclear response to external fields

The properties of collective modes can be investigated through the nuclear response to external probes. To this purpose it is useful to compute the strength functions

$$
\begin{aligned}
\mathcal{S}(E\lambda,\omega) &= \sum_\nu B_\nu(E\lambda)\,\delta(\omega-\omega_\nu) \\
&\approx \sum_\nu B_\nu(E\lambda)\,\rho_\Delta(\omega-\omega_\nu),
\end{aligned}
\tag{9.24}
$$

where ω is the energy variable, ω_ν the energy of the transition of multipolarity $E\lambda$ from the ground to the ν_{th} excited state $\Psi_\lambda^{(\nu)}$ of spin $J=\lambda$, and

$$
\rho_\Delta(\omega-\omega_\nu) = \frac{\Delta}{2\pi}\frac{1}{(\omega-\omega_\nu)^2+(\frac{\Delta}{2})^2} \ , \tag{9.25}
$$

is a Lorentzian of width Δ, which replaces the δ function as a weight of the reduced transition probability

$$
B_\nu(E\lambda) = \sum_\mu |\langle\Psi_{\nu\lambda\mu}|\mathcal{M}(E\lambda\mu)|\Psi_0\rangle|^2 \ . \tag{9.26}
$$

For all the $E\lambda$ transitions, we adopt the standard multipole operator

$$
\mathcal{M}(E\lambda\mu) = \frac{e}{2}\sum_{i=1}^{A}(1-\tau_3^i) r_i^\lambda Y_{\lambda\mu}(\hat{r}_i) \ , \tag{9.27}
$$

where $\tau_3 = 1$ for neutrons and $\tau_3 = -1$ for protons.

It may be also useful in some cases to compute the running sums

$$\begin{aligned} \Sigma_0^{(N)}(E\lambda) &= \sum_{i=1}^{N} B_{\nu_i}(E\lambda), \\ \Sigma_1^{(N)}(E\lambda) &= \sum_{i=1}^{N}(E_i - E_0)B_{\nu_i}(E\lambda). \end{aligned} \tag{9.28}$$

In the limit $N \to \infty$, the two sums define the $m_0(E\lambda)$ and $m_1(E\lambda)$ momenta. They are just the non-energy and energy-weighted sums of the $E\lambda$ operator.

For a Hamiltonian which does not contain momentum dependent and exchange potentials, the following standard formula (72; 74) holds

$$\begin{aligned} S_{EW}(E\lambda) &= \frac{1}{2}\sum_{\mu}\langle[\mathcal{M}^{\dagger}(E\lambda\mu,\tau),[H,\mathcal{M}(E\lambda\mu,\tau)]]\rangle \\ &= \frac{\lambda(2\lambda+1)^2}{16\pi}\frac{\hbar^2}{2m}A\langle r^{2\lambda-2}\rangle \ . \end{aligned} \tag{9.29}$$

For the dipole operator, the above formula yields

$$S_{EW}(E1) = \frac{9}{16\pi}\frac{\hbar^2}{2m}A \ , \tag{9.30}$$

which is the well known Thomas-Reiche-Kuhn sum rule for N=Z nuclei. For a generic multipole, if constant density and sharp surface are assumed, we get

$$\langle r^n \rangle = \frac{3}{3+n}R^n \ , \tag{9.31}$$

with $R = 1.2A^{1/3}$. Thus, the EWSR is practically insensitive to ground state correlations. Because of this property, it is often consider a benchmark for many theoretical and experimental investigations.

9.3 Application of the EMPM to nuclear collective excitations

Our calculations will focus mainly on the study of the giant dipole resonance (GDR). This is the most famous and most studied nuclear resonance observed in all nuclei. It appears as a large hump of width $\sim$ 5 MeV around a main peak (117; 118; 119). Its centroid lies at an energy

$$E_{1^-}^{(GR)} \sim 79A^{-1/3}. \tag{9.32}$$

It has clearly an isovector character. In fact, Eq. (9.27) shows that the isoscalar component of the dipole operator is just proportional to the CM coordinates. In the classical context (120; 121), indeed, it originates from a translational oscillation of proton versus neutron fluids (Fig. 9.2).

The GDR cross section is given by

$$\sigma_{int} = \int_{E_0}^{E_1} \sigma(\omega)d\omega = \frac{16\pi^3 e^2}{9\hbar c}\int_{E_0}^{E_1} \omega\mathcal{S}(E1,\omega)d\omega \ , \tag{9.33}$$

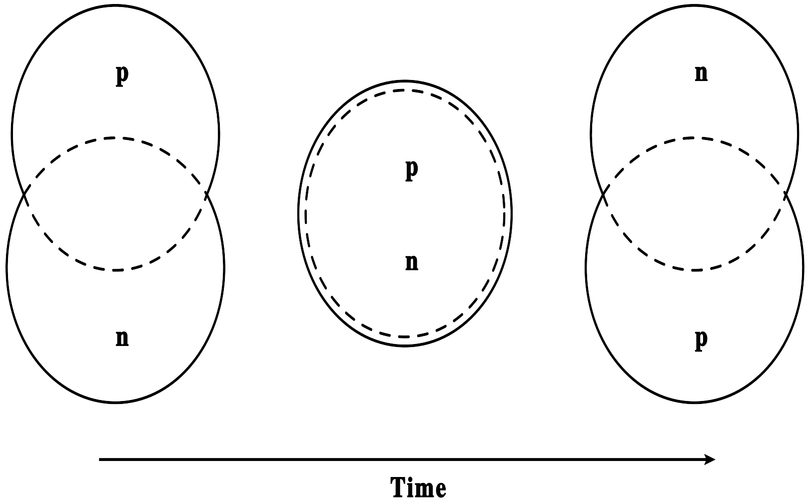

Figure 9.2: GDR vibration : Schematic picture of the GDR in the Goldhaber and Teller model, (120).

where ω_ν are the $E1$ excitation energies. When integrated from $E_0 = 0$ to $E_1 = \infty$, σ_{int} may be compared with the Thomas-Reiche-Khun (TRK) sum rule

$$\sigma_{TRK} = 60\frac{NZ}{A}(\text{MeV mb}) \,. \tag{9.34}$$

The GDR exhausts more than 100 % of the TRK sum rule. The contribution in excess comes from velocity dependent and exchange terms of the two-body nuclear potential.

In nuclei with neutron excess, a weaker resonance should appear around the neutron threshold. This is called Pygmy dipole resonance (PDR) and is supposed to originate from a translational oscillation of the neutron skin against the core. The motion is illustrated in Fig. 9.3.

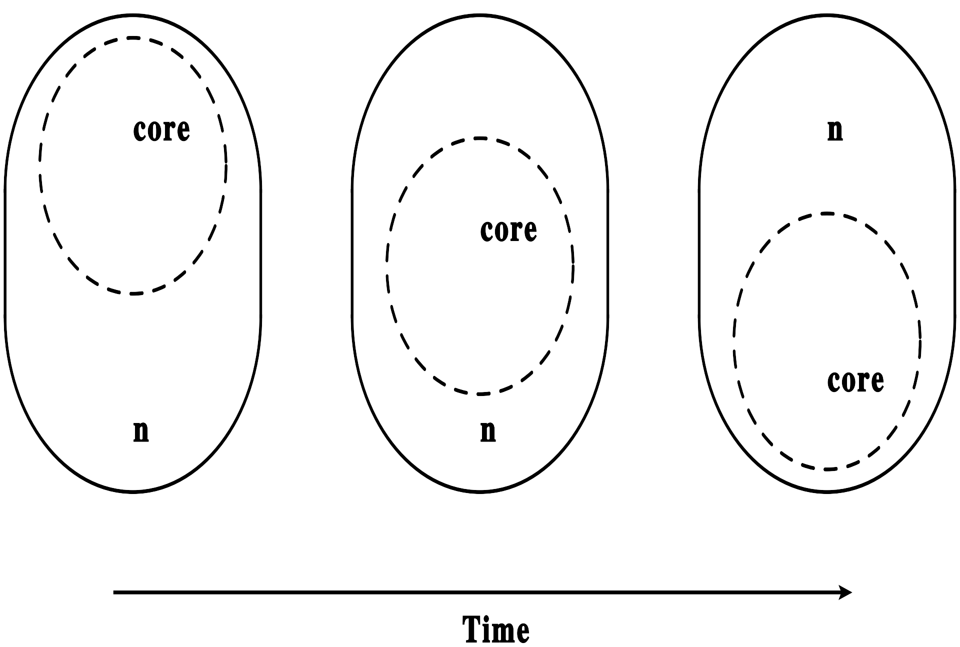

Figure 9.3: PDR interpretation as a translational oscillation of neutron skin against the core.

This is the picture proposed by the many theoretical investigations performed in recent years (see (122) for a review). Experiments on radioactive neutron-rich nuclei seem to support this assumption and experimental investigations (123)-(129).

The interest of studying this excitation mechanism goes beyond the field of theoretical nuclear structure physics. In fact, it has been pointed out that a systematic appearance of low-lying dipole strength in neutron-rich nuclei may affect the estimate of element abundances in the r-process of the nucleosynthesis (130).

The EMPM is an ideal tool for testing the proposed interpretation of the phenomenon. It can ascertain if the mode comes from the *ph* dipole channel only or gets contribution also from more complex excitations.

We will use the EMPM in the *ph* formalism to study the GDR in the double-magic ^{16}O. We will then adopt the same method in its quasiparticle version to study both the GDR and the PDR in the neutron rich nuclei $^{18-22}$O.

9.3.1 GDR in ^{16}O

^{16}O was already studied within the EMPM in its old version (131). Here it is used as a testing ground for the new formulation of the method.

In spite of being double magic, in fact, this nucleus has a very complex structure and represents an ideal benchmark for testing nuclear models. Shell model and mean-field calculations describing its properties were performed already in the sixties (132; 133). It was shown that treating the low-lying parity states as $4p-4h$ deformed configurations qualitatively explains the observed energy spectrum.

Useful information on the phonon structure of the states in ^{16}O was provided by Feshbach and Iachello in a schematic approach based on the interacting Boson model (134; 135).

The first large scale SM calculation was performed by Haxton and Johnson (136) in a SM space including excitations up to $4\hbar\omega$. They pointed out the crucial role of $2p-2h$ and $4p-4h$ configurations in the low lying spectrum and the extreme importance of the coupling between the vacuum and the $2p-2h$ configurations as well as between $2p-2h$ and $4p-4h$ subspaces. The importance of neglecting the monopole self-energy terms was stressed by Warburton and Brown (137).

Recently, the SM space was enlarged so as to include $6p-6h$ states in a no core SM calculation of the ground state only(138).

The importance role played by $3p-3h$ on the low-lying negative parity levels in ^{16}O was stressed by a calculation carried out within the old version of the EMPM (90; 131).

Here, our EMPM calculations will focus on the study of the giant dipole resonance (GDR). This has been studied recently in the second RPA (139) using a density dependent Skyrme potential.

We will investigate the effect of the coupling of this mode to complex configurations described by multiphonon states. The crucial importance of taking explicitly into account the ground state correlations will be pointed out. We will also show how our results compare with the experiments.

We will use realistic two-body potentials, like a Brueckner G-matrix derived from the CD-Bonn NN potential, or a V_{low_k} derived from several NN interactions. We threat the Hamiltonian in both Nilsson and HF bases. The configuration space used includes up to the (p, f) shells. The number of states increases very rapidly as we increase the number of phonons. Thus, while keeping all two-phonon states, we were forced to truncate the $n = 3$-phonon space by keeping all the states up some maximum energy value.

When the Nilsson basis is adopted, the TDA strength is peaked around ~ 22 MeV, in agreement with experiments. The strength distribution does not change in going from the TDA to the multiphonon spaces(Fig. 9.4). The strength, however, is pushed up in energy by ~ 16 MeV if the two-phonon space is added. It is shifted again downward when we include the $n = 3$-phonon states. The downward shift increases as we bring the energy-cut threshold from 25 to 30 MeV. In order to determine the complete shift we should go further and include all $n = 3$-phonon states. This, however, would require too long computing time.

If we shift downward the energy of the peaks by hands, we get a cross section in good agreement with experiments (Fig. 9.5).

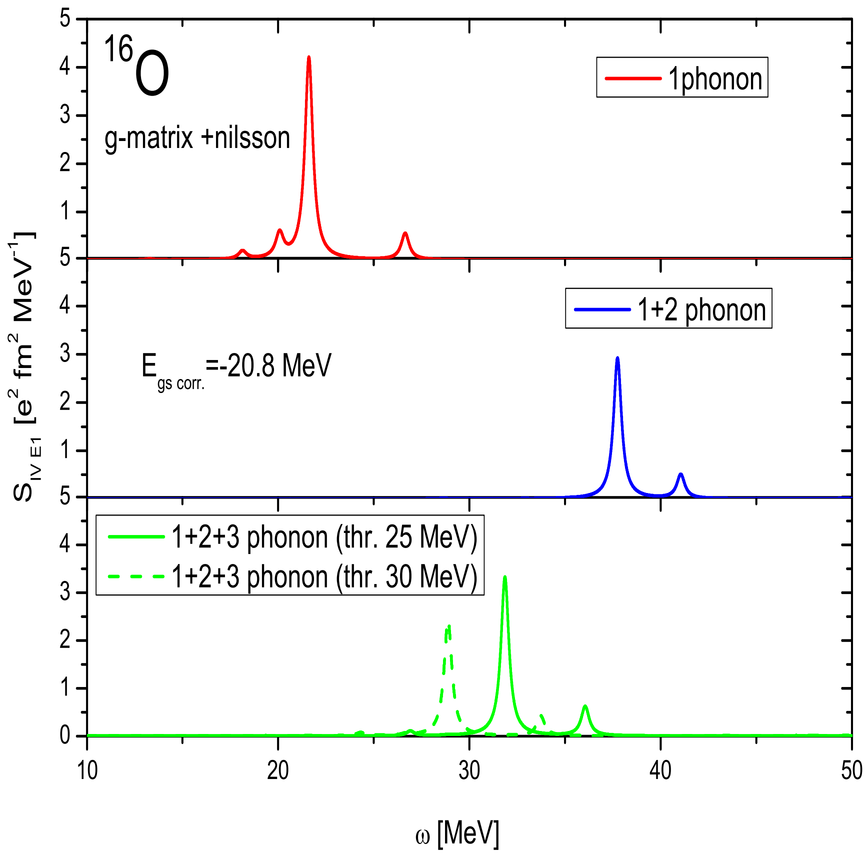

Figure 9.4: $E1$ strength function calculated using a Nilsson basis in ^{16}O. The calculations for the 3-phonon space have been done with two different energy treshold. The observed energy shift is discussed in the text.

If a HF basis is adopted, the $E1$ response gets considerably more fragmented already at the TDA level, as shown in Fig. 9.6. The peak, however, is several MeV above the experimental one. The phonon coupling is much weaker than in the Nilsson basis. In fact, the $n = 2$-phonon space pushes further up the peaks by ~ 5.5 MeV only, while $n = 3$-phonon states bring the strength back to the TDA energies. The net result is that the GDR remains centered around ~ 30 MeV, well above the experimental peak.

The mechanism responsible for this energy shifts can be understood if we have in mind that the coupling between the spaces differing by two phonons is much stronger than the one between spaces differing by one-phonon. This implies that the ph vacuum $|0\rangle$ is strongly coupled to the $|n = 2, \alpha\rangle$ two-phonon states, the one-phonon states $|\lambda\rangle$ couple strongly to the three-phonon states $|n = 3, \alpha\rangle$ and so on.

It follows that, if the space includes up to two-phonon states, only the ground state is pushed down in energy while the one-phonon states are little affected. The one-phonon states

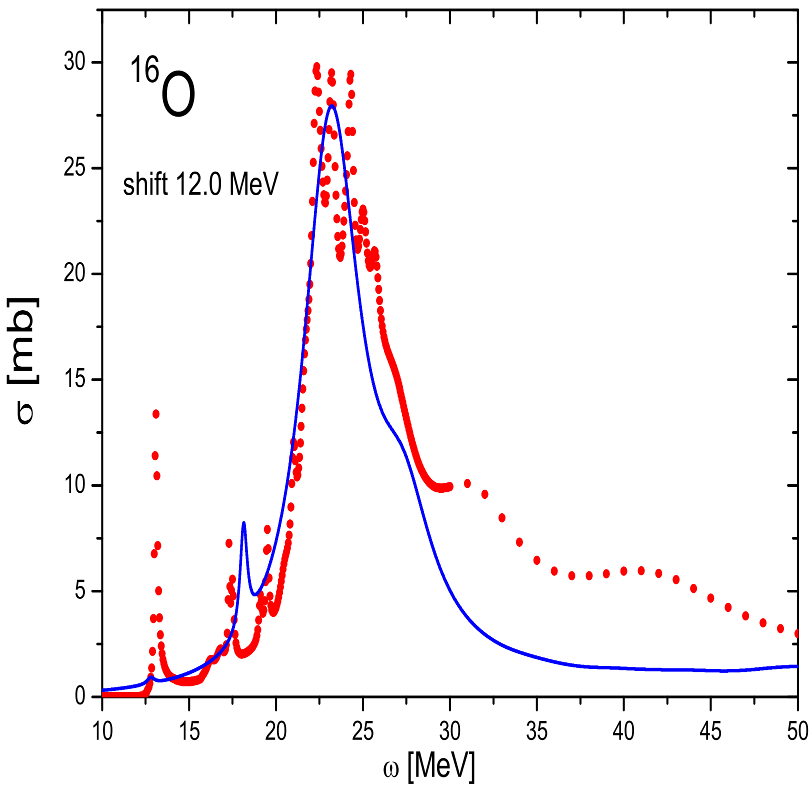

Figure 9.5: EMPM versus experimental $E1$ cross section in ^{16}O.

are pushed down once the three-phonon states are included.

This hierarchy in the phonon coupling is also reflected in the phonon composition of the total wavefunctions. As shown in Fig. 9.7, the ground state is dominantly composed of the ph vacuum with a large two-phonon component ($\sim 25\%$). The amplitudes of the $n = 1$ and $n = 3$-phonon components are negligible.

If we consider the other two 0^+_2 states, we observe that both of them have a dominant two-phonon component. This couples strongly to the four-phonon states. Thus, in order to push down the energy of the excited 0^+ states toward the experimental energies we need to include up to the $n = 4$-phonon subspace, at least. This is consistent with the results obtained in the large scale shell model calculations by Haxton and Johnson (136).

Let us now look at the 1^- excitation. From Fig. 9.8 one can see that the first two 1^- states, including the one corresponding to the strongest peak, have a dominant one-phonon structure. This explains why the strength distribution is little affected by the multiphonon states. Only the third one has a large three-phonon component suggesting a strong coupling to the $n = 5$-phonon space.

9.3.2 E1 response in neutron rich O isotopes

The oxygen isotopic chain has been object of several investigations aiming at establishing the neutron drip-line in this light region. In spite of theoretical calculations (140; 141), which predicted the stability of ^{26}O and ^{28}O, the neutron drip line was shown to be located at $A = 24$

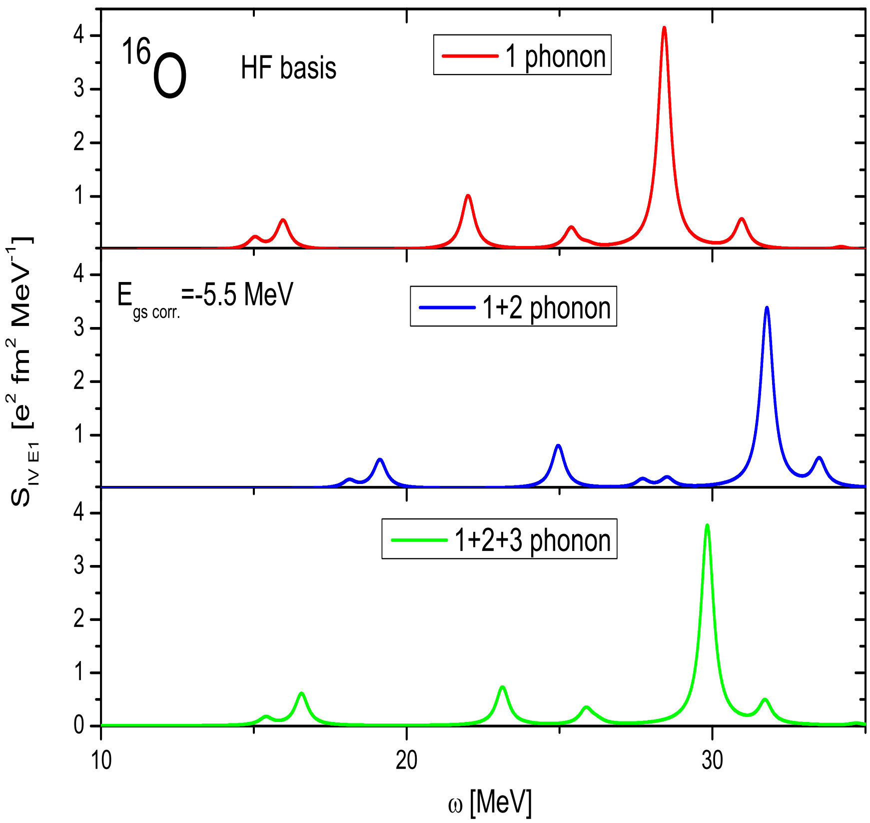

Figure 9.6: $E1$ strength function calculated using a HF basis in ^{16}O.

(142; 143).

Among the studies focused on the oxygen isotopes, few of them were devoted to the $E1$ response. Their goal was to investigate how the energy distribution of the $E1$ strength evolves as the number of valence neutrons increases. Special effort was paid to the search of low-energy peaks around the neutron threshold and to their characterization.

An experiment was performed in Ref. (144), where the dipole response of the $^{18-22}$O up to an excitation energy of 30 MeV was investigated. It was found that, in all neutron-rich oxygen isotopes investigated, the dipole strength appears to be strongly fragmented with a considerable fraction observed at energies lower than ~ 15 MeV, therefore well below the giant dipole resonance. This is in contrast to the dipole response of stable nuclei, where the giant dipole resonance is localized at excitation energies of $20 \div 30$ MeV. This low-lying strength was found to exhaust a sizable fraction of the classical sum rule, up to 12%, and was associated to the pygmy resonance.

Theoretical calculations were carried within the shell model framework by Sagawa and Suzuki (145), and in a QRPA plus phonon coupling by Coló and Bortignon (146). In both approaches, the configurations excluded by the QRPA space were found to enhance strongly the fragmentation of the $E1$ strength. It was also shown that several low-energy peaks appear and should correspond to the pygmy resonance.

There are valid theoretical reasons why, in nuclei with neutron excess, configurations excluded by the $1p-1h$ space should enhance the fragmentation of the GDR and affect the pygmy resonance. In these nuclei, in fact, the positive parity phonons, like the quadrupole mode, fall

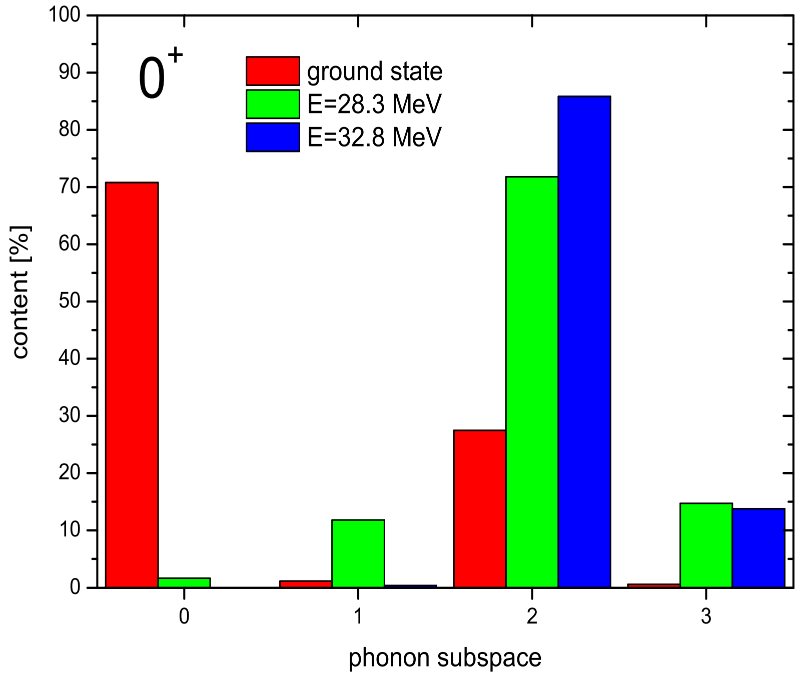

Figure 9.7: Phonon composition for the ground state and two excited 0^+ states.

at very low energy. They arise from $0\hbar\omega$ two quasiparticle excitations, in contrast to ^{16}O, where the positive parity phonons are promoted by $2\hbar\omega$ $1p-1h$ excitations. These low-energy mode couple to the $1\hbar\omega$ negative parity phonons generating two-phonon 1^- states of energy comparable to the the energy of the GDR peaks. In particular, the coupling between octupole and quadrupole phonons may generate two-phonon states which fall in the same energy region of pygmy resonance.

It is, therefore, of great interest to apply our EMPM to the neutron-rich oxygen isotopes, (147) . Dealing with open shell nuclei we have to use the qp formulation of the method, where the TDA phonons are composed of two-quasiparticle states. The TDA phonons were generated in a configuration space which includes the $(0p, 1s, 0d)$ shells. The negative parity phonons generated in this space are built of $1\hbar\omega$ $1p-1h$ excitations, while the main components of the positive parity phonons are the $0\hbar\omega$ neutron two-quasiparticle states. These are the main ingredients which should be sufficient to provide a realistic characterization of the $E1$ response. We have checked, indeed, that the TDA $E1$ response is insensitive to the dimensions of the configuration space.

Figs. 9.9 shows for ^{18}O the $E1$ reduced strengths computed in TDA and in EMPM. One may notice the extremely strong quenching and fragmentation of the strength once the $n = 2$-phonon space is added. The impact of the $n = 3$-phonon space is milder, though not negligible. Analogous results are obtained for ^{20}O (Figs. 9.10)and ^{22}O(Figs. 9.11).

From inspecting the above figures, one may notice that the giant resonance gets more spread as we move from ^{18}O to ^{22}O. In particular, low-lying peaks appear and become more pronounced in the most rich neutron isotopes.

Figs. 9.12-9.14 show the evolution of the $E1$ cross section with the number of phonons and the number of neutrons. Once again, we observe that the spreading of the resonance increases very much as the $n = 2$-phonon space is added to the TDA phonons, while the three-phonons

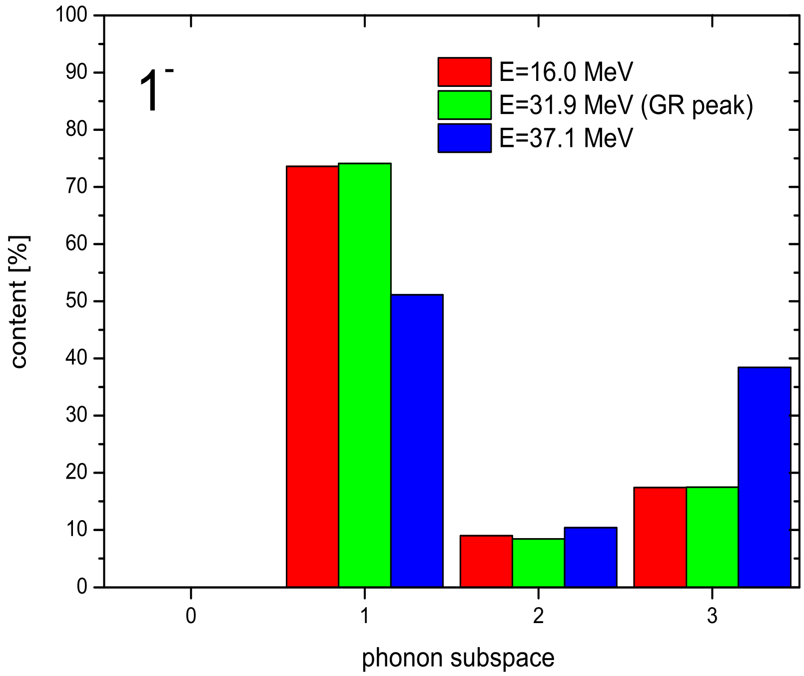

Figure 9.8: Phonon composition for three excited 1^- states.

have a considerably less important role. The situation is completely reversed as compared to the case of ^{16}O. Let us investigate the reason of such a strongly contrasting behavior. In ^{16}O, the negative parity $n = 3$-phonon states are built of three $1\hbar\omega$ negative parity TDA phonons, while the $n = 2$-phonon states of the same negative parity are composed of $1\hbar\omega$ negative parity plus a $2\hbar\omega$ positive parity phonons. Thus both $n = 2$ and $n = 3$-phonon states have approximately the same $\sim 3\hbar\omega$ energy. On the other hand, the $n = 3$-phonon phase space is much larger and couples much more strongly to the $n = 1$-phonon space. This explains the strong impact of the three-phonon states on the $E1$ response in ^{16}O.

In neutron rich oxygen isotopes, instead, the dominant positive parity phonons are composed of the $\sim 0\hbar\omega$ neutron two-quasiparticle states and, therefore fall at very low energy. When coupled to the lowest negative parity phonons composed of $\sim 1\hbar\omega$ $1p-1h$ states, a two-phonon negative parity phonon of about the same $\sim 1\hbar\omega$ $1p-1h$ energy is formed. They get, therefore, easily admixed with the negative parity 1^- phonons. The three phonon states, so important in ^{16}O, are at much higher energy $\sim 3\hbar\omega$ and, therefore are much less effective.

As already mentioned, as the excess of neutrons increases, low-lying peaks appear and get more pronounced. They are candidates for being pygmy resonance. To identify the nature of the peaks, we have computed the transition densities. Figs.9.15 and 9.16 show these transition densities for a high GDR peak and a low energy peak.

As shown in Figs.9.15, the proton and neutron transition densities are in opposition of phase in all isotopes for a high energy peak. This clearly is part of the GDR.

For the low energy peaks in all Oxygen isotopes considered here, we notice from Figs.9.16 a neutron excess with respect to protons. This is an indication that these peaks describe a pygmy resonance. The neutron excess is less pronounced in ^{22}O. This is due to the neutron sub-shell closure which inhibits the neutron diffuseness.

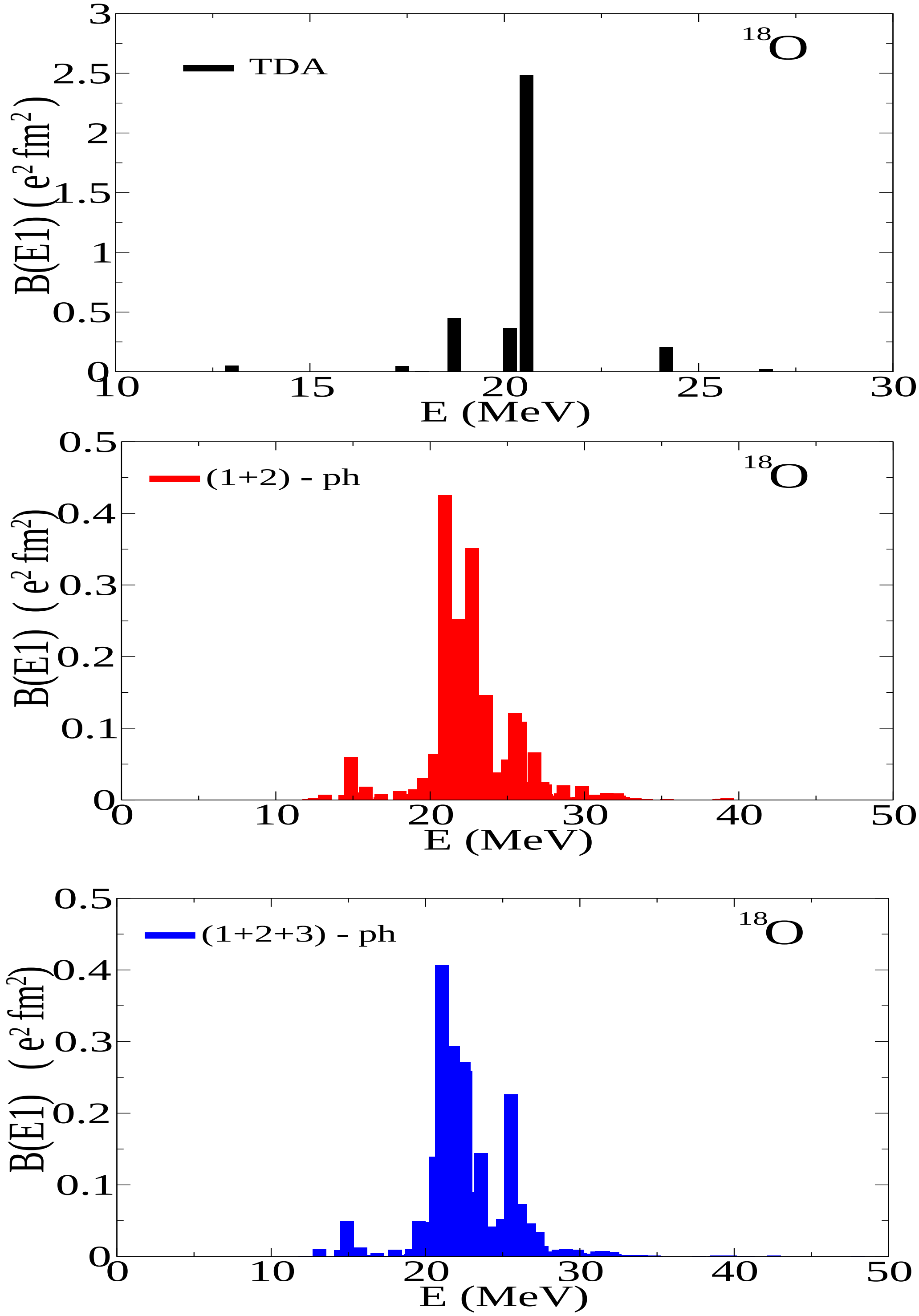

Figure 9.9: TDA versus EMPM $E1$ reduced transition probabilities in ^{18}O.

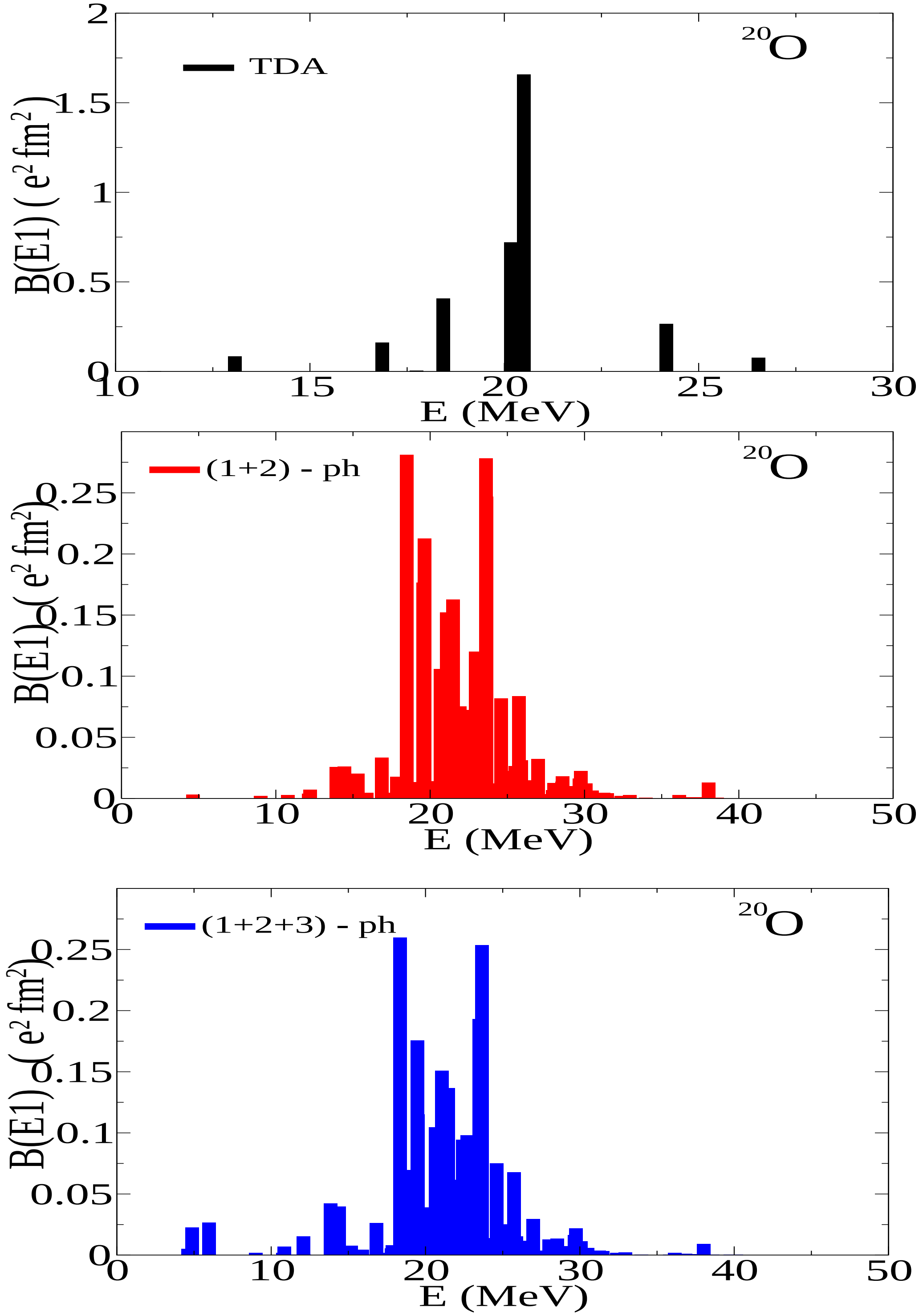

Figure 9.10: TDA versus EMPM $E1$ reduced transition probabilities in ^{20}O.

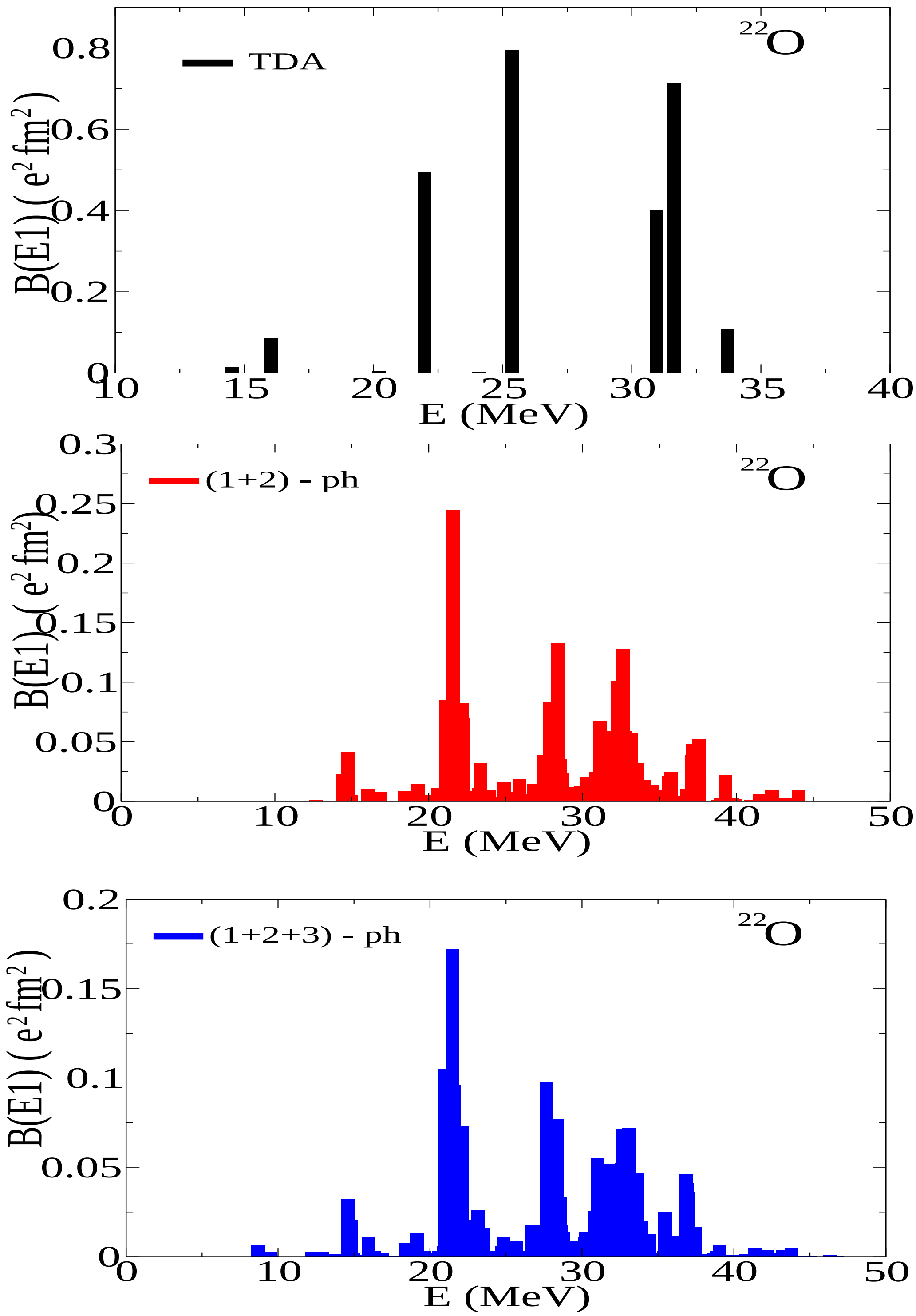

Figure 9.11: TDA versus EMPM $E1$ reduced transition probabilities in ^{22}O.

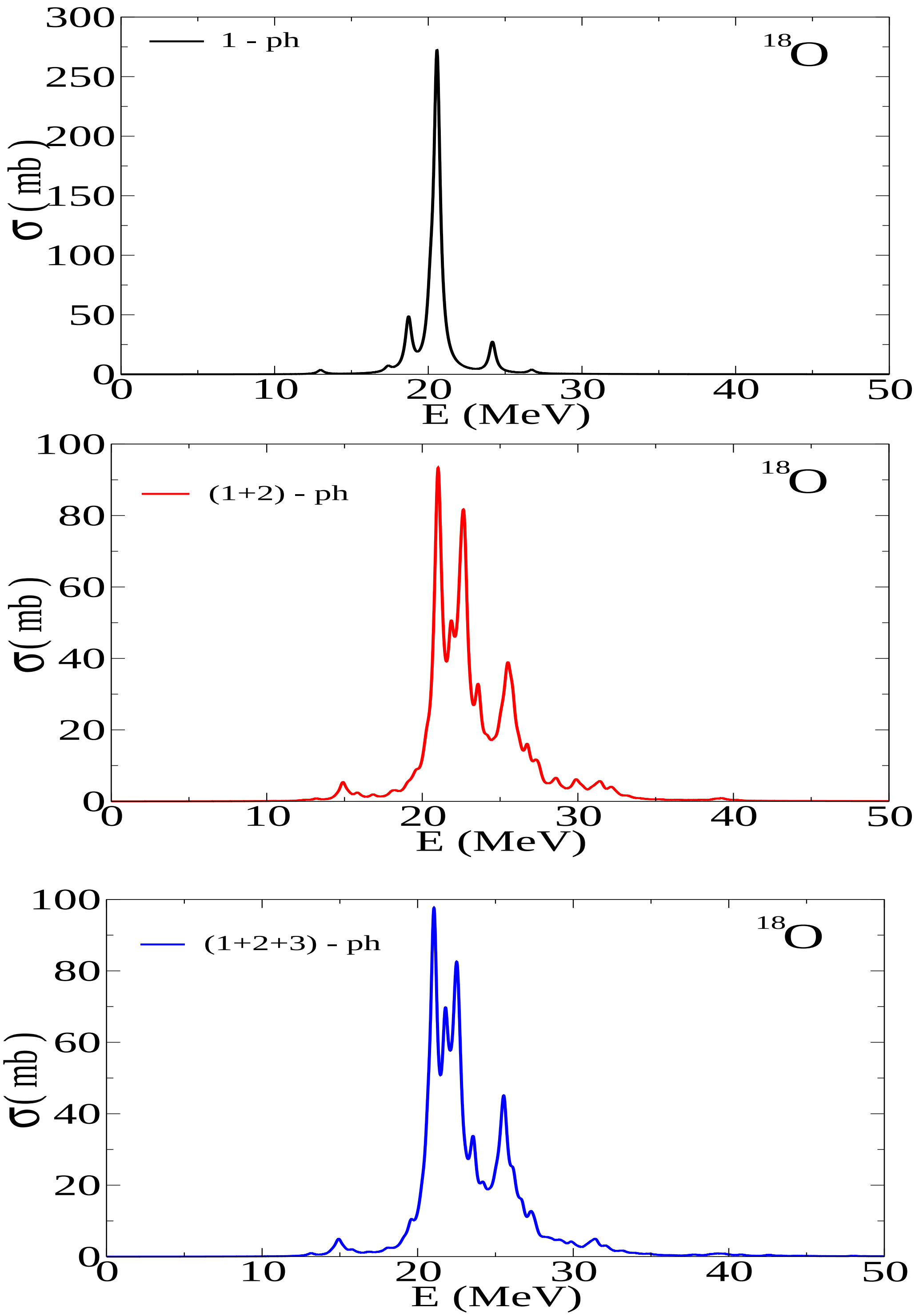

Figure 9.12: TDA versus EMPM $E1$ cross section in ^{18}O.

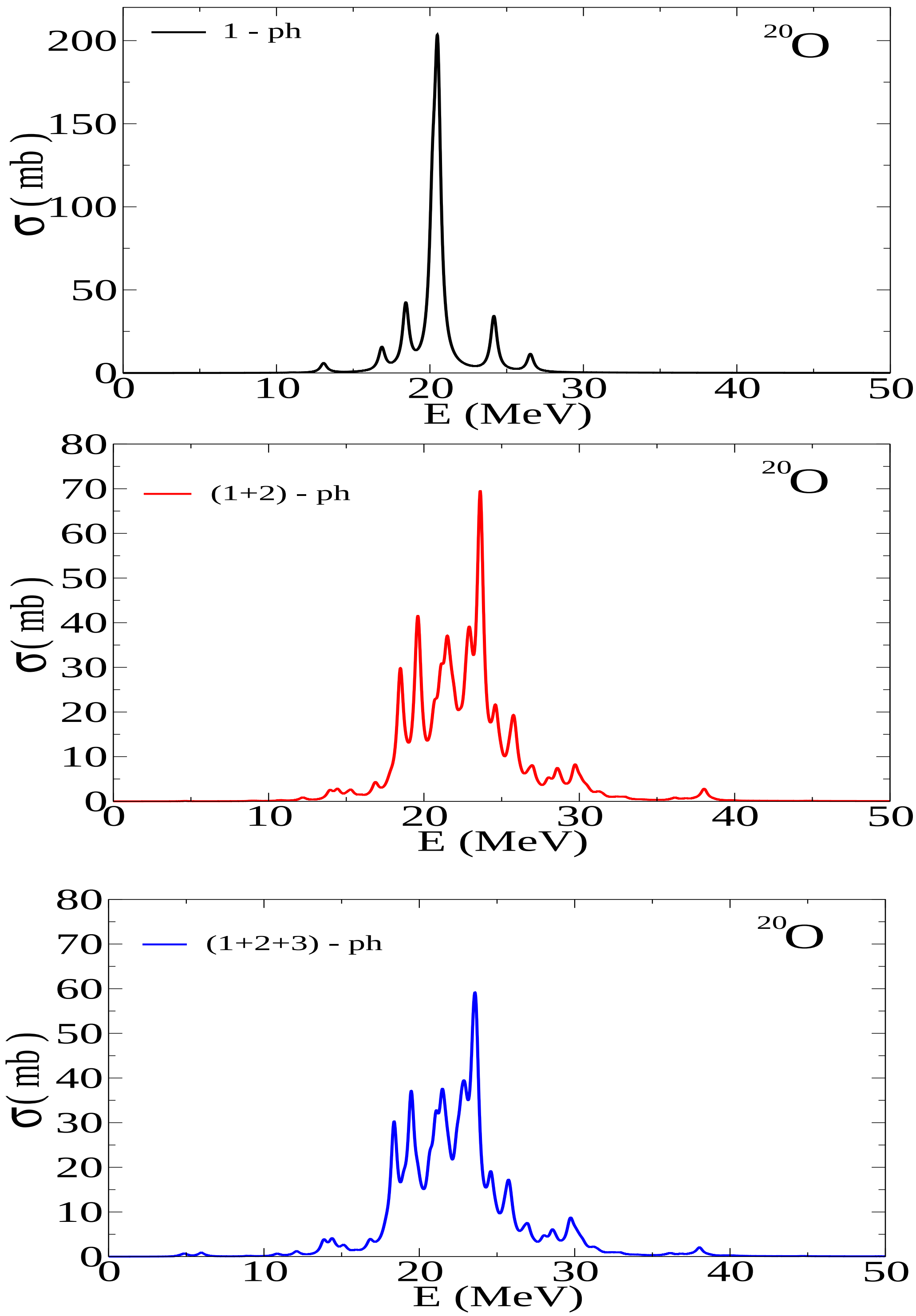

Figure 9.13: TDA versus EMPM $E1$ cross section in ^{20}O.

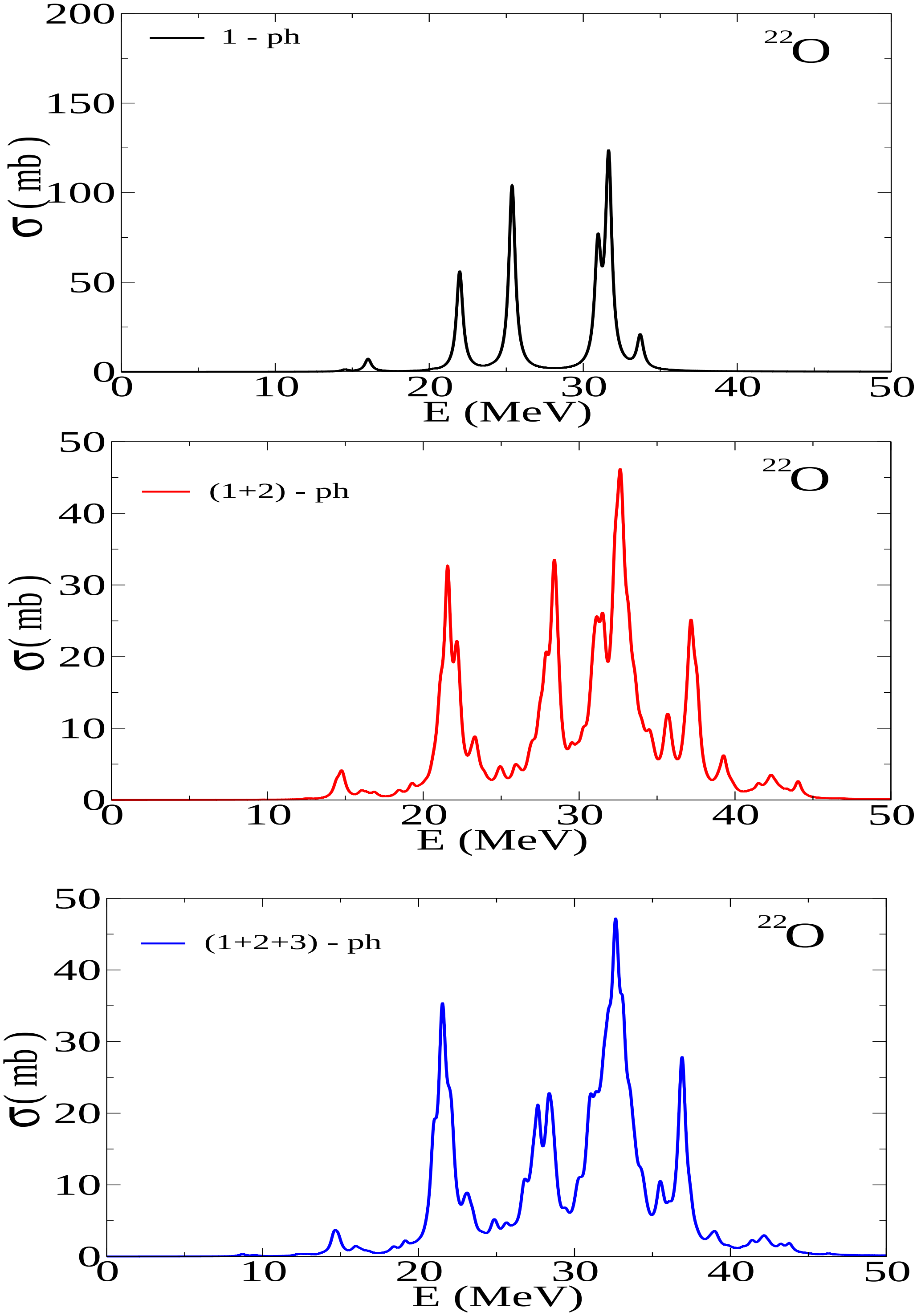

Figure 9.14: TDA versus EMPM $E1$ cross section in ^{22}O.

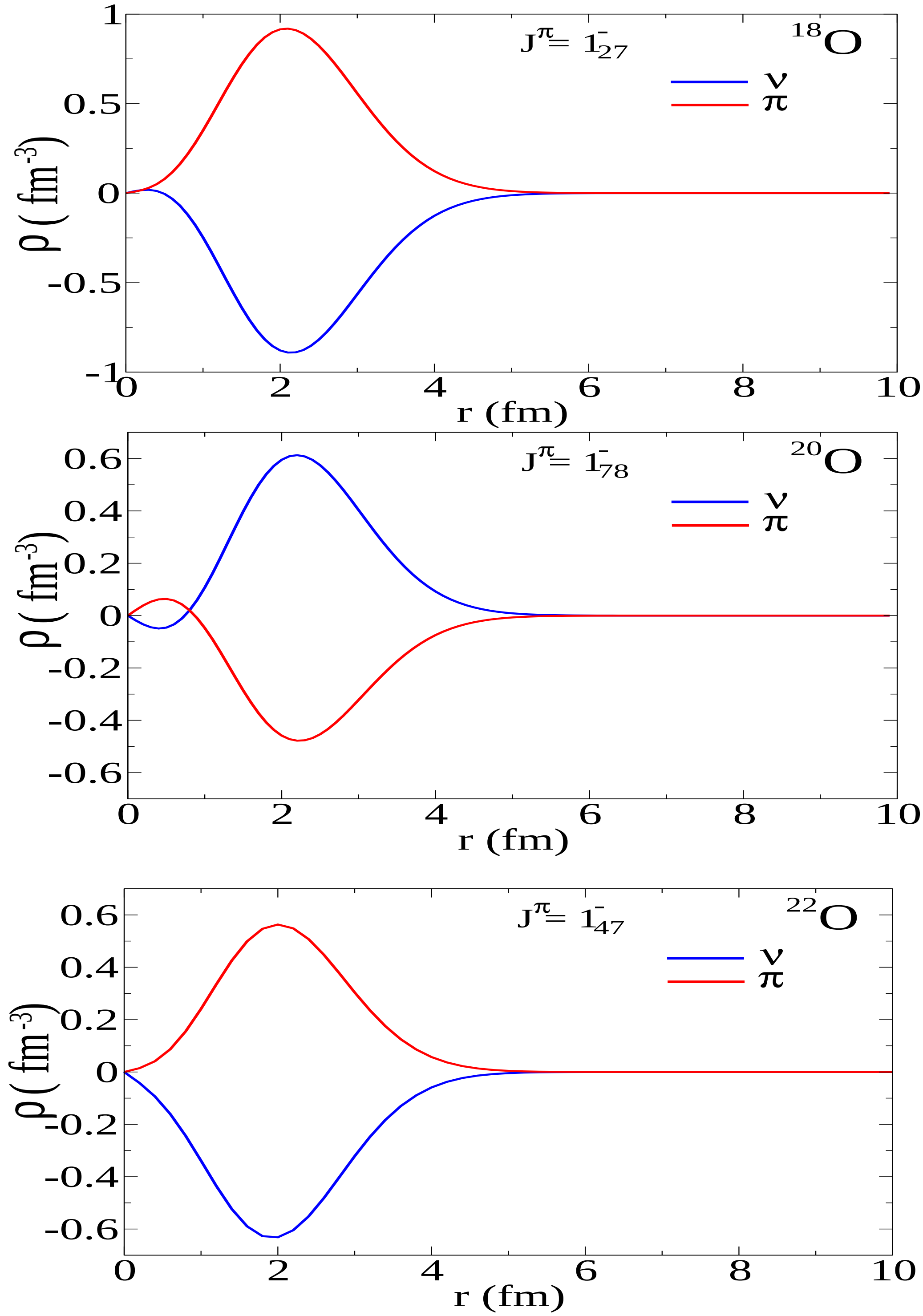

Figure 9.15: $E1$ transition densities inducing a typical DGR peak.

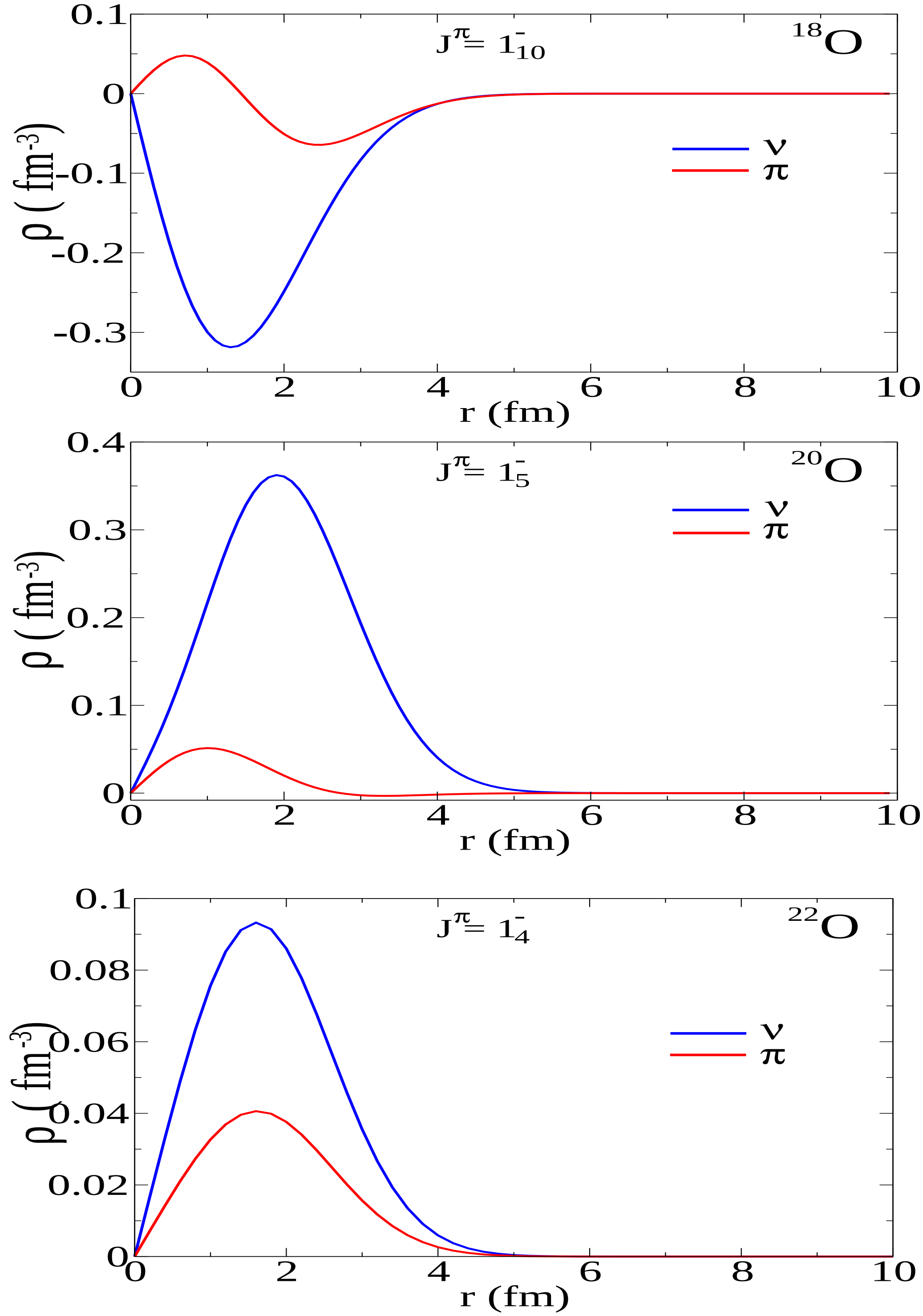

Figure 9.16: $E1$ transition densities inducing a typical PDR peak.

Chapter 10

Conclusions

The two methods described in the present work, namely the SM algorithm and the EMPM, are in many ways complementary. The SM algorithm applies to low-energy spectroscopy, the EMPM is more suited to collective modes and, in particular, to giant resonances.

We have accomplished the first implementation of the SM algorithm in the uncoupled m-scheme and proposed a new sampling for reducing effectively the dimensions of the shell model space.

We have seen that the method allows to safely diagonalize Hamiltonian matrices of dimensions of the order of $N \sim 10^8$. Within these limits, the method yields an almost arbitrary number of eigenvalues and eigenvectors. It can therefore be fruitfully applied to medium-heavy nuclei not too far from the proton or the neutron shell closures.

An exampled was offered by ^{132}Xe. We have provided a rather complete description of the low lying spectroscopic properties of this nucleus. We have, in particular, tested the symmetry of the low-lying states with respect to the exchange of protons versus neutrons through the analysis of the $E2$ and $M1$ transitions.

We have also seen that the sampling procedure yields sequences of energy levels converging rapidly to their asymptotic values even for Hamiltonian matrices of dimensions $N \sim 10^9$. This fast convergence has enabled us to generate a complete low-lying spectrum for ^{130}Xe.

The convergence, however, deteriorates for the transition strengths, especially the $M1$ transitions, which are quite sensitive to small components of the wavefunctions. Because of this poor convergence, we were not able to make reliable estimates of the electromagnetic transition strengths for ^{130}Xe. This establishes the limits of applicability of the algorithm in its present formulation. There is, nonetheless, room for improvement.

One possible advance may come from a more rational and efficient exploitation of the sparsity of the Hamiltonian matrix, which should reduce drastically the number of operations. A procedure for achieving this improvement is under investigation.

A major step forward may be made by elaborating a parallel version of the implementation code. This, however, requires a longer effort.

Concerning the other method, we have presented an upgraded formulation of the EMPM which expresses all quantities only in terms of TDA phonons.

The outcome of the method is a set of eigenvalue equations which can be solved iteratively to generate a basis of multiphonon states to be used for a final diagonalization of the residual nuclear Hamiltonian.

As stressed previously, the method is free of approximations and includes explicitly correlations in the ground state. It represents, therefore, a meaningful progress with respect to RPA and its extensions, based on the quasiboson approximation.

We implemented the method in the particle-hole and the quasiparticle formalism, the first suited to double magic nuclei, the second to open shell nuclei.

In both cases, we solved the multiphonon eigenvalue problem in spaces that include all states spanning up to the $n = 3$-phonon subspace. This is the first calculation, using a realistic Hamiltonian, in which three-phonon states come into play. Previous approaches were confined to two-phonon states only and, moreover, had to resort to more or less restricting approximations.

The application of the method to the double magic ^{16}O has unveiled the importance of including the multiphonon states and of taking into full account the coupling between spaces with different numbers of phonons. We have seen that such a coupling is especially effective between spaces differing by two phonons.

Thus, for instance, the ground state gets strongly depressed due to the coupling to the two-phonon space. This space does not affect the other levels, including the peaks of the DGR, which, therefore, are pushed at too high energy with respect to the ground state. In order to bring back the dipole peaks, it is necessary to include the three-phonon space.

The role of multiphonon states has emerged also from the quasiparticle EMPM applied to neutron rich oxygen isotopes. A largely visible effect is the strong fragmentation of the dipole resonance induced by the phonon coupling. We have also pointed out the appearance of low energy peaks which have the properties typical of the pygmy resonance.

The EMPM study was confined to light nuclei. It can be easily extended to heavy nuclei if the space is confined to one- plus two-phonons.

If, on the other hand, we intend to enclose more phonons into the scheme, we need to find a reliable method for selecting the multiphonon states which contribute to energies and transitions of interest. In other words, we need a reliable sampling for achieving a severe truncation of the multiphonon space. This is the route we intend to follow in the immediate future.

Appendix A

Matrix decomposition

Two classical matrix decomposition methods, namely the QR and Cholesky algorithm, are briefly discussed in this appendix. The main reference for what is treated here is the book by Wilkinson, (23).

The QR decomposition is used for solving the full eigenvalue problem of an Hermitean matrix. The so-called QR diagonalization can be shown to be, between the methods for finding all the eigenvalues and eigenvectors, the fastest. It has been used in the complete diagonalizations needed from both the SM algorithm and the EMPM.

The Cholesky decomposition splits a real and symmetric matrix into a product of a lower (upper) triangular matrix with its transpose, allowing a fast calculation of the matrix rank and determinant. Its role is fundamental for extracting a linear independent set out of the EMPM basis states.

A.1 QR decomposition

Consider a $(n \times n)$ matrix $\mathbf{A}$. The QR methods writes $\mathbf{A}$ as the product of an orthogonal matrix, $\mathbf{Q}$, and an upper triangular matrix, $\mathbf{R}$

$$\mathbf{A} = \mathbf{QR}\,. \tag{A.1}$$

There are several known implementation of the QR decomposition. Here we discuss the procedure due to Householder, which is one of the most used in practical application. In this approach, one considers the Householder reflection

$$\mathbf{P} = \mathbf{I} - 2\mathbf{w}\mathbf{w}^T\,, \tag{A.2}$$

where $\mathbf{w}$ is a real vector with euclidean norm $||\mathbf{w}||_2 = 1$. The transformation implemented by $\mathbf{P}$ is unitary and orthogonal, since

$$\begin{aligned}\mathbf{P}^2 &= (\mathbf{I} - 2\mathbf{w}\mathbf{w}^T)(\mathbf{I} - 2\mathbf{w}\mathbf{w}^T)\\ &= \mathbf{I} - 4\mathbf{w}\mathbf{w}^T + 4\mathbf{w}(\mathbf{w}^T\mathbf{w})\mathbf{w}^T\\ &= \mathbf{I}\,,\end{aligned} \tag{A.3}$$

from which $\mathbf{P} = \mathbf{P}^{-1}$, and because it is easily verified the relation $\mathbf{P} = \mathbf{P}^T$.

The matrix $\mathbf{P}$ can be expressed as a function of a real vector $\mathbf{u}$, not normalized

$$\mathbf{P} = \mathbf{I} - \frac{\mathbf{u}\mathbf{u}^T}{H}\,, \tag{A.4}$$

whit H defined by

$$H = \frac{1}{2}||\mathbf{u}||_2\,. \tag{A.5}$$

The vector $\mathbf{u}$ can be chosen in such a way to have the product of a generic vector $\mathbf{x}$ by $\mathbf{P}$ giving a result proportional to a vector of the natural basis, $\mathbf{e_i}$

$$\mathbf{Px} = \alpha\mathbf{e_i} \,. \tag{A.6}$$

In order to make $\mathbf{u}$ fulfilling the above relation, one has to impose the condition

$$\alpha\mathbf{e_i} = \mathbf{Px} = \left(\mathbf{I} - 2\frac{\mathbf{u}\mathbf{u}^T}{\mathbf{u}^T\mathbf{u}}\right)\mathbf{x} = \mathbf{x} - \mathbf{u}\frac{2\mathbf{u}^T\mathbf{x}}{\mathbf{u}^T\mathbf{u}} \,, \tag{A.7}$$

that is

$$\mathbf{u} = \mathbf{x} - \alpha\mathbf{e}_i \,. \tag{A.8}$$

Moreover, one can ask the transformation to preserve the norm, imposing to the coefficients the condition $\alpha = \pm||\mathbf{x}||_2$, which means

$$\mathbf{u} = \mathbf{x} \mp |\mathbf{x}|\mathbf{e}_i \,. \tag{A.9}$$

If $\mathbf{x}$ if a column of $\mathbf{A}$, the multiplication by $\mathbf{P}$ nullifies all the elements but the i-th. It can be demonstrated that with successive applications of the Householder reflectors the matrix $\mathbf{A}$ converges to the form of A.1

The QR algorithm is an iterative direct diagonalization algorithm, due to Francis (43; 44), which solves the full eigenproblem of a given matrix $\mathbf{A}$, starting from its QR decomposition. At the k-th step, the matrix is decomposed as a

$$\mathbf{A}^{(k)} = \mathbf{Q}^{(k)}\mathbf{R}^{(k)} \,. \tag{A.10}$$

The next-step matrix, $\mathbf{A}^{(k+1)}$, is then formed as

$$\mathbf{A}^{(k+1)} = \mathbf{R}^{(k)}\mathbf{Q}^{(k)} \,, \tag{A.11}$$

which is equivalent to

$$\mathbf{A}^{(k+1)} = \mathbf{Q}^{(k)T}\mathbf{Q}^{(k)}\mathbf{R}^{(k)}\mathbf{Q}^{(k)} = \mathbf{Q}^{(k)T}\mathbf{A}^{(k)}\mathbf{Q}^{(k)} \,, \tag{A.12}$$

given the orthogonality of $\mathbf{Q}^{(k)}$.

It can be shown that the matrix elements under the main diagonal go to zero as

$$a_{ij}^n = \left(\frac{\lambda_i}{\lambda_j}\right)^n \,, \tag{A.13}$$

where $\lambda_i < \lambda_j$. If one eigenvalue λ_i is next to λ_j, the convergence can be increased using the split technique. This means that the algorithm is applied to the matrix $\mathbf{A} - k\mathbf{I}$, for which the convergence goes like the ratio

$$\frac{\lambda_i - k_n}{\lambda_j - k_n} \,. \tag{A.14}$$

Moreover, one can demonstrate that the number of operations needed for the implementation of the algorithm increases as $\mathrm{O}(n^3)$.

A.2 Cholesky decomposition

If a square matrix $\mathbf{A}$ is symmetric and positive definite, it can be decomposed more efficiently using the Cholesky algorithm. This method decomposes the matrix as a product of a lower triangular matrix, $\mathbf{L}$, and its transpose, $\mathbf{L}^T$

$$\mathbf{A} = \mathbf{L}\mathbf{L}^T \ . \tag{A.15}$$

Writing this equality in components, one finds that the diagonal elements of $\mathbf{L}$ have the structure

$$L_{ii} = \left(a_{ii} - \sum_{k=0}^{i-1} L_{ik}^2 \right)^{1/2} \ . \tag{A.16}$$

Moreover, the off-diagonal elements can be calculated as

$$L_{ji} = \frac{1}{L_{ii}} \left(a_{ij} - \sum_{k=0}^{i-1} L_{ik} L_{jk} \right) \ . \tag{A.17}$$

This decomposition is extremely stable from a numerical point of view.

Cholesky decomposition is often used for finding the matrix rank and determinant. In fact, once the symmetric and positive definite matrix, $\mathbf{A}$, has been decomposed, its determinant is given by

$$det(\mathbf{A}) = det(\mathbf{L}) \times det(\mathbf{L}^T) \ , \tag{A.18}$$

that is, from the product of the square of the diagonal term of $\mathbf{L}$, $(\prod_i L_{ii})^2$.

The determinant can then be calculated on-line while doing the decomposition. If at the $(j+1)$-th step of the decomposition the determinant is nullified, one has determined the matrix rank $r = j < n$.

Appendix B

Hartree-Fock

This appendix describes the mean field approach for the determination of the nuclear ground state wave function.

The first section is devoted to discuss the Hartree-Fock (HF) theory. Borrowed from atomic physics, this self-consistent field method is the basis for every mean-field based approach.

The second section introduces the quasi-particle formalism, and the generalization of the method through the unitary Bogolyubov transformation.

B.1 Hartree-Fock theory

The Hartree-Fock procedure aims to find the best form for the mean-field potential, U, in which the nucleons move as independent particle. This is achieved imposing on the energy expectation to be stationary

$$\delta\langle\phi|H|\phi\rangle = \langle\delta\phi|H|\phi\rangle = 0 \, . \tag{B.1}$$

The above equation can be written explicitly using the second quantized form of the Hamiltonian

$$H = \sum_{ij} t_{ij} c_i^\dagger c_j + \frac{1}{4} \sum_{ijkl} V_{ijkl} c_i^\dagger c_j^\dagger c_l c_k \, , \tag{B.2}$$

where $c_i^\dagger$ (c_i) are creation (annihilation) operators with respect to the nucleon vacuum, obeying the anticommutation relations

$$\{c_i \, , \, c_j\} = 0 \, , \quad \{c_i^\dagger \, , \, c_j\} = \delta_{ij} \, , \tag{B.3}$$

t_{ij} are the single particle matrix elements of the kinetic operator, and V_{ijkl} the antisymmetrized matrix elements of the two-body potential

$$V_{ijkl} = \langle ij|V|kl\rangle - \langle ij|V|lk\rangle \, , \tag{B.4}$$

which fulfill the symmetry conditions

$$V_{ijkl} = -V_{jikl} = -V_{ijlk} = V_{jilk} \, . \tag{B.5}$$

The following step is to define a new set of creation and annihilation operators by the unitary transformation

$$a_i^\dagger = \sum_j D_{ij} c_j^\dagger \, , \, \sum_k D_{ki}^* D_{kj} = \delta_{ij} \, . \tag{B.6}$$

Enforcing the variation with respect to the coefficient D_{ij}, one obtains the HF eigenvalue equations

$$t_{ij} + \sum_h V_{ihjh} = \epsilon_i \delta_{ij} \, . \tag{B.7}$$

The iterative solution of the above equations yields the HF single particle energies (ϵ_i) and eigenvectors. The generic Hartree-Fock Slater determinant ϕ_i can be written as

$$|\phi_i\rangle = |\nu_1, \nu_2, \dots, \nu_A\rangle = a^\dagger_{\nu_1} \cdots a^\dagger_{\nu_A}|0\rangle \ . \tag{B.8}$$

For closed shell nuclei, the lowest eigenvalue of H_0 is non degenerate and the corresponding HF Slater determinant describes a configuration corresponding to the complete filling of the lowest shells up to the Fermi surface. It is therefore convenient to define this state, denote by $|\rangle$, as the particle-hole vacuum

$$\begin{aligned} a_p|\rangle &= 0 \ , \\ b_h|\rangle &= a^\dagger_h|\rangle = 0 \ , \end{aligned} \tag{B.9}$$

where p and h denote single particle states above and below the Fermi surface. Particle and hole states are defined respectively as

$$\begin{aligned} |p\rangle &= a^\dagger_p|\rangle \ , \\ |h^{-1}\rangle &= b^\dagger_h|\rangle = a_{\bar{h}}|\rangle \ , \end{aligned} \tag{B.10}$$

where

$$a_{\bar{\nu}} = (-1)^{j_\nu + m_\nu} a_{j_\nu, -m_\nu}. \tag{B.11}$$

The phase is required for the hole operator to transform as an irreducible spherical tensor (7).

In this self consistent HF basis, the Hamiltonian B.2 takes the form

$$H = \sum_i^A \epsilon_i a^\dagger_i a_i - \frac{1}{2}\sum_{ij}^A V_{ijij} + \frac{1}{4}\sum_{ijkl}^A V_{ijkl} : a^\dagger_i a^\dagger_j a_l a_k : \ , \tag{B.12}$$

where the residual two-body interaction is written in normal order with respect to HF ground state, $|\rangle$. The ground state energy is then given by the expectation value

$$E_0 = \langle|H|\rangle = \sum_i^A \epsilon_i - \frac{1}{2}\sum_{ij}^A V_{ijij} \ . \tag{B.13}$$

B.2 Quasi-particle and Hartree-Bogoliubov theory

The HF description is often not completely satisfactory, especially if one deals with open-shell nuclei. The Hartree-Bogolyubov theory aims to go beyond the HF method, including explicitly the correlations introduced by the residual interaction, while retaining the simplicity of the independent particle model.

HB method introduces the generalized fermion creation (annihilation) operators, $\alpha^\dagger_\nu$ (α_ν), also called quasi-particle operators, defined by the unitary Bogoliubov transformations

$$\begin{array}{ll} \alpha_\nu = u_\nu a_\nu - v_\nu a^\dagger_{\bar{\nu}} & a_\nu = u_\nu \alpha_\nu + v_\nu \alpha^\dagger_{\bar{\nu}} \\ \alpha^\dagger_\nu = u_\nu a^\dagger_\nu - v_\nu a_{\bar{\nu}} & a^\dagger_\nu = u_\nu \alpha^\dagger_\nu + v_\nu \alpha_{\bar{\nu}} \\ \alpha_{\bar{\nu}} = u_\nu a_{\bar{\nu}} + v_\nu a^\dagger_\nu & a_{\bar{\nu}} = u_\nu \alpha_{\bar{\nu}} - v_\nu \alpha^\dagger_\nu \\ \alpha^\dagger_{\bar{\nu}} = u_\nu a^\dagger_{\bar{\nu}} + v_\nu a_\nu & a^\dagger_{\bar{\nu}} = u_\nu \alpha^\dagger_{\bar{\nu}} - v_\nu \alpha_\nu \end{array} \ , \tag{B.14}$$

in which a barred suffix refers to the single-particle state

$$\phi_{j\bar{m}} = (-1)^{j+m}\phi_{j-m} \ , \tag{B.15}$$

and the u and v factors are required to satisfy the normalization condition

$$u_\nu^2 + v_\nu^2 = 1 \; . \tag{B.16}$$

Assuming $|0\rangle$ to be the bare-particle vacuum, the state

$$|0\rangle_{qp} = \prod_{\nu>0} \left(u_\nu + v_\nu a_\nu^\dagger a_{\bar{\nu}}^\dagger \right) |0\rangle \; , \tag{B.17}$$

can be proved to be the quasi-particle vacuum,

$$(u_\mu a_\mu - v_\mu a_{\bar{\nu}}^\dagger) \prod_{\nu>0} \left(u_\nu + v_\nu a_\nu^\dagger a_{\bar{\nu}}^\dagger \right) |0\rangle = 0 \; . \tag{B.18}$$

The HB method seeks a ground state wave function with the form B.17. The numerical value of the parameters and the single particle wave functions are then determined in a self-consistent way.

The state defined in B.17 is not made up of a defined number of particle. There is then, in general, the need to introduce a redefined Hamiltonian H'

$$H' = H - \lambda n \; , \tag{B.19}$$

where λ is a Lagrange multiplier chosen to ensure the correct value for the mean particle number

$$\langle 0|n|0\rangle_{qp} = N_0 \; . \tag{B.20}$$

The λ parameter is a function of the number of particles, N_0, and its value is given by the variational condition

$$\frac{\partial}{\partial N_0} \langle 0|H'|0\rangle_{qp} = 0 \; , \tag{B.21}$$

or

$$\lambda = \frac{\partial}{\partial N_0} \langle 0|H|0\rangle_{qp} \; , \tag{B.22}$$

which identifies λ with the chemical potential.

Making use of the second quantized form of the Hamiltonian, Eq. (B.2), H' takes the form

$$H' = \sum_{\nu\nu'} \left(t_{\nu\nu'} - \lambda \delta_{\nu\nu'} \right) \alpha_\nu^\dagger \alpha_{\nu'} + \frac{1}{4} \sum_{\mu\nu\mu'\nu'} V_{\mu\nu\mu'\nu'} \alpha_\mu^\dagger \alpha_\nu^\dagger \alpha_{\nu'} \alpha_{\mu'} \; . \tag{B.23}$$

Substituting Eq. (B.14) into the above equation, one obtains four terms for the transformed Hamiltonian

$$H' = U + H_{11} + H_{20} + V_{res} \; , \tag{B.24}$$

where U is constant, and

$$\begin{array}{lcl} H_{11} & \sim & \alpha^\dagger \alpha \\ H_{20} & \sim & \alpha^\dagger \alpha^\dagger + \alpha\alpha \\ V_{res} & \sim & \alpha^\dagger \alpha^\dagger \alpha^\dagger \alpha^\dagger + \alpha^\dagger \alpha^\dagger \alpha^\dagger \alpha + \cdots + \alpha\alpha\alpha\alpha \end{array} \; . \tag{B.25}$$

The minimization of the energy expectation of the quasi-particle vacuum, $\langle 0|H'|0\rangle_{qp}$, with a direct calculation can be shown to be equivalent to require the term H_{20} to vanish. Generally one also requires the term H_{11} to be diagonal, from which one finds

$$t_{\nu\nu'} + \sum_\mu V_{\mu\nu\mu\nu'} v_\mu^2 = \epsilon_\nu \delta_{\nu\nu'} \; , \tag{B.26}$$

a relation which is equivalent to the HF condition B.7. With this additional condition, the expression for H_{20} becomes

$$H_{20} = \sum_{\nu} \left[(\epsilon_\nu - \lambda) u_\nu v_\nu - \frac{1}{2} \Delta_\nu (u_\nu^2 - v_\nu^2) \right] (\alpha_\nu^\dagger \alpha_{\bar{\nu}}^\dagger + \alpha_{\bar{\nu}} \alpha_\nu) \ , \tag{B.27}$$

where delta, the gap parameter, is defined as

$$\Delta_\nu = -\frac{1}{2} \sum_{\mu} V_{\bar{\mu}\mu\bar{\nu}\nu} u_\mu v_\mu \ . \tag{B.28}$$

Imposing the H_{20} term to vanish

$$(\epsilon_\nu - \lambda) 2 u_\nu v_\nu - \Delta_\nu (u_\nu^2 - v_\nu^2) = 0 \ , \tag{B.29}$$

together with the normalization and number conservation conditions, one finds the following expressions for u and v

$$u_\nu^2 = \frac{1}{2} \left(1 + \frac{\epsilon_\nu - \lambda}{\sqrt{(\epsilon_\nu - \lambda)^2 - \Delta_\nu}} \right) \ , \quad v_\nu^2 = \frac{1}{2} \left(1 - \frac{\epsilon_\nu - \lambda}{\sqrt{(\epsilon_\nu - \lambda)^2 - \Delta_\nu}} \right) \ , \tag{B.30}$$

and consequently the equations for Δ

$$\Delta_\nu = -\frac{1}{4} \sum_{\nu'} \frac{V_{\bar{\nu}\nu\bar{\nu}'\nu'}}{\sqrt{(\epsilon_{\nu'} - \lambda)^2 - \Delta_{\nu'}}} \Delta_{\nu'} \ , \tag{B.31}$$

and λ

$$\frac{1}{2} \sum_{\nu} \left(1 - \frac{\epsilon_\nu - \lambda}{\sqrt{(\epsilon_\nu - \lambda)^2 - \Delta_\nu}} \right) = N_0 \ . \tag{B.32}$$

The HB equations, in general, have several solutions, some of which are trivial, corresponding to the HF solutions. As in HF method, the HB approach does not necessary preserve the symmetries of the wave function,. There can be solutions with the right symmetry properties, but they are not necessary the lowest in energy.

The ground energy is given by the constant term in the H' Hamiltonian

$$U = \sum_{\nu} \left[(\epsilon_\nu - \lambda) - \frac{1}{2} \sum_{\mu} V_{\mu\nu\mu\nu} v_\mu^2 \right] v_\nu^2 - \frac{1}{2} \sum_{\nu} \Delta_\nu u_\nu v_\nu \ . \tag{B.33}$$

The single particle energies, given by the expectation value of the H_{11} term

$$H_{11} = \sum_{\nu} E_\nu \alpha_\nu^\dagger \alpha_\nu \ , \tag{B.34}$$

include now all the contribution, from both extra-core and core particles, which are no longer distinguished, as in the HF case

$$E_\nu = (\epsilon_\nu - \lambda)(u_\nu^2 - v_\nu^2) + 2 \Delta_\nu u_\nu v_\nu = \sqrt{(\epsilon_\nu - \lambda)^2 + \Delta_\nu^2} \ . \tag{B.35}$$

Bibliography

[1] M. Mayer, Phys. Rev. **75**, 1969 (1949).

[2] O. Haxel, J. H. D. Jensen and H. E. Suess, Phys. Rev. **75**, 1766 (1949).

[3] R.D. Woods and D.S. Saxon, Phys. Rev. **95**, 577 (1954).

[4] S. G. Nilsson, Mat. Fys. Medd. Dan id. Selsk. **29**, 16 (1955).

[5] C. Gustafsson, I. L. Lamm, B. Nilsson, and S. G. Nilsson, Ark. Fys. **36**, 613 (1967).

[6] W. Nazarewicz, J. Dudek, R. Bengtsson, T. Bengtsson, and I. Ragnarsson, Nucl. Phys. **A435**, 397 (1985).

[7] A. Bohr and B. R. Mottelson, *Nuclear Structure*, Vol. I (Benjamin, New York, 1969).

[8] K. Suzuki, S. Y. Lee, Prog. Theor. Phys. **64**, 2091 (1980).

[9] F.Andreozzi, Phys. Rev. C, **54**, 684 (1996).

[10] M. Hjorth-Jensen, E. Osnes, and T. T. S. Kuo, Phys. Rep. **261**, 125 (1995).

[11] See, for instance, B. D. Day, Rev. Mod. Phys., **39**, 719 (1967).

[12] T. T. S. Kuo and G. E. Brown, Nucl. Phys. **85**, 40 (1966).

[13] E. M. Krenciglowa, T. T. S. Kuo, Nucl. Phys. A **235**, 171 (1974).

[14] S. Bogner, T. T. S. Kuo and L. Coraggio, Nucl. Phys. A **684**, 432 (2001).

[15] S.K. Bogner, T.T.S. Kuo and A. Schwenk, Phys. Rep. **386**, 1 (2003).

[16] L. Coraggio, A. Covello, A. Gargano, N. Itaco and T. T. S. Kuo, Prog. Part. Nucl. Phys. **62**, 135 (2009).

[17] V. G. J. Stoks, R. a. M. Klomp, C. P. F. Terheggen and J. J. de Swart, Phys. Rev. C **48**, 792 (1993).

[18] R. B. Wiringa, V. G. J. Stoks, and R. Schiavilla Phys. Rev. C **51**, 38 (1995).

[19] R. Machleidt, F. Sammaruca, and Y. Song, Phys. Rev. C **53**, R1483 (1996).

[20] D. R. Entem and R. Machleidt, Phy. Lett. B, **524**, 93 (2002).

[21] D. R. Entem and R. Machleidt, Phys. Rev. C **68**, 041001(R) (2003).

[22] L. Coraggio, A. Covello, A. Gargano, N. Itaco, D. R. Entem, T. T. S. Kuo, and R. Machleidt, Phys. Rev. C **75**, 024311 (2007).

[23] J. H. Wilkinson, *The Algebric eigenvalue problem*, Oxford University Press, New York (1965).

[24] Cornelius Lanczos, J. Res. Nat. Bur. Standards **45**, 2133 (1950).

[25] G. H. Golub and C. F. Van Loan, *Matrix Computations*, (John Hopkins University Press, Baltimore, 1996).

[26] E. Caurier et al., Rev. Mod. Phys. **77**, 427 (2005).

[27] F. Nowacki, E. Caurier, coupled code NATHAN, Strasbourg (1995).

[28] E. Caurier and F. Nowacki, Acta Phys. Pol. B **30**, 705 (1999).

[29] B. A. Brown and W. D. M. Rae, NUSHELL@MSU, MSUNSCL Report, 2007 (unpublished).

[30] R.R. Whitehead, A. Watt, B. J. Cole and I. Morrison Adv. in Nuc. Phys. **9**, 123 (1977).

[31] E. Caurier, computer code antoine, C.R.N., Strasbourg (1989).

[32] S. E. Koonin, D. J. Dean, and K. Langanke, Phys. Rep. **278**, 1 (1997).

[33] J. A. White, S. E. Koonin, and D. J. Dean, Phys. Rev. C **61**, 034303 (2000).

[34] N. Metropolis, A. W. Rosenbluth, M. N. Rosenbluth, A. H. Teller, and E. Teller, J. Chem. Phys. **21**, 1087 (1953).

[35] T. Otsuka, M. Honma, T. Mizusaki, N. Shimizu e Y. Utsuno, Progress in Nuclear and Particle Physics **47**, 319 (2001).

[36] S.R. White, Phys. Rev. B **48**, 10345 (1993.)

[37] K. G. Wilson, Rev. Mod. Phys. **47**, 773 (1975).

[38] J. Dukelsky and S. Pittel, Phys. Rev. C **63**, 061303 (2001).

[39] B. Thakur, S. Pittel, and N. Sandulescu, Phys. Rev. C **78**, 041303 (2008).

[40] F. Andreozzi, A. Porrino and N. Lo Iudice, J. Phys. A **35**, L61 (2002).

[41] F. Andreozzi, N. Lo Iudice and A. Porrino, J. Phys. G **29**, 2319 (2003).

[42] I. Shavitt, C. F. Bender, A. Pipano and R. P. Hosteny, J. Comp. Phys. **11**, 90 (1973).

[43] J. G. F. Francis, The Computer Journal **4**, 265 (1961).

[44] J. G. F. Francis, The Computer Journal **4**, 332 (1962).

[45] D. Bianco, F. Andreozzi, N. Lo Iudice, A. Porrino, and F. Knapp, J. Phys. G **38**, 025103 (2011).

[46] D. Bianco, F. Andreozzi, N. Lo Iudice, A. Porrino, and F. Knapp, Phys. Rev. C **84**, 024310 (2011).

[47] E. Dikmen, O. Öztürk, and M. Vallieres, J. Phys. G : Nucl. Part. Phys. **36**, 045102 (2009).

[48] See, for instance, J. Duflo and A.P. Zuker, Phys. Rev. C **59**, R2347 (1999), and reference therein.

[49] H. von Garrel, P. von Brentano, C. Fransen, G. Friessner, N. Hollmann, J. Jolie, F. Käppeler, L. Käubler, U. Kneissl, C. Kohstall, L. Kostov, A. Linnemann, D. Mücher, N. Pietralla, H. H. Pitz, G. Rusev, M. Scheck,1, K. D. Schilling, C. Scholl, R. Schwengner, F. Stedile, S. Walter, V. Werner, and K. Wisshak, Phys. Rev. C **73**, 054315 (2006).

[50] T. Ahn, L. Coquardc, N. Pietralla, G. Rainovskid, A. Costinb, R.V.F. Janssens, C.J. Lister, M. Carpenter, S. Zhu, K. Heyde, Phys. Lett. **B 679**, 19 (2009).

[51] L. Coquard, N. Pietralla, G. Rainovski, T. Ahn, L. Bettermann, M. P. Carpenter, R. V. F. Janssens, J. Leske, C. J. Lister, O. Möller, W. Rother, V. Werner, and S. Zhu, Phys. Rev. C **82**, 024317 (2010).

[52] A. Arima, T. Otsuka, F. Iachello, and I. Talmi, Phys. Lett. **B 66**, 205 (1977).

[53] A. Arima and F. Iachello, Adv. Nucl. Phys. **13** 139 (1984)

[54] F. Iachello and A. Arima, *The interacting boson model*, (Cambridge University Press, Cambridge, U.K., 1987).

[55] N. Lo Iudice and F. Palumbo, Phys. Rev. Lett.**41**, 1532 (1978).

[56] D. Bohle, A. Richter, W. Steffen, A. E. L. Dieperink, N. Lo Iudice, F. Palumbo, and O. Scholten, Phys. Lett. **B137**, 27 (1984).

[57] N. Lo Iudice, Riv. Nuovo Cimento **23** (9), 1 (2000).

[58] K. Heyde, P. von Neumann-Cosel, A. Richter, Rev. Mod. Phys. **82**, 2365 (2010).

[59] W. D. Hamilton,, A. Irbäck, J. P. Elliott, Phys. Rev. Lett. **53**, 2469 (1984).

[60] G. Molnár, R. A. Gatenby, S. W. Yates, Phys. Rev. C **37**, R898 (1988).

[61] N. Pietralla, C. Fransen, D. Belic, P. von Brentano, C. Friessner, U. Kneissl, A. Linnemann, A. Nord, H. H. Pitz, T. Otsuka, I.Schneider, V. Werner, and I. Wiedenhover, Phys. Rev. Lett. **83**, 1303 (1999).

[62] U. Kneissl, N. Pietralla and A. Zilges, J. Phys. G: Nucl. Part. Phys. **32**, R217 (2006).

[63] N. Pietralla, P. von Brentano, and A. F. Lisetskiy, Prog. Part. Nucl. Phys. **60**, 225 (2008).

[64] A. F. Lisetskiy, N. Pietralla, C. Fransen, R.V. Jolos, P. von Brentano, Nucl. Phys. **A 677**, 1000 (2000).

[65] N. Lo Iudice and Ch. Stoyanov, Phys. Rev. C **62**, 047302 (2000).

[66] N. Lo Iudice and Ch. Stoyanov, Phys. Rev. C **65**, 064304 (2002).

[67] N. Lo Iudice, Ch. Stoyanov, and D. Tarpanov, Phys. Rev. C **77**, 044310 (2008).

[68] N. Lo Iudice, Ch. Stoyanov, and N. Pietralla, Phys. Rev. C **80**, 024311 (2009).

[69] K. Sieja, G. Martinez-Pinedo, L. Coquard, and N. Pietralla, Phys. Rev. C **80**, 054311 (2009).

[70] A. A. Sonzogni, Nucl. Data Sheets **103**, 1 (2004).

[71] D. J. Rowe, *Nuclear Collective Motion* (Methuen, London, 1970).

[72] P. Ring and P. Schuck, *The Nuclear Many-Body Problem* (Springer-Verlag, New York, 1980).

[73] P.F. Bortignon, A. Bracco, and R. A. Broglia, *Giant Resonances* (Harwood academic publishers, Amsterdam, 1998).

[74] A. Bohr and B. R. Mottelson, *Nuclear Structure*, Vol. II (Benjamin, New York, 1975) and references therein.

[75] M. Kneissl, H. H. Pitz and A. Zilges, Prog. Part. Nucl. Phys. **37**, 439 (1996)

[76] M. Kneissl, N. Pietralla and A. Zilges, J. Phys. G: Nucl. Part. Phys. **32** R217 (2006)

[77] N. Pietralla, P. von Brentano, and A. F. Lisetskiy, Prog. Part. Nucl. Phys. **60**, 225 (2008)

[78] N. Frascaria, Nucl. Phys. A **482** 245c (1988)

[79] T. Auman, P. F. Bortignon, H. Hemling, Ann. Rev. Nucl. Part. Sci. **48** 351 (1998)

[80] S. T. Belyaev and V. G. Zelevinsky, Nucl. Phys. **39** (1962) 582.

[81] T. Marumori, M. Yamamura, and A. Tokunaga, Progr. Thor. Phys. **31** (1964) 1009.

[82] For a review see A. Klein and E. R. Marshalek, Rev. Mod. Phys. **63** (1991) 375.

[83] T. Otsuka, A. Arima, and F. Iachello, Nucl. Phys. **A309**, 1 (1978).

[84] P. F. Bortignon, R. A. Broglia, D. R. Bes, and R. Liotta, Phys. Rep. **30** (1977) 305 and references therein.

[85] V. G. Soloviev, *Theory of atomic nuclei : Quasiparticles and Phonons* (Institute of Physics, Bristol, 1992).

[86] V. Yu. Ponomarev, P. F. Bortignon, R. A. Broglia, and V. V. Voronov, Phys. Rev. Lett. (2000) **85** 1400.

[87] N. Lo Iudice, A. V. Sushkov, and N. Yu. Shirikova, Phys. Rev. C **70**, 064316 (2004); Phys. Rev. C **72**, 034303 (2005).

[88] C. Pomar, J. Blomqvist, R. J. Liotta, and A. Insolia, *Nucl. Phys.* **A515**(1990) 381.

[89] M. Grinberg, R. Piepenbring, K. V. Protasov, B. Silvestre-Brac, *Nucl. Phys.* **A597** (1996) 355.

[90] F. Andreozzi, F. Knapp, N. Lo Iudice, A. Porrino, and J. Kvasil, Phys. Rev. C **75**, 044312 (2007).

[91] D. Bohm and D. Pines, Phys. Rev. **92**, 609 (1953).

[92] D. J. Thouless, Nucl. Phys. **22**, 78 (1961).

[93] D. J. Rowe, Rev. Mod. Phys. **40**, 153 (1968).

[94] J. Sawicki , Phys. Rev. **126**, 2231 (1962).

[95] C. Yannouleas, M. Dworzecka, and J. J. Griffin, Nucl. Phys. **A 397**, 239 (1983).

[96] C. Yannouleas, Phys. Rev. C **35**, 1159 (1987).

[97] D. J. Rowe, Rev. Mod. Phys. **40**, 153 (1968).

[98] B. Schwesinger and J. Wambach, Phys. Lett. **134B**, 29 (1984).

[99] B. Schwesinger and J. Wambach, Nucl. Phys. **A 426**, 253 (1984).

[100] P. Papakonstantinou, R. Roth, Phys. Lett. B **671**, 356 (2009).

[101] J. S. Dehesa, S. Krewald, J. Speth, and A. Faessler Phys. Rev. C **15**, 1858 (1977).

[102] P. F. Bortignon and R. A. Broglia Nucl. Phys. **A 371**, 405 (1981).

[103] G.F. Bertsch, P.F. Bortignon, R.A. Broglia, Rev. Mod. Phys. 55 (1983) 287.

[104] J. Wambach, V. K. Mishra, and L. Chu-Hsia, Nucl. Phys. **A 380**, 285 (1981).

[105] S. Kamerdzhiev, J. Speth, G. Tertychnya, Phys. Rep. **393**, 1 (2004).

[106] V. I. Tselyaev, Yad. Fiz. **50**, 1252 (1989) [Sov. J. Nucl. Phys. **50**, 780 (1989).

[107] V. I. Tselyaev, Phys. Rev. C **75**, 024306 (2007).

[108] E. Litvinova, P. Ring, D. Vretenar, Phys. Lett. **B 647**, 111 (2007).

[109] E. Litvinova, P. Ring, V. Tselyaev, Phys. Rev. C **78**, 014312 (2008).

[110] E. Litvinova, P. Ring, V. Tselyaev, Phys. Rev. Lett. **105**, 022502 (2010).

[111] D. Gambacurta, M. Grasso, and F. Catara, Phys. Rev. C **81**, 054312 (2010).

[112] D. J. Rowe, J. Math. Phys. **10**, 1774 (1969)

[113] J. P. Elliott and T. H. Skyrme, Proc. R. Soc. Lond. A **232**, 561 (1955).

[114] F. Palumbo, Nucl. Phys. A **99**, 100 (1967).

[115] D. H. Gloeckner and R. D. Lawson, Phys. Lett. **53**B, 313 (1974).

[116] N. Paar, P. Papakonstantinou, H. Hergert, and R. Roth, Phys. Rev. C **74**, 014318 (2006).

[117] E. G. Fuller, Phys. Rep. **127**, 187 (1985).

[118] A. Vessiere *et al.*, Nucl. Phys. **A227**, 513 (1974).

[119] B. L. Berman, At. Data Nucl. Data Tables **15**, 319 (1975).

[120] M. Goldhaber and E. Teller, Phys. Rev. **74**, 1046 (1948).

[121] H. Steinwedel and J. H. D. Jensen, Z. Naturforschung **5A**, 413 (1950).

[122] N. Paar *et al.*, Rep. Prog. Phys. **70**, 691 (2007).

[123] P. Adrich *et al.*, Phys. Rev. Lett. **95**, 132501 (2005).

[124] A. Klimkiewicz *et al.*, Nucl. Phys. **A788**, 145 (2007).

[125] T. Aumann, Nucl. Phys. **A805**, 198c (2008).

[126] J. Gibelin *et al.*, Phys. Rev. Lett. **101**, 212503 (2008).

[127] O. Wieland *et al.*, Phys. Rev. Lett. **102**, 092502 (2009).

[128] A. Carbone *et al.*, Phys. Rev. C **81**, 041301(R) (2010).

[129] J. Endres *et al.*, Phys. Rev. Lett **105**, 212503 (2010).

[130] S. Goriely, Phys. Lett. **B 436**, 10 (1998).

[131] F. Andreozzi, F. Knapp, N. Lo Iudice, A. Porrino, and J. Kvasil, Phys. Rev. C **78**, 054308 (2008).

[132] W. H. Bassichis and G. Ripka, Phys. Lett. **15**, 320 (1965).

[133] G. E. Brown and A. M. Green, Nucl. Phys. **75**, 401 (1966).

[134] H. Feshbach and F. Iachello, Ann. Phys. **84**, 2111 (1974).

[135] H. Feshbach and F. Iachello, Phys. Lett. B **45**, 7 (1973).

[136] W. C. Haxton and C. J. Johnson, Phys. Rev. Lett. **65**, 1325 (1990).

[137] E. K. Warburon et. al., Phys. Lett. B **293**, 7 (1992).

[138] T. Dytrych, K. D. Sviratcheva, C. Bahri, J. P. Draayer, J.P. Vary, Phys. Rev. Lett. **98**, 162503 (2007).

[139] D. Gambacurta, F. Catara and M. Grasso, Phys. Rev. C **80**, 014303 (2009).

[140] P.E. Haustein, At. Data Nucl. Tables **39**, 185 (1988).

[141] E.K. Warburton, J.A. Becker, B.A. Brown, Phys. Rev. C **41**, 1147 (1990).

[142] O. Tarasov et al., Phys. Lett. B **409**, 64 (1997).

[143] H. Sakurai et al., Phys. Lett. B **448**, 180 (1999).

[144] A. Leistenschneider et al., Phys. Rev. Lett. **86**, 5442 (2001).

[145] H. Sagawa and T. Suzuki, Phys. Rev. C **59**, 3116 (1999).

[146] G. Coló and P.F. Bortignon, Nucl. Phys. A**696**, 427 (2001).

[147] N. Lo Iudice, D. Bianco, F. Knapp, F. Andreozzi, A. Porrino, and P. Vesely, to be published on Proceedings of the Fourteenth International Symposium on Capture Gamma-Ray Spectroscopy and Related Topics, August 28 - September 2, 2011, University of Guelph, Guelph, Ontario, Canada.